Impact of Aluminosilicate Additives on Potassium Retention during Biomass Combustion

David Charles Nichols, MChem

Thesis submitted to the University of Nottingham for the degree of

Doctor of Engineering, September 2018

Abstract

The slagging and fouling characteristics of biomass fuels can act as a barrier to their use as a fuel for thermal power generation. Biomasses with high alkali metal and alkaline earth metal contents, in particular those with high potassium contents, have high slagging and fouling propensities due to the formation of low melting temperature mineral phases.

Under slow heating conditions using a muffle furnace, olive cake ashes have been produced at low temperature to retain inorganic volatile compounds while fully oxidizing carbon. These ashes have subsequently been heated with and without kaolin additives in different ratios to high temperatures, under both slow and fast heating rate conditions, in a muffle furnace and drop tube furnace respectively. Particular focus has been on the interactions of olive cake and kaolin in drop tube furnace combustion at temperatures ranging between 1000-1450°C and in 10% O_2 – conditions representative of pulverized fuel combustion.

Two additive ratio test series were conducted involving additive ratios ranging from 20% kaolin in olive cake ash (equivalent to 2% additive in raw fuel) to 50% kaolin in olive cake ash (equivalent to 10% additive in raw fuel). These tests were conducted at two temperatures: 1150°C and 1300°C. It was found that as the additive ratio increased, a threshold level for retention of volatile potassium was approached for each temperature. At 1150°C this value was 100% while at 1300°C this threshold level was approximately 80%.

Furthermore, log curves were produced from the results obtained. These approximations serve to offer an insight into the levels of retention that might be achieved as a function of additive ratio. Notably, it would appear that high levels of retention are attainable with small additive ratios at the optimum temperature of 1150°C.

From these additive ratio experiments it can clearly be seen that the combustion temperature has a significant effect on the efficacy of the kaolin additive. To further investigate this, an experimental test series was conducted involving DTF testing with 50% kaolin in olive cake ash at 1000°C and 1450°C. It was found that the level of retention at 1000°C was similar to that found at 1300°C (approximately 70%) while at 1450°C, 40% retention was measured. It is expected that at 1000°C the reaction is not under thermodynamic control and so the reduced retention is due to the slower kinetics at that temperature. This is not the case at the two higher temperatures of 1300°C and 1450°C. At these very high temperatures it is possible that there may be some degradation of the kaolinite additive which reduces its ability to react with the potassium.

Following the experiments with olive cake and kaolin, some further tests were conducted with miscanthus and wood as alternative feedstocks with different levels of potassium. While these tests were limited in number, they did show significant signs of substantial retention of volatile potassium. With wood in particular being a favoured feedstock in large scale biomass combustion (in part due it its low ash content) further research in this area is expected. Additionally, the use of an alternative aluminosilicate additive was explored. The additive

chosen was coal fly ash due to its high availability and low cost. When compared with the results achieved with kaolin, the coal fly ash that was used performed poorly. The notable contrast between the fly ash and the kaolin additive was a much lower alumina to silica ratio. When considering the ternery mineral phase diagram for the system K-Al-Si and the area of high melting temperature phases that exist where higher ratios of alumina are present, it is expected that the alumina to silica ratio of the additive is key to its performance. To further investigate this, further coal fly ash additives comprising of higher alumina to silica ratios should be tested.

The use of Mineral Liberation Analysis in this research afforded the opportunity to examine the form of potassium species (by association) present in olive cake ash samples. By using this method, it was observed that the volatile potassium present in the starting fuel existed primarily as KOH. By comparing this starting material with the ash following combustion with and without kaolin at 1150°C and 1300°C, it was possible to see the transformations that occur to the potassium species. In the absence of the additive it was found that while all KOH was volatilised and lost, some of this volatile potassium migrated to form potassium silicates. In the presence of the additive however, this migration did not occur. In preference, a large proportion (up to 100%) of the KOH reacted with the aluminosilicate additive to form potassium aluminium silicate mineral phases. Thermodynamic data available in literature demonstrates that this is due to the favourable ΔG energies of formation for this reaction. By further analysis of the molar ratios of elements present in the mineral phases detected, it was possible to speculate as to the identity of potential specific compounds

in the ash samples. These include the most commonly reported products of the reaction of K with Al-Si: kalsilite and leucite. By using this method it was found that the reaction product kalsilite was most likely to exist in large quantities in the samples.

Acknowledgements

This research is funded by the UK Engineering and Physical Sciences Research Council (EPSRC) through the CDT (grant: EP/L016362/1) for the Flex-E-Plant project (grant: EP/K021095/1). Without this funding it would not have been possible to conduct this research.

My sincere thanks go to my academic supervisor, Professor Colin Snape for his advice, guidance and supervision over the previous four years.

I would also like to express my gratitude to my co-academic supervisor, Associate Professor Robin Irons for his advice on the writing of this thesis.

Many thanks also go to those who have assisted in the collection of data throughout this research. Notably: Adrian Quinn for his continued technical support with furnace operation and repair; Dr Jackie Deans at the University of Birmingham for her unwavering assistance and accommodation in facilitating the collection of XRF data; Teresa Needham for her generosity in providing an alternative XRF service on such short notice; and Dr Elisabeth Steer for her patience, support and instruction on the use of SEM-EDX with MLA.

I also wish to extend my wholehearted appreciation to my family – particularly my parents, my friends, and my girlfriend Shelli. Their continued support and assistance throughout the course of this work has been invaluable.

Contents

List of Tables

List of Figures

Abbreviations

GHG – Greenhouse Gases

SEM – Scanning Electron Microscopy

EDX – Energy Dispersive X-Ray Spectroscopy

MLA – Mineral Liberation Analysis

GXMAP – Grain-Based X-Ray Mapping

CCSEM – Computer Controlled Scanning Electron Microscopy

QEMSCAN – Quantitative Evaluation of Minerals by Scanning Electron Microscopy

DTF – Drop Tube Furnace

TGA – Thermogravimetric Analysis

CFA – Coal Fly Ash

PF – Pulverised Fuel

NFFO – Non Fossil Fuel Obligation

1 Introduction

1.1 General Background

With global a rise of +2.2% in 2017 (the fastest since 2013) it is clear that our thirst for primary energy is showing no sign of abatement (Figure 1.1) (BP Statistical Review). What is also clear is that the anthropogenic emission of greenhouse gases (GHG), particularly CO_2, is causing irreversible and damaging change to our climate. In 2016, 81% of this energy was produced from non-renewable fossil fuels (Figure 1.2). The need to reduce the emissions of harmful GHGs associated with the production of energy is therefore indisputable.

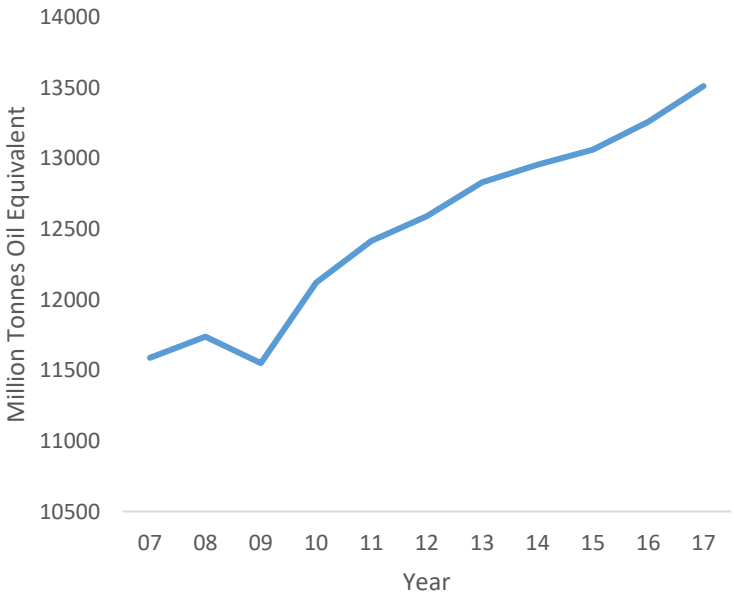

Figure 1.1 Global Growth in Primary Energy Consumption in the last decade (data taken from the BP Annual Statistical Review)

To achieve this, nations around the world are committing to reduce their emissions. As demand for energy continues to grow, it is clear this must be achieved by the adoption of cleaner means of supply.

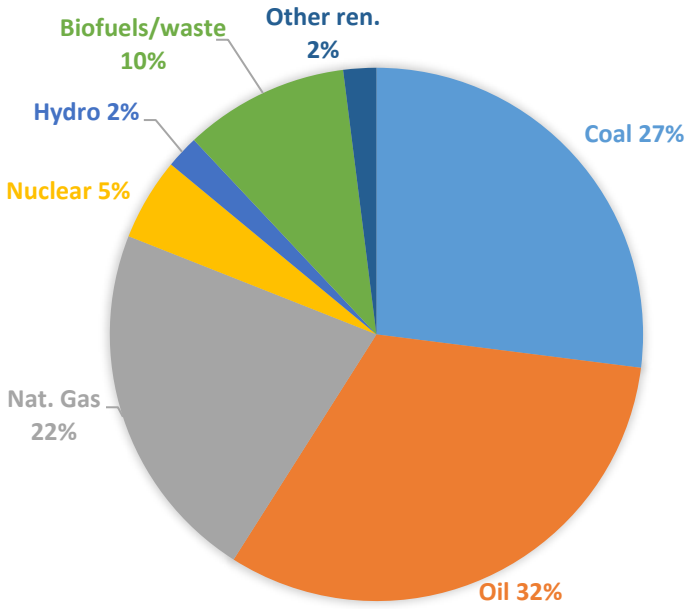

Figure 1.2 Total Primary Energy Supply by Fuel 2016 (data taken from IEA)

Fuel switching provides a means of maintaining a reliable and flexible supply while (depending on the fuel) reducing carbon emissions.

1.2 Why Biomass?

The primary greenhouse gas (GHG) that is released from combustion is carbon dioxide. With the combustion of fossil fuels, this CO_2 comes from carbon that was previously sequestered for millions of years; its release therefore results in a net increase in atmospheric CO_2. One of the ways in which we can significantly reduce our use of fossil fuels (and therefore our net carbon emissions) is by using biomass for thermal power generation (Anderson and Fergusson, 2006; Ladanai and Vinterbäck, 2009).

1.3 Properties of biomass

When considering the use of biomass as a fuel replacement for coal, the differences in its properties and combustion behaviour must be examined. In

general, biomass is less energy dense than coal. This means that for an equivalent energy output, a greater volume of biomass must be transported and stored. Furthermore, biomass must be kept dry to prevent rot. Biomass is also more volatile than coal and measures must be taken to avoid fire in storage.

1.4 Problems with biomass combustion

Due to the different properties of biomass when compared with coal, untreated biomass cannot be fired in boilers that were designed purely for the combustion of coal (Saidur et al. 2011). This is due to a higher propensity of biomass for slagging and fouling in boilers (Munir 2010). This occurs due to the volatilisation of alkali and alkaline earth metals that form low melting temperature ashes. Given the significant economic benefits of using existing coal boilers for future biomass combustion, any measures to mitigate these adverse ash problems could act to reduce the expense of switching.

1.5 Biomass in the UK

To incentivise the adoption of biomass combustion by generators, the UK Government has introduced a number of strategies where subsidies can be earned for full or partial conversion. This began with the Non Fossil Fuel Obligation (NFFO) which ran from 1990-2002 and which compelled energy companies to source a fixed percentage of their power from renewable sources (Pearson and Watson, 2012). However, this primarily served to support nuclear power rather than other renewables such as biomass. The introduction of the Renewables Obligation in 2002 did encourage significant uptake of biomass

combustion in the form of biomass-coal co-firing. This was initially done with olive residue in ratios of up to 8% biomass. The government later moved to support only full conversion from coal to biomass. Since then several operators have adopted 100% biomass firing, most notably Drax Power with their combustion of wood pellets. Electricity generation from bioenergy has, as a result, increased to 27.6 TWh in 2017 (DECC, 2018)

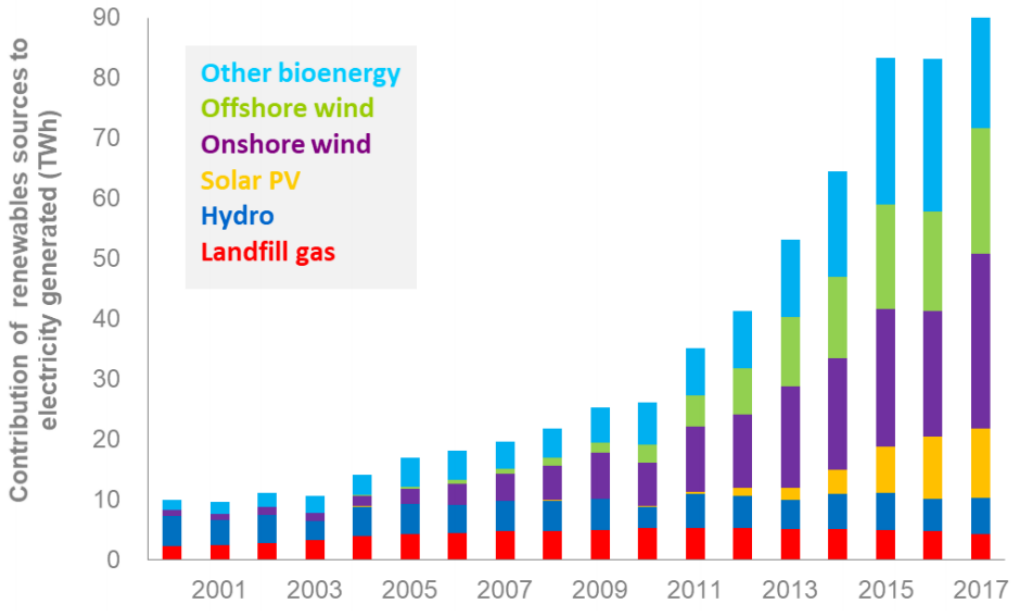

Figure 1.3. Electricity from renewable sources since 2000 (DECC, 2018)

1.6 Use of additives in biomass combustion

The use of additives has previously been shown to inhibit the volatilisation of alkali and alkaline earth containing species during combustion and therefore reduce the slagging and fouling issues associated with biomass combustion (Tran et al. 2005). There remains however, to be a limited understanding of the process of formation of ash particles from biomass. Aluminosilicate additives show a great deal of promise in mitigating alkali metal release (Wang et al.

2016; Niu et al. 2016; Jensen et al. 2016) and for this reason, these additives have taken the primary focus of this work.

1.6 Motivation for this study

Of particular interest to this research is the behaviour of aluminosilicate additives in pulverised fuel (PF) biomass combustion. This is because of the prevalence of this type of combustion in power grids around the world and because it is possible to convert coal PF boilers for biomass firing – albeit with some adaptations often necessary for successful conversion. Fluidised bed combustion has seen some extensive research on mitigation of bed agglomeration by use of fuel additives and developments have offered kaolin as a good choice to solve ash-related problems in fluidised bed combustion (Vamvuka et al. 2008; Niu et al. 2015). However, limited research has been conducted on the effect of kaolin and other aluminosilicate additives in pulverised fuel and grate firing combustion and this has been identified as an area which would benefit from further study.

1.7 Aims and objectives

The aims and objectives of the study are as follows:

- To obtain data on potassium retention by aluminosilicate additives in different ratios and at different temperatures
- To compare the effectiveness of additives on different biomass types
- To make use of MLA to characterise combustion ashes
- To use MLA to obtain data on the fate of potassium during biomass combustion with and without additives

- To understand the mechanisms involved in potassium retention in the presence of aluminosilicate additives

1.8 Thesis structure

This thesis is divided into 8 chapters which are presented as follows:

- Chapter 2 presents a review of literature on the topic of biomass composition and its combustion for power generation. Particular attention is drawn to reported research on the use of additives during biomass combustion and on optimal characterisation methods.
- Chapter 3 details the materials and experimental methods used in this research and the means of data analysis.
- Chapter 4 presents the results of a fundamental study on the use of kaolin clay as an additive during combustion of olive cake at 815°C in a muffle furnace.
- Chapter 5 presents the results of all drop tube furnace experiments conducted. This chapter includes a number of experiments beginning with the effectiveness of kaolin at fixing potassium in ashes over a range of variables including additive ratio, combustion temperature and residence time. Kaolin experiments conducted with miscanthus and wood are then explored and finally, the use of coal fly ash as an alternative to kaolin is tested.
- Chapter 6 presents the use of Mineral Liberation Analysis (MLA) software with a scanning electron microscope with energy dispersive x-ray spectroscopy (SEM-EDX) to characterise the ashes of a selection of

olive cake and kaolin experiments. This technique allows the rapid analysis of $>10^4$ particles and, significantly, identifies multiple phases within single particles. The migration of potassium in the biomass during combustion and the effect on this of the additive is shown in this chapter on a semi-quantitative basis.

- Chapter 7 presents the overall conclusions from the study and suggests areas for future research

2 Literature Review

2.1 Introduction to Biomass

Derived from living, or recently living organisms, biomass is formed primarily of biological material. It is carbon based consisting mainly of hydrogen, oxygen and nitrogen containing organic molecules, but also with small quantities of metals such as alkali metals, and alkaline earth metals (Vassilev et al., 2010). While there are often carbon emissions associated with the processing and transport of the biomass, the European Commission requires that ratio of energy output from the biomass to the fossil energy used to deliver the biomass, should exceed 7:1.

2.1.1 Biomass Sources and Types

Biomass is a broad term and applies to a diverse range of fuels. The different types of biomass used as fuels can be arranged within 5 main categories:

- Virgin wood
- Energy crops
- Agricultural residues
- Food waste
- Industrial waste and co-products

Virgin wood refers to wood generally from forestry; energy crops are grown specifically for energy applications; agricultural residues come from harvesting or processing of other crops; food waste comes from manufacture, processing,

and post-consumer waste; and industrial waste comes from manufacturing and industrial processes (UK Government, 2013).

In the UK, the primary sources of biomass are wood, energy crops, and agricultural residues (Marsh et al., 2008). In his 2003 paper, Cannell presents an overview of the potential for substitution of energy from fossil sources with "modern" forms of biomass, namely energy crops or industrial forest residues (Table 2.1)(Cannell, 2003).

Table 2.1. Estimates of Carbon Substitution using Energy Crops for the World, the EU15 and the UK (Mt carbon/yr)(Cannell, 2003)

	Theoretical potential	**Realistic potential**	**Conservative achievable**
World	2000–5000	600–900	40–60
Europe	1000–2000	200–300	5–20
UK	200–1000	100–200	1–6

The use of energy crops relies on dedicating arable land for their production. This has sparked a contentious food vs fuel debate which could serve as a significant barrier to the widespread production of energy crops (Levidow et al., 2014). However, such is the scale of current plant growth (more than five times the ~8 billion tons of carbon released annually from fossil fuel combustion) that the diversion of only a small fraction could satisfy the majority of global energy needs (Field et al., 2008).

2.1.2 The Use of Biomass in Power Generation

The use of biomass to generate heat is not a new concept; wood has been used for this purpose for thousands of years. In addition, biomass combustion is not

limited by the weather as other sources of renewable energy are and it can be used flexibly. Flexibility is vital to ensure electricity supply meets demand but nuclear power and most other renewables are not able to achieve this. Biomass combustion can therefore be considered to be an important contributor to a balanced, low carbon energy system (Saidur et al., 2011). Biomass boilers for thermal power generation have existed for as long as coal plants, however the favourable combustion properties of coal have meant that coal generation is by far the more prevalent (BP, 2015). With the ever growing concerns about climate change however, the use of biomass as an alternative to coal is increasingly being employed as a way of reducing carbon emissions. To incentivise the use of biomass as a replacement to coal for power generation, in 2002 the UK government introduced the Renewables Obligation. This required all licensed electricity suppliers to supply a fixed percentage of their power from certified renewable generators. The generators received renewable obligations certificates for each MWh of electricity produced, which could then be traded (Thornley, 2006). This resulted in a large increase in biomass/coal co-firing over the following three years. Co-firing biomass with coal is a way in which carbon emissions can be reduced with relatively low capital investment (Baxter, 2005). This is because it reduces the impact of biomass combustion on the operation of boilers that have been designed purely for coal. This was a significant advantage given the high capital costs associated with building new plants and infrastructure. In 2002, at Ferrybridge power station in Yorkshire, up to 8% by mass of olive residue was co-fired into all four 500 MWe boilers, generating around 100 MWe of renewable power

(Livingston, 2016). This proved to be very successful and led all other coal plant operators to initiate their own co-firing programmes. It was eventually deemed by the government however that co-firing at such low levels of biomass was providing an insufficient reduction in carbon emissions and legislation now only encourages dedicated biomass firing. Drax Power Ltd have responded to these subsidies and have now converted four out of six units to 100% biomass firing. This is equivalent to around 2000 MWe, approximately 4% of the UK electricity supply. To achieve this, Drax had to convert all of their mills supplying the four units from coal to wood pellet processing. They have also had to invest heavily in new infrastructure at the plant for the transport and storage of the biomass. This is largely due to the fact that unlike coal, biomass must be kept dry. To facilitate the wood pellets, four 75,000 tonne capacity, storage domes have been constructed (Livingston, 2016). There have also been successful conversions of pulverised coal boilers to 100% biomass at two other UK power plants. At Tilbury three 300 MWe boilers were converted and operated for two years before the station closed down. Ironbridge power station also fully converted its two 500 MWe coal units to dedicated biomass combustion and operated for several years before its closure in 2015.

In its white paper in 2011, the government stated its expectation that biomass combustion should continue to make a significant contribution towards achieving the UK's renewable energy targets (UK Government, 2011). Indeed, Drax has stated its aim to cease all coal combustion by 2025. When using biomass in coal boilers however, operational issues are incurred. These are primarily caused by the different chemical composition of the biomass (when

compared with coal) which, on combustion, results in an increased propensity for problematic ash-related issues (Saidur et al., 2011).

2.2 Introduction to Coal

When considering the use of biomass as a source of primary energy an understanding of the properties and combustion behaviours of coal is very worthwhile – particularly if biomass is to be used as a replacement for coal in a process such as power generation.

Coal is an organic sedimentary rock derived from peat. It is comprised of a heterogeneous mixture of organic and inorganic constituents (Van Krevelen, 1993). The organic components exist in the form of macerals: substances formed from plant matter that have been subjected to decay, and then as a mixture with sediment, compacted, hardened, and chemically altered over time by geological processes. The inorganic component comes from sediment during the formation of the coal (Neavel, 1979).

The word “coal” is a broad term and refers to a wide range of materials of different age and composition. Indeed its use is similar to that of the term “crude oil” or “petroleum” (Speight, 2015). Given the differences found between types of coal, it is useful to classify different coals. It is possible to rank coals based on the carbon content and gross calorific value.

2.2.1 The Use of Coal in Power Generation

Coal was one of the first choices as a fuel for power generation. As the fuel that powered the industrial revolution, the first coal power stations were operated by reciprocating steam engines. Over time boiler systems developed and steam

turbines were introduced. There are several different boiler designs currently used in coal-fired power stations. There are three main types; pulverised fuel (PF) boilers, fluidised bed boilers, and grate fired boilers. With PF boilers, the coal is pulverised to a fine powder in mills before being carried by hot air to the burners. These burners can be arranged in a variety of configurations depending in part on the rank of coal being combusted. The main configurations are front-wall-fired (burners on one wall), opposed-wall-fired (burners on opposite walls)(Figure 2.1), tangential-corner-fired (burners in each corner firing at tangents to a central spiral), and roof firing (burners firing downwards towards the centre of the boiler) (Couch, 1994). 30% of primary energy worldwide comes from the combustion of coal (BP, 2015).

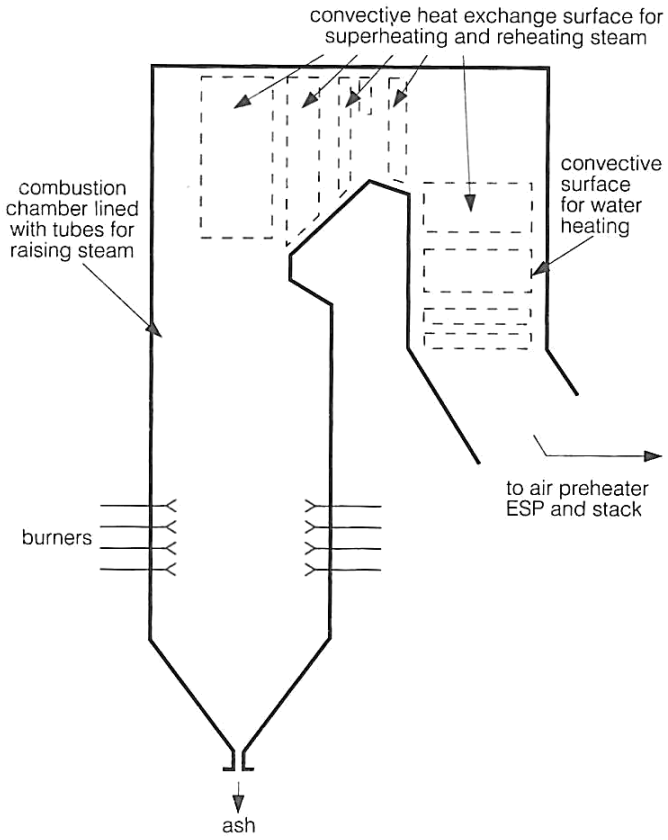

Figure 2.1. Conventional PF-Fired Boiler Configuration (Modified from Couch 1994)

Fluidised bed boilers make use of a bubbling fluidised bed of ash and other particulate solids (such as limestone and sand) into which the fuel is added and combusted (Figure 2.2). The oxygen required for combustion is provided by the hot air that is bubbled through the mixture. There are several advantages to fluidised bed combustion including uniform particle mixing and the use of a lower combustion temperature which allows for the use of fuels with lower ash melting temperatures. This means that fluidised bed boilers have greater fuel flexibility. Fluidised bed boilers also recirculate unburnt fuel particles, increasing efficiency.

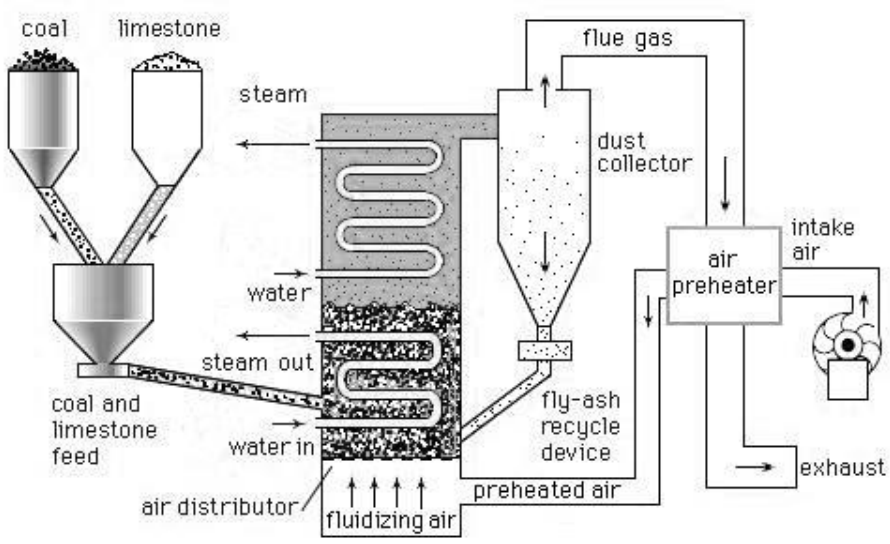

Figure 2.2. Fluidised Bed Combustion Boiler (Pisupati, 1999)

The majority of coal that is used for power generation worldwide is Lignite or subbituminous coal as higher ranked coals are more expensive and ignite with more difficulty due to their lower volatile matter content (Speight, 2015).

2.3 Introduction to Ash Related Boiler Issues

The inorganic constituents of coal and biomass form ash on combustion. Deposition of ash on surfaces in boilers causes reductions in efficiency,

materials corrosion, and can cause unplanned shut-downs (Livingston, 2014). There are two main types of ash deposition in boilers: slagging and fouling. Slagging refers to conglomeration of ash at high temperatures on the boiler surfaces and involves bulk melting of the ash material, whilst fouling refers to lower temperature ash deposition on heat transfer surfaces, where the bulk of the ash does not melt. Figure 2.3 shows the areas of a conventional PF boiler that are susceptible to slagging and fouling. Slagging occurs in the hottest parts of the furnace, those which are directly exposed to flame radiation. Fouling occurs in the cooler part of the boiler, such as amongst the closely spaced tubes in the convection sections (Couch, 1994).

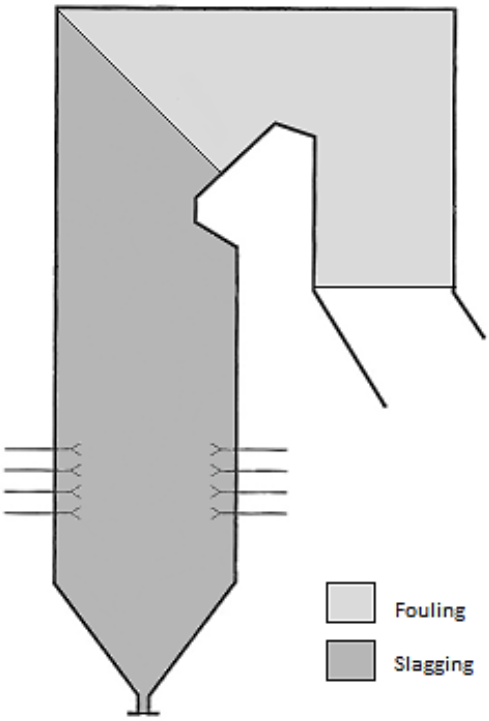

Figure 2.3. Slagging and Fouling in a Conventional PF Boiler (Modified from Couch 1994)

It is very important to minimise the risk of slagging, fouling, and corrosion in boilers as these processes can cause major issues to the operation of the boiler. The combustion of biomass incurs a higher risk of slagging and fouling than coal.

There is also a higher risk of corrosion of surfaces caused either by gas phase species, deposits, or both (Saidur et al., 2011) and this is influenced by the chemical composition of the fuel – see below.

2.4 Biomass Composition

Biomass consists both of natural constituents derived from plants or products of animal digestion, and of technogenic products from the subsequent processing of the natural matter. It's therefore no surprise that the properties of different biomasses vary a great deal. There are however, notable differences between biomass and coal. Biomass has less carbon; more oxygen; a lower heating value; a much higher volatile content; and less carbon (Figure 2.4). Biomass generally also has a significantly higher level of alkali/alkaline earth metals.

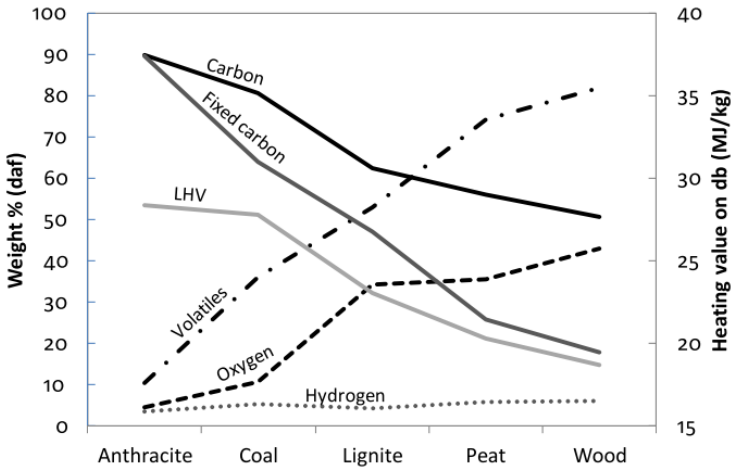

Figure 2.4. Properties for various types of solid fuels (daf, dry ash free basis; db, dry basis) (Hupa et al., 2017)

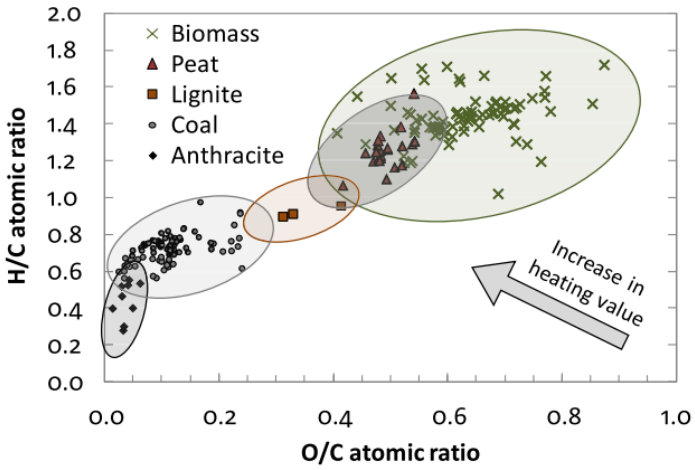

Figure 2.5. Van Krevelen diagram of various fuels (Hupa et al., 2017)

Figure 2.5 shows how biomass fuels compare with various coals. It can be seen that biomass fuels have both a higher O/C atomic ratio and higher H/C atomic ratio. The most common form of biomass is lignocellulosic biomass (Sánchez and Cardona, 2008). Lignocellulosic biomass refers to plant matter from higher plants, softwood, and hardwood. The main components are cellulose, hemicellulose, and lignin (Klass, 1998).

2.4.1 Organic Material in Biomass

The organic material in lignocellulosic biomass consists primarily of cellulose, hemicellulose, and lignin. Cellulose is a polymer of β-glucose and provides much of a plant's strength (Mohan et al., 2006). Cellulose accounts for ~40–50 wt % of dry wood (Pettersen, 1984). Hemicellulose is a second major constituent of wood with 25%–35% of the mass of dry wood being comprised of a variety of hemicelluloses. Unlike cellulose, hemicellulose exists as a mixture of various, polymerised monosaccharides. Accounting for between 16 and 33% of the mass of wood is the third major constituent of biomass: lignin (Mohan et al., 2006; Pettersen, 1984). Lignin has a complex, cross-linked, amorphous

structure, consisting of an irregular array of hydroxy- and methoxy- substituted phenylpropane units (Figure 2.6).

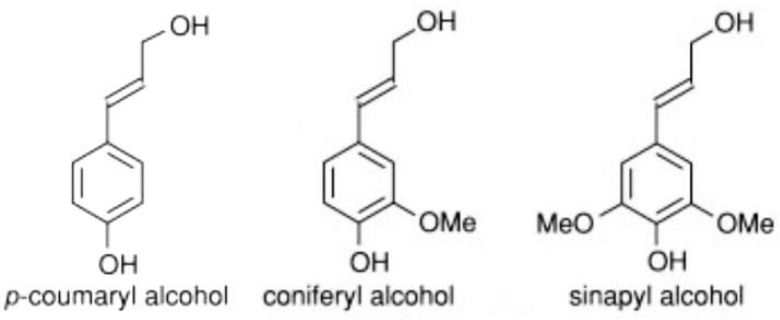

Figure 2.6. The Phenolic Building Blocks of Lignin (Modified from Boerjan et al. 2003)

2.4.2 Inorganic Material in Biomass

While plants are primarily made up of organic matter consisting mainly of carbon, hydrogen, and oxygen, they also contain small quantities of many inorganic elements that are essential for life (Table 2.2). Furthermore, in addition to minerals from the body of the plant matter in biomass, inorganic elements from external sources often exist in the fuel. During coalification the quantity of these inherent elements is substantially diminished; combusting biomass however, means the introduction of higher amounts of certain inorganics to boiler systems.

Table 2.2. Essential Plant Nutrients Relative to Nitrogen Content (Modified from Masiá 2010)

Name	%w in plant (relative to N)	Function in plant	Nutrient category
Nitrogen	100	Proteins, amino acids	
Potassium	25	Catalyst, ion transport	Primary macronutrients
Phosphorus	6	Nucleic acids, ATP	
Calcium	12.5	Cell wall component	
Magnesium	8	Part of chlorophyll	Secondary macronutrients
Sulphur	3	Amino acids	

Chlorine	0.3	Photosynthesis	
Iron	0.2	reactions	Micronutrients
Boron	0.2	Chlorophyll synthesis Cell wall component	

It is possible to group ash formation from biomass fuels into four types: water soluble salts, elements associated with the inorganic materials of the biomass, intrinsic minerals in the biomass structure, and extraneous minerals present in the mixture (Wang et al., 2012b). Figure 2.7 shows the metal content in a variety of biomass fuels and in sub-bituminous coal. It can be seen that the coal has predominantly Si, Al and Ca with a small amount of K. By comparison, the biomass samples (in particular the wheat straw) have significantly higher levels of potassium.

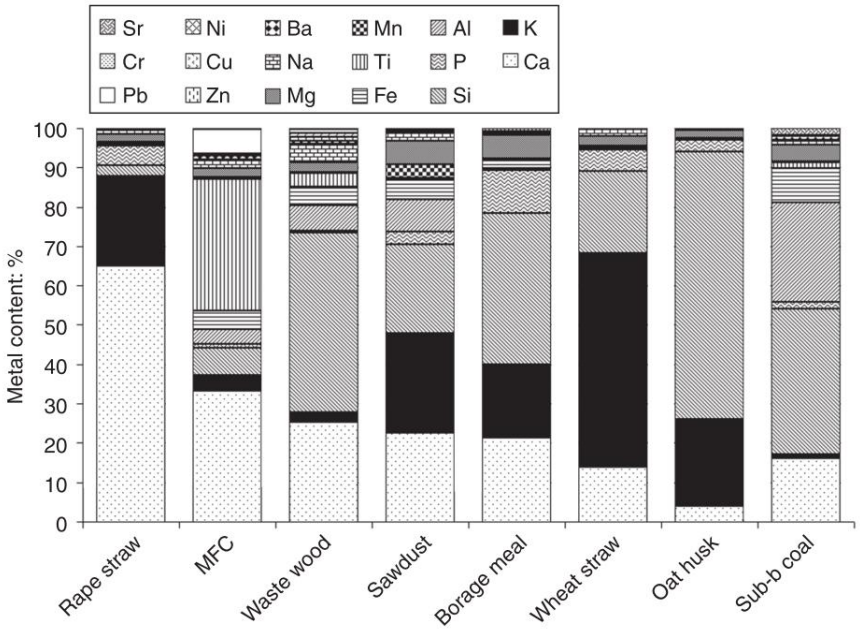

Figure 2.7. Metal Content in Biomass Ash Samples (Marsh et al., 2008)

2.5 Biomass Combustion

While the sequence of combustion of biomass is the same as coal, the combustion behaviour of biomass has distinct differences. These differences alone result in different flame properties (Lu et al., 2008), char forming tendencies (Wornat et al., 1995), and ashing behaviour (Vassilev et al., 2014). In order to be used at all, most biomass requires at least some form of pre-treatment prior to combustion. Various reasons to do this include improving the grindability of the fuel (for PF combustion) by decomposing the fibrous structure; decrease the moisture content; decreasing the amount of volatile matter (to increase the energy density of the fuel); and to make the fuel easier to transport and store. Biomass typically has a volatile matter content of 70-80% compared to the 10-50% found in coal (Vassilev et al., 2010). This means that homogeneous ignition is more likely. The oxidation of this volatile matter releases less energy than the oxidation of coal char. This, combined with its significantly lower energy density, means that biomass has a lower calorific value than coal (Saidur et al., 2011; Vassilev et al., 2015). In addition, while biomass has a lower ash content than coal, biomass ash is rich in alkali and alkaline earth metals (Munir, 2010). High moisture and ash contents in biomass fuels cause a decrease in adiabatic flame temperature which can result in flame stability issues (Sami et al., 2001).

There are several stages that occur during the combustion of solid fuels such as biomass and coal. The first stage is the loss of moisture, followed by the release and oxidation of volatile gases. This release of volatile matter is referred to as

devolatilisation or pyrolysis. In general, pyrolysis of biomass begins at a lower temperature than that of coal (Biagini et al., 2002) and (as with coal) depends greatly on heating rate (Sami et al., 2001). Hemicelluloses are rich in volatile matter and volatilise at temperatures of 200–260°C. Cellulose decomposes at 240–350°C, and lignin decomposition occurs at 280–500°C. All metals are largely retained in biomass char during devolatilisation.

After devolatilisation, char is combusted. Incomplete char burnout of biomass is a serious issue that must be considered if biomass combustion is to be employed on a large scale. Incomplete combustion products can be precursors to pollutants and when present in ash can render it unsuitable for use in cement production and other applications (Moghtaderi, 2007). The results of a study on the transformations of biomass chars during combustion at 1600 K in a laminar flow reactor can be seen in Table 2.3. Early in the char conversion process, large amounts of oxygen and hydrogen are lost. This is primarily in the form of volatiles such as CO, CO_2, and H_2O. Despite this however, oxygen levels remain higher in biomass char than found in that of high-rank coals. Sodium and potassium vaporise during char burnout (Knudsen et al., 2004).

Table 2.3. Element Retention in Biomass Chars (Modified from Wornat et al. 1995)

Char Conversion (% DAF)	Mass[a]	Normalized fractional retention in the char								
		C	H	O	N	Na	Mg	Al[b]	K	Ca
Southern pine										
0	1.00	1.00	1.00	1.00	1.00	1.00	1.00	1.00	1.00	1.00
52.8[c]	0.47	0.56	0.08	0.16	0.69	1.00	0.98	0.76	0.98	1.00
73.0[c]	0.27	0.31	0.05	0.13	0.53	0.46	0.93	0.69	0.89	0.96
86.4[c]	0.14	0.15	0.02	0.09	0.39	0.45	0.92	0.73	0.60	0.97
94.6	0.05	0.05	0.01	0.05	0.17	0.31	0.83	0.88	0.47	0.79
Switchgrass										
0	1.00	1.00	1.00	1.00	1.00	1.00	1.00	1.00	1.00	1.00
48.0	0.52	0.63	0.15	0.24	0.58	0.85	1.00	1.00	0.95	1.00

76.3	0.24	0.23	0.04	0.12	0.35	0.59	0.91	0.98	0.72	0.92
90.7	0.09	0.10	0.02	0.07	0.22	0.43	0.74	0.95	0.49	0.79
93.9	0.06	0.07	0.02	0.06	0.13	0.06	0.70	0.75	0.44	0.68

[a] Normalised char mass on a DAF basis.
[b] Al values more uncertain for pine char due to low absolute Al levels.
[c] These samples produced at 6% O_2; all other samples produced at 12% O_2.

Following the large initial release of oxygen and hydrogen, steady losses in carbon and nitrogen are seen as the char conversion proceeds. The results also show retention of nitrogen by the biomass, relative to carbon. This is the reverse of what is found with coal and is likely due to the nature of the carbon present in biomass when compared with coal. In biomass char the carbon is mostly aliphatic whereas in coal char it predominantly exists in aromatic systems. Aliphatic C-C bonds have lower bond dissociation energies than aromatic C-N which in turn are lower than aromatic C-C bonds (Clayden et al., 2008).

2.5.1 Release of Inorganic Metals during Combustion

During combustion of biomass, certain inorganic elements are released to the gas phase (van Lith et al., 2006, 2008). The formation and deposition of acidic or high mass pollutants derived from these elements are responsible for slagging, fouling, and corrosion in boiler systems (Baxter and Nielsen, 1997; Baxter et al., 1998; Couch, 1994; Knudsen et al., 2004; Miles et al., 1996; Munir, 2010; Nutalapati et al., 2007). The reason for the increased risk of these issues is the higher content of alkali metals such as sodium and potassium that is found in biomass (Vassilev et al., 2010). Alkali and alkaline earth metals are effective fluxes for alumina-silicates (Munir, 2010). This process results in the formation of alkali silicates that melt at relatively low temperatures (~700˚C).

These can form a sticky surface on the inside of the boiler, aiding deposition of ash (Miles et al., 1996; Saidur et al., 2011).

As can be seen in Table 2.2, plants require a relatively high amount of potassium during growth. Indeed, potassium salts are the primary alkali metal containing species released during combustion (Jones et al., 2007). These are mainly found as gases in the form of KCl and KOH but also (at lower temperatures) as condensed sulphates, chlorides, and silicates. The volatility of potassium is generally increased by the presence of chlorine and sulphur (Nielsen et al., 2000).

The use of molecular-beam mass spectrometry has been used to detect released vapour species during combustion (Dayton et al., 1999, 1995). It was found that alkali metals were volatilised during char burnout following the prior release of HCl and SO_2 during devolatilisation. Further research has identified relationships between the rate of release of potassium and the proportion of potassium released (Mason et al., 2016, 2015). On release to the gas phase, potassium can form a number of problematic species. These include potassium salts such as KCl, K_2SO_4, and K_2CO_3 which have melting points as low as 770°C and can get carried by combustion gases through the boiler where they cause fouling. Also produced are potassium silicates. Formed by reaction of potassium salts with silicon/silicates and with a melting temperature as low as 600°C; binary K_2O-SiO_2 can cause bed sintering and agglomeration in fluidised bed systems. Potassium phosphates are also formed and readily melt resulting in ash sintering and slagging (Wang et al., 2012b).

Interestingly, a higher proportion of sodium is released during char burnout than of potassium relative to starting quantities (Table 2.3). This is suggested to be as a result of intercalation of potassium within carbon structures due to its greater electropositivity than sodium (Wigmans et al., 1983). This intercalation will prevent volatilisation. Silica is abundant in biomass and reaction of sodium with SiO_2 forms sodium silicates above particle temperatures of 1600°C. While some forms of sodium exist as volatile species such as Na_2O and NaCl, this interaction of sodium (or potassium) oxides with SiO_2 and/or Al_2O_3 may prevent their vaporisation due to the formation of silicates and/or alumina-silicates (Wornat et al., 1995). The higher retentions of magnesium, aluminium, and calcium found during conversion may be attributed to coalescence and sintering in addition to silicate conversion. Calcium in particular, as CaO, will bind with SiO_2 at temperatures between 800 and 1400°C.

Leaching of the biomass is a very effective way of improving the combustion properties of some biomass fuels. Indeed, reductions of >80% of potassium and sodium and >90% of chlorine in biomass fuels, achieved by leaching with water, have been shown to yield significant reductions in the gas phase alkali salts present on combustion (Gudka et al., 2016; Yanqing Niu et al., 2016; Vamvuka et al., 2008). However, there are significant drawbacks associated with leaching of biomass. The primary drawback is the obvious expense and time cost that is incurred when adding any extra processing stages. In addition, following any wet process, the biomass must be dried sufficiently to avoid rot during storage.

2.6 Ash Deposition in Biomass Boilers

2.6.1 Ash deposition mechanisms

As previously stated, the deposition of ash in boilers can induce many operational problems. These include a reduction in heat transfer in the furnace walls and convective pass tubes and a decrease in the boiler efficiency and capacity. In this section, an overview of the types and mechanisms of ash deposition will be covered.

There are four principal mechanisms for ash deposition: inertial impaction, condensation of vapours, thermophoresis, and chemical reactions. These can be seen below in Figure 2.8.

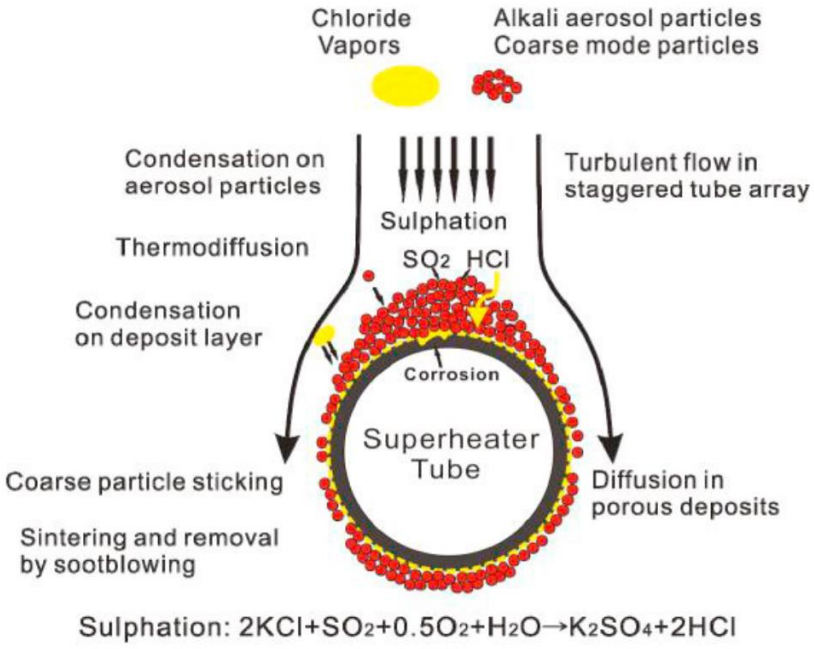

Figure 2.8. Mechanisms of ash formation and deposition on a super-heater tube surface

(Yongtie et al., 2017)

Inertial impaction occurs when particles larger than 10 µm have sufficient inertia to impact on heat transfer surfaces. The ratio of particles impacting the

heat transfer surface to the overall number of particles flowing towards the surface is defined by the impaction rate. This is dependent on several factors including the properties of the gas flow; the impaction angle and velocity; particle size, density and shape; and target geometry.

Thermophoresis involves the transport of particles within the gas flow as a result of a local temperature gradient. This most commonly affects particles smaller than 10 μm and when the temperature difference between the flue gas and heat transfer surface is large enough. For example, where a low temperature layer presents at the heat transfer surface, thermophoretic effects may be observed until the deposit grows such that the temperature gradient decreases, whereby the deposition by thermophoresis decreases and eventually stops entirely. Thermophoretic deposits are typically fine and evenly distributed on the incident surface (Yongtie et al., 2017).

Condensation occurs where inorganic vapours pass through the heat transfer zones and collect on surfaces cooler than the local gas. This can be directly on the heat transfer surfaces themselves or on top of already-deposited particles. Two of the aforementioned K-containing species (KCl and K_2SO_4) are prime culprits of this kind of fouling and where high levels of these gases are found, problematic fouling typically follows. Condensation deposits are usually evenly distributed and sticky.

The final mechanism for ash deposition is caused by heterogeneous chemical reactions between the formed deposits and incident gas phase species. The most significant of these reactions in terms of further deposit formation are

oxidation, sulphation, alkali absorption and eutectics. Potassium and sodium compounds, most commonly in the form of condensed hydroxides and chlorides are the principal sulphating species.

Figure 2.9 describes the main transport mechanisms by which particles deposit on superheater tubes (Zbogar et al., 2009). These can be split into two types. Diffusion and thermophoresis act on vapours and small particles which are carried in the gas flow around the tubes Figure 2.9 (a) and which adhere in deposits by the mechanisms described above. Inertial impaction affects larger particles with inertia sufficient to continue directly towards and impact with the tube rather than being carried around by the gas Figure 2.9 (b).

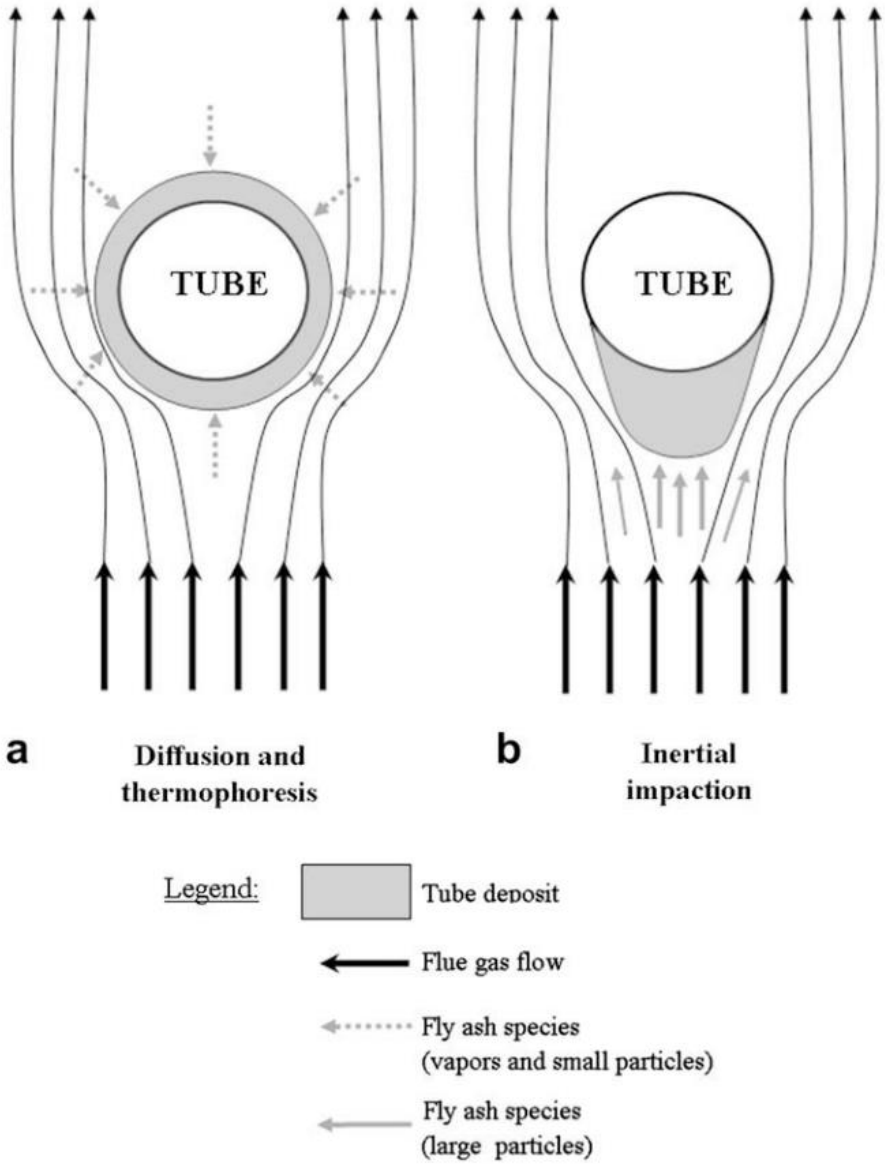

Figure 2.9. Formation of ash deposit on the superheater tube (Zbogar et al., 2009)

2.6.2 Ash Sintering

Ash sintering is the process by which particles attach to each other during deposit consolidation. Sintering therefore results in the formation of large plate-like features where the solid phase is all interconnected. The driving force behind sintering is particle surface energy. However, there are several different mechanisms of material transfer which lead to the sintering of ash particles (Zbogar et al., 2009). "Evaporation-condensation sintering" involves the

transfer of material due to variations in vapour pressure present as a result of surface curvature. A particle surface with a positive radius of curvature will have a higher vapour pressure and will tend to transfer material to an area with a negative radius of curvature and therefore a lower vapour pressure. “Liquid state sintering” describes sintering which is caused by melts. The amount of formed melt controls the level of resultant sintering. “Viscous flow sintering” occurs where the liquid state involved is highly viscous (eg. melted silicates) and its rate is dependent on the viscosity of the glassy phase and time. “Sintering with a reactive liquid” involves the partial dissolution of the solid phase in the liquid phase at sintering temperature. This results in densification and is driven by the capillary pressure of the liquid phase. “Chemical reaction sintering” between two ash particles involves the formation of a third component. A typical example of this would be the sulphation of deposited species. The formed sulphate can then go on to cause further deposition through melt formation. “Solid state sintering” may occur due to the difference in free energy or chemical potential between the ash particle and deposit surface. This mechanism relies on other types of material transfer to also be present (vapour transport or diffusion) and is a slower sintering process than those involving melts (Zbogar et al., 2009).

2.6.3 Industrial techniques for deposit removal

While some ash deposits may shed naturally over time, it is typically necessary to employ deposit removal techniques to maintain boiler efficiency and manage deposit build-up. There are several techniques that may be adopted for different deposit types and in different locations within the boiler.

Sootblowing is a commonly used technique for the removal of ash deposits from heat transfer surfaces. Sootblowing involves application of high pressure water, air or steam to the deposit and which causes its fracture due to the induced thermal and mechanical stress. The success of sootblowing is usually related in part to the level of sintering found in the deposit. Deposits with low sintering and which are not adhered strongly to the surface are often removed quickly and effectively, leaving an almost clean tube surface. More highly sintered deposits however, are significantly more challenging to remove and may leave a thin layer of deposit on the surface. In these cases, subsequent deposition on the residual layers is common. Sootblowing can be quite costly due to the large amounts of high pressure steam required and it can cause abrasion and erosion on the boiler tubes (Zbogar et al., 2009).

Another method of cleaning boiler surfaces is called acoustic cleaning and involves the use of sound waves. These act on the air in the boiler to cause oscillations which can shake deposits free. This technique is highly reflective which means that deposits may be released where they couldn't otherwise be reached. The technique is also gentle in nature and so doesn't damage the internal surfaces of the boiler. In cases of heavy fouling, detonation wave techniques can be employed for deposit removal. Typically, where detonation techniques are used, a fuel-oxidant mixture is detonated in a special chamber adjacent to the area requiring cleaning. The detonation creates a shockwave which serves to propagate through the chamber and impact on the deposit. Shot cleaning is a method of removing deposits through the directional use of

metal shot. This method can cause erosion however if the shot impacts on bare, undeposited surfaces (Zbogar et al., 2009).

2.6.4 The role of potassium in slagging and fouling

While slagging concerns the formation of melts/deposits in the combustion zone of the furnace, fouling refers to the condensation/deposition of ash in the cooler, convective areas of the boiler. The role of potassium as a cause of ash build-up is significant for both of these areas. During combustion, K is released in the combustion zone in the form of $KCl_{(g)}$, $KOH_{(g)}$ and $K_{(g)}$. These gases will then often deposit directly on the fireside, radiative surfaces of the boiler but also continue through the boiler where they will deposit on heat transfer surfaces by the previously described mechanisms of ash deposition.

Ash-related issues in furnaces can be attributed not only to alkali induced slagging but also silicate melt-induced slagging. Silicate melt-induced slagging is closely related to the ash fusion characteristics of the biomass. Quantitative information on the properties of different biomasses for prediction of silicate melt-induced slagging can be derived from the standard ash fusion test (AFT). Initial deformation temperature (IDT) in particular, is dependent on the proportions of the elements in biomass ash and is therefore typically employed to guide boiler design (Yanqing; Niu et al., 2016). Silicate melt-induced slagging is influenced in part by the alkali metal content, but also by the mineral composition of the biomass. Indeed, as the levels of MgO, CaO, Fe_2O_3 and Al_2O_3 increase, so do ash fusion temperatures. Conversely, as K_2O increases, ash fusion temperatures decrease. Furthermore, it has been reported by Vassilev

et al., that refractory minerals such as quartz, metakaolinite, mullite, etc., increase ash fusion temperatures whereas fluxing minerals such as anhydrite, calcium silicate and hematite, reduce them (Vassilev et al., 1995). Research in this area has therefore focused primarily on the analysis of the elemental and mineral compositions of biomass ashes (or simulated biomass ashes) by advanced electron/X-ray methods such as X-ray fluorescence spectroscopy (XRF), inductively coupled plasma mass spectrometry (ICP-MS), scanning electron microscopy with energy dispersive X-ray spectroscopy (SEM-EDX), X-ray diffraction (XRD), thermogravimetric analysis (TGA) and ash fusion characteristic testing instruments.

2.7 The Use of Additives in Biomass Combustion

A number of strategies can be used to reduce the number of undesirable compounds (primarily alkali metal species) in the gaseous state during combustion (Davidsson et al., 2008). These include leaching of the fuel prior to combustion, the use of alkali-metal-binding additives (to alter the ash composition), or the addition of sulphur to form K_2SO_4 (less corrosive than KCl). By use of these methods, some of the problems found in biomass combustion can be reduced (Wang et al., 2012b). This is achieved by decreasing the concentration of problematic species, changing the ash chemistry, or increasing the ash melting temperature. In this section the use of additives will be reviewed.

Different potential mechanisms for abatement of biomass ash related problems by use of additives include:

- Chemical reaction (alkali-getter effects). Use of additives to convert compounds with low melting point to those with higher melting temperature.
- Physical adsorption. Use of porous additives with high surface area to capture and transport particulate ashes out of the boiler system.
- Introduction of inert materials and elements (SiO_2 and Al_2O_3) into ash residues to raise ash melting temperature.
- Dilution of ash and restraint of ash melt formation and accumulation.

The most problematic compound formed during combustion is KCl (Aho and Ferrer, 2005). This is because it easily vaporises and condenses on heat exchange surfaces. As such, the majority of additives that have been tested have targeted the chemical capture of KCl and conversion to species with a high melting point.

Additives can be categorised by their reactive components:

2.7.1 Aluminium silicate-based additives

Potassium silicates and potassium aluminium silicates with a high SiO_2 content can have melting temperatures of ca. 700°C or less. This can be seen on a ternery mineral diagram as shown in Figure 2.10 below by the area in the red circle.

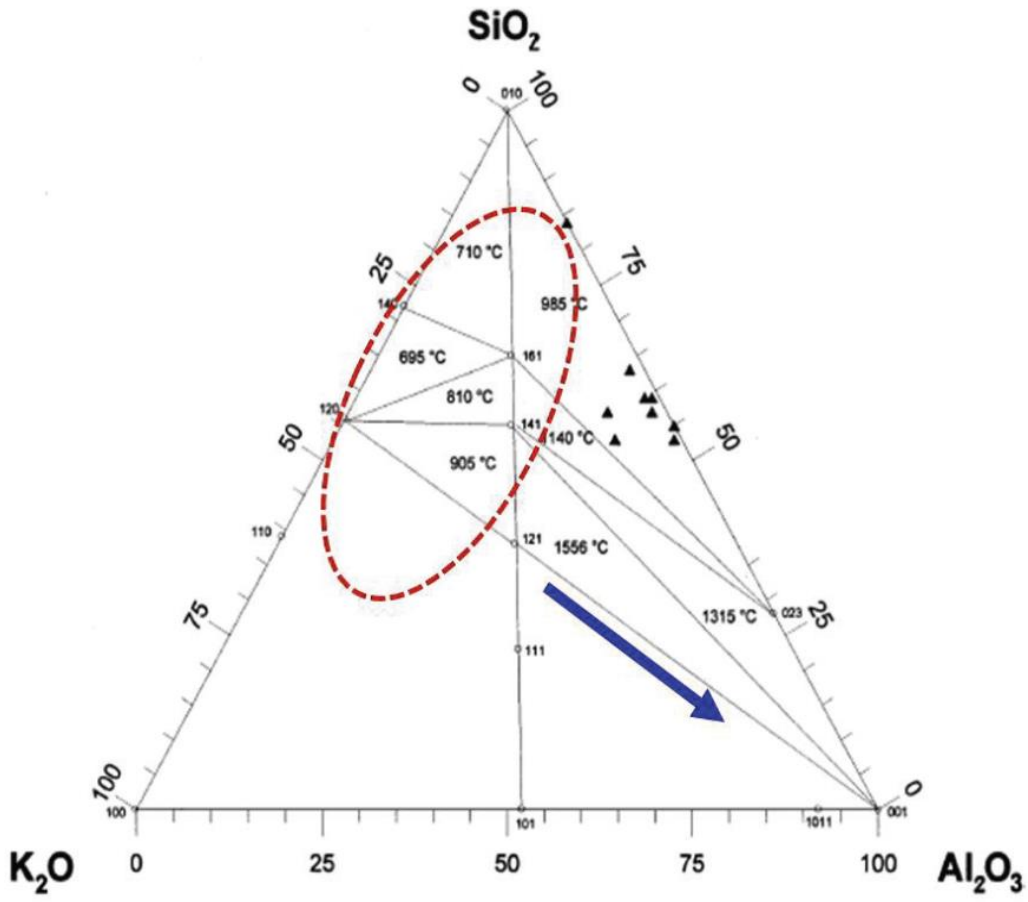

Figure 2.10. Formation of Potassium -Silicates and -Aluminium Silicates (Wang et al., 2012b)

The addition of aluminium oxide in the form of aluminium silicates such as kaolin clay yields potassium-aluminium-silicates. This change is shown by the blue arrow (Wang et al., 2012b). Kaolinite, $Al_2Si_2O_5(OH)_4$, is the main mineral in kaolin clay. Kaolinite decomposes and releases entrained moisture at temperatures between 450°C and 600°C (endothermic de-hydroxylation) to form an amorphous mixture of alumina and silica called meta-kaolinite (Yanqing; Niu et al., 2016). It is this meta-kaolinite which subsequently suppresses the release of volatile potassium from the biomass by reacting with the gaseous potassium compounds to form potassium aluminium silicates. The binding by kaolin of potassium compounds from biomass fuels can be described

by the following reactions (Boström et al., 2009; Steenari et al., 2009; Wang et al., 2012a):

$$Al_2Si_2O_5(OH)_4 \rightarrow Al_2O_3.2SiO_2 + 2H_2O \quad (2.1)$$

$$Al_2O_3.2SiO_2 + 2MCl + H_2O \rightarrow 2MAlSiO_4 + 2HCl \quad (2.2)$$

$$Al_2O_3.2SiO_2 + M_2SO_4 \rightarrow 2MAlSiO_4 + SO_3 \quad (2.3)$$

$$Al_2O_3.2SiO_2 + 2MOH \rightarrow 2MAlSiO_4 + H_2O \quad (2.4)$$

$$Al_2O_3.2SiO_2 + M_2O \rightarrow 2MAlSiO_4 \quad (2.5)$$

$$Al_2O_3.2SiO_2 + 2MCl + 2SiO_2 + H_2O \rightarrow 2MAlSi_2O_6 + 2HCl \quad (2.6)$$

$$Al_2O_3.2SiO_2 + M_2SO_4 + 2SiO_2 \rightarrow 2MAlSi_2O_6 + SO_3 \quad (2.7)$$

$$Al_2O_3.2SiO_2 + 2MO + 2SiO_2 \rightarrow 2MAlSi_2O_6 + H_2O \quad (2.8)$$

$$Al_2O_3.2SiO_2 + M_2O + 2SiO_2 \rightarrow 2MAlSi_2O_6 \quad (2.9)$$

The main products from the reaction of kaolinite with KCl are kalsilite ($KAlSiO_4$) and leucite ($KAlSi_2O_6$) and have been found to have melting points of over 1500°C (Steenari et al., 2009). The addition of aluminosilicates to biomass fuels during combustion has therefore been found to be an effective way of reducing KCl fouling by fixing potassium in ash minerals and has been widely reported (Schmitt and Kaltschmitt, 2013; Steenari et al., 2009; Wang et al., 2013, 2012b). However, the majority of these studies have been performed either on a lab scale and aimed at small-scale grate-fired combustors or similar (Steenari et al., 2009; Steenari and Lindqvist, 1998; Wang et al., 2013; Zheng et al., 2008), or fluidised bed systems (Öhman and Nordin, 2000; Vamvuka et al., 2008). This is important as it has been found that the ability of aluminosilicates to fix potassium varies under different temperatures and conditions. Indeed, the levels of potassium capture by kaolin pellets have been seen to decrease with

increasing temperature (Zheng et al., 2008). This has been attributed partly to changes in porosity and a reduction in the active surface area of the additive pellet (Tran et al., 2005). Additionally, in a study using gaseous KCl with pelletised kaolin in a fixed bed reactor, it was reported that above temperatures of 950°C, meta-kaolinite dissociates into amorphous silica and aluminosilica spinel. At 1000°C aluminosilica spinel then converts to pseudomullite. Both of these products appear to have low potential to react with KCl when compared with meta-kaolinite. The results of exposure temperature on the weight gain of different sorbent pellets when saturated with KCl can be seen below in Figure 2.11.

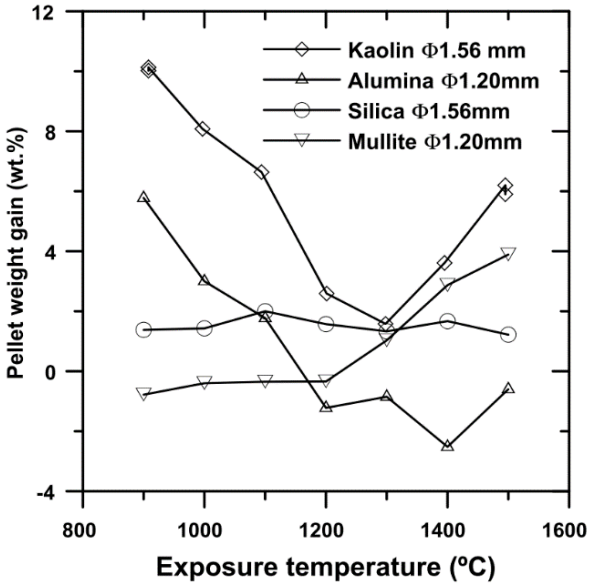

Figure 2.11. Effect of reaction temperature on potassium capture by different sorbent materials (Zheng et al., 2008)

The results from this study show that of the samples tested, kaolin holds the greatest potential to capture potassium across the entire temperature range. The use of kaolin as an additive therefore appears to be a good option to mitigate ash-related problems at the temperatures used in circulating fluidised

bed systems. For higher temperature combustion systems such as PF firing, there has been less research. Some significant progress has been made in this area nonetheless. In 2007, full-scale experiments on a 250 MWth straw pellet fired suspension drum-type boiler were conducted. Four additives were used: “sand, dicalciumphosphate (DCP), chalk, and bentonite, thereby representing both both Al-Si and P-Ca type substances”. For each of the additives, 5% by mass of the straw was added. Chalk and DCP were found to be unsuitable as additives due to the white deposits formed, but sand and bentonite showed promise. It was reported that more testing would be required before conclusive evaluations could be made but that bentonite is too expensive to be used on a large scale (Tobiasen et al., 2007).

Spent Bleaching Earth (SBE) is a by-product of the bleaching process that is used for the physical refinement of palm oil. The spent earth currently does not have any practical uses and is typically disposed of in landfill sites in large quantities. The use of SBE as an alternative additive to kaolinite in the combustion of straw and the subsequent effects on ash chemistry and deposition behaviour has also been investigated, this time in an entrained flow reactor (Wu et al., 2011). It was found that the levels of Cl were significantly reduced due to the presence of the additives, attributable to both simple dilution and also chemical reactions. Less Cl in the fly ash would significantly reduce corrosion problems. While the SBE was found to be a less effective additive than kaolinite, its use was still deemed to be attractive due to its economic benefit as a waste product (Wu et al., 2011).

The use of coal fly ash as an aluminosilicate-based additive for PF combustion of wood was been investigated by Wu et al. in 2013. An advanced probe system was employed to study deposit formation at two points within a full-scale (800 MWth) boiler. Coal fly ash, at a level four times that of the mass of the wood ash, was added and was found to greatly impact the fly ash properties and its deposition behaviours. The first detection point was at a temperature of 1300°C. At this location, where previously there had been a considerable amount of K_2SO_4, negligible water-soluble alkali species were found. At the second location in the boiler, at a temperature of 800°C, where relatively large quantities of potassium had previously been found in formed deposits, significant reductions were also found. In particular, almost no KCl appeared in the deposits here (Wu et al., 2013).

Another study of note is that of Paneru et al. and their research on deposit formation in wood pellet combustion (Paneru et al., 2016). By feeding a solid additive in powder form with milled wood pellets simultaneously in a 20 kW vertical tube furnace (much like a drop tube furnace) at temperatures of around 1300°C, conditions representing large scale PF combustion were achieved. The samples tested consisted of two different wood pellets and two different aluminosilicate based additives. It was found that even at high temperatures and under short residence times, interaction between potassium species and additive is possible. Thermodynamic equilibrium modelling was employed to determine both the relative distribution of potassium species over various temperatures (Figure 2.12) and then subsequently, the influence of the amount of additive on the K-phase distribution (Figure 2.13).

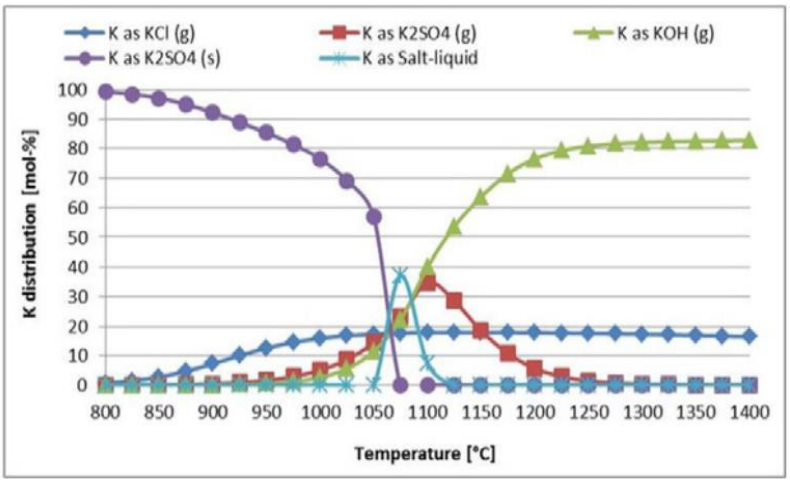

Figure 2.12. Relative distribution of K-species in equilibrium against temperature (Paneru et al., 2016)

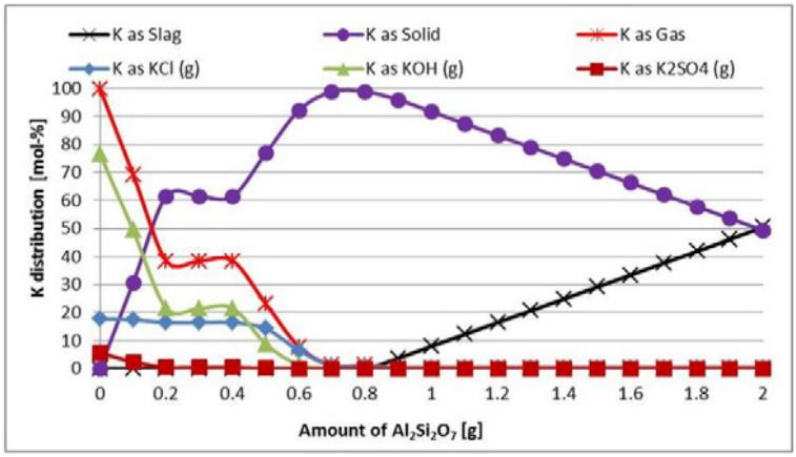

Figure 2.13. Influence of variation of $Al_2Si_2O_7$ additive on K-phase distribution at 1200°C (Paneru et al., 2016)

It can clearly be seen from these results that without the presence of the additive the potassium in the fuel predominantly exists as KOH and KCl above 1200°C. It can then be seen that when the additive is used at the optimum level, at 1200°C, 100% of the potassium can exist as a solid. This provides further strong evidence of the potential of kaolin as an additive even when used at high temperatures.

In 2018, in research conducted by Leeds University, gas phase potassium release profiles for combustion of biomass in a flame with aluminosilicate

additives were determined by the use of flame emission spectroscopy. The release of potassium was profiled over the three stages of combustion (volatilisation, char combustion, and "ash cooking"). These release profiles have been found to vary depending on the biomass type. In addition to analysing the release of gases from the samples, the resultant ashes were also tested to find the elemental mass balances at different temperatures and with different levels of the additive. It was reported that, without the presence of any additive, the loss of potassium at combustion temperature is 80% for wood pellets, 50% for wheat straw and 40% for olive residue. When additives were used, the levels of potassium retention in the ash were 70-100% for wood, 60-80% for wheat straw, and 70-100% for olive cake (Clery et al., 2018).

2.7.2 Other additives

2.7.2.1 Calcium based additives

The addition of calcium, most commonly as oxides from lime, has been found to significantly reduce the formation of slags during biomass combustion (Boström et al., 2009). This addition of CaO, $CaCO_3$ and $Ca(OH)_2$ reduces the formation of the low melting temperature minerals seen in the red circle in Figure 2.14 and promotes the release of gaseous potassium by the dissolution of and replacement by Ca^{2+} in potassium silicate melts. The result of this process is shown by the blue arrow in Figure 2.14. The formation of calcium silicates with higher melting temperatures reduces ash melt formation, ash sintering, and slagging.

$$K_2O.SiO_2 + 2CaCO_3 \rightarrow 2Ca.K_2O.SiO_2 + 2CO_2 \qquad (2.10)$$

Calcium additives have been more successful in biomasses that are rich in phosphorus and potassium (Steenari et al., 2009). This is due to the enhancement of Ca in potassium phosphates to form species with high melting temperatures. This can be seen in Figure 2.15 by the blue arrow.

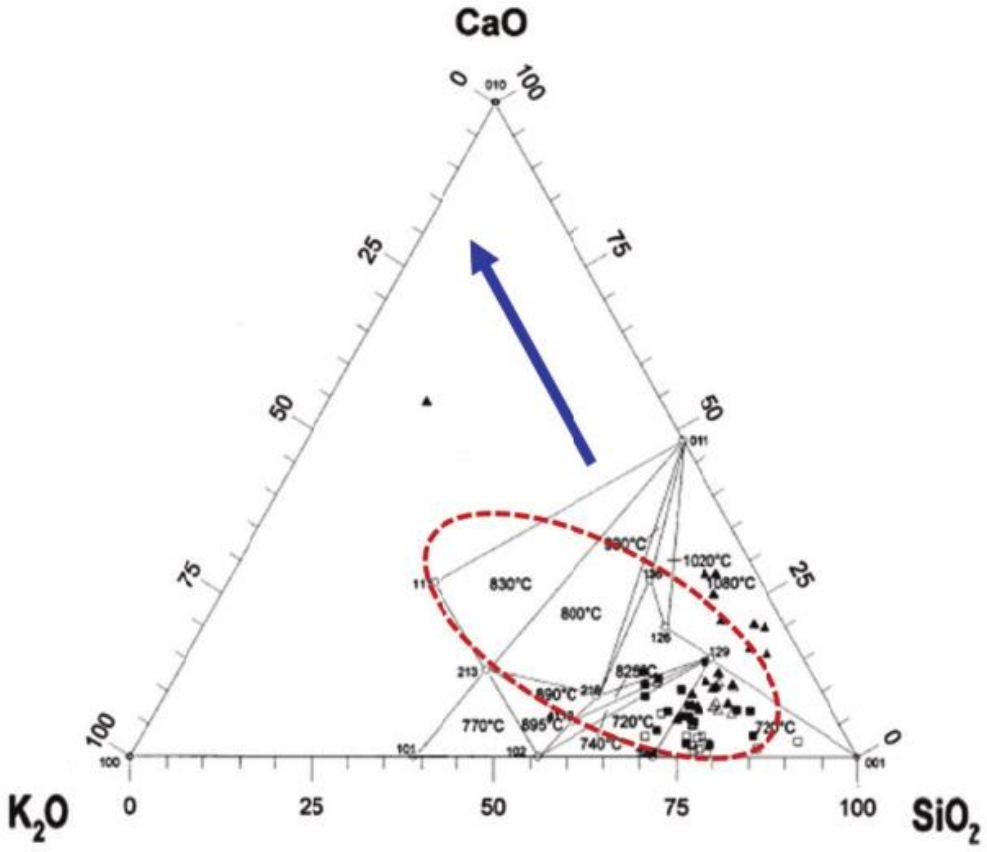

Figure 2.14. Ternery K_2O-CaO-SiO_2 system (Wang et al., 2012b)

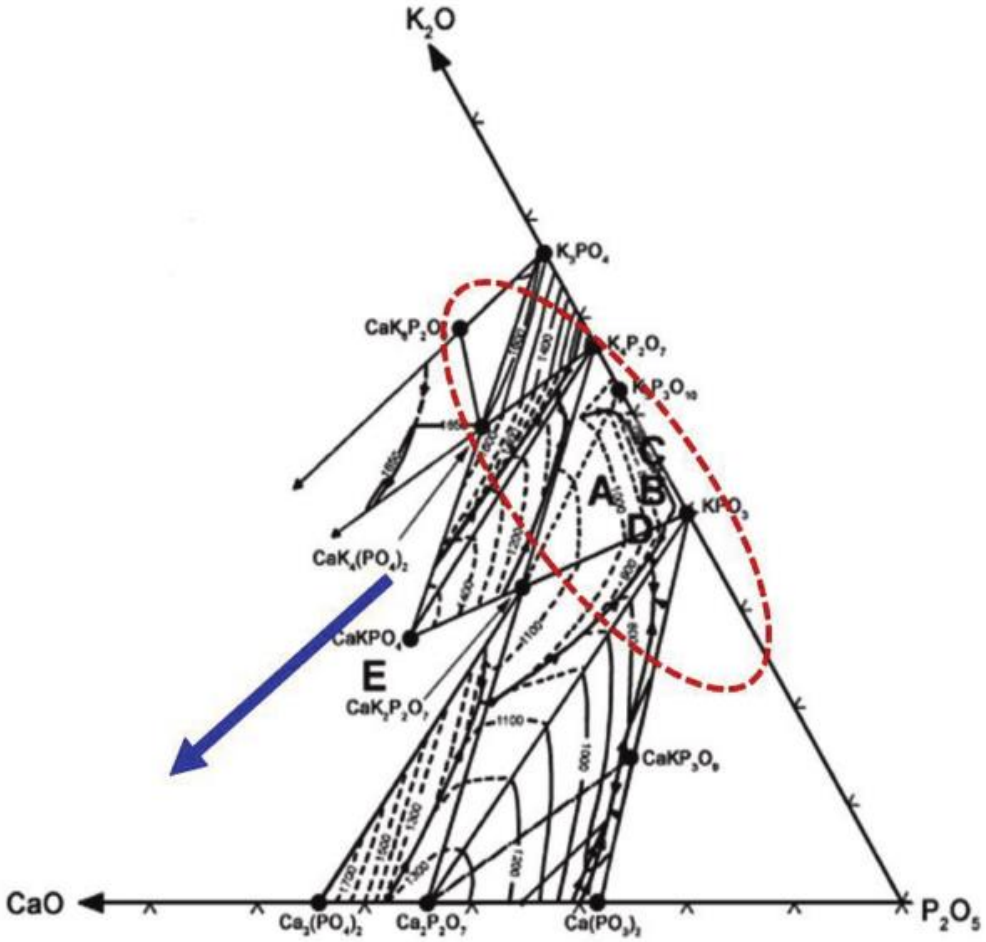

Figure 2.15. Ternery K_2O-P_2O_5-CaO (Wang et al., 2012b)

2.7.2.2 Phosphorous rich additives

Another approach to reducing the content of available potassium is the addition of phosphoric acid. This enables the formation of potassium rich phosphates which may further react with calcium oxide (Grimm et al., 2011). It has also been found that phosphorus addition aids the capture potassium by the formation of K_2O-P_2O_5-CaO systems with higher melting temperatures (Figure 2.15)(Ren and Li, 2015).

2.7.2.3 Sulphur based additives

Rather than changing the composition ratios of the minerals formed, the effect when using sulphur based additives is the conversion of KCl to K_2SO_4 (seen in reaction 11). K_2SO_4 has a higher melting temperature than KCl.

$$SO_3 + KCl + H_2O \rightarrow 2HCl + K_2SO_4 \qquad (2.11)$$

In a study on the efficacy of fuel leaching and additives in mitigating the ash related combustion issues of olive kernel in a fluidised bed furnace, Vamvuka et al reported notable reductions in the concentrations of potassium, sodium, chlorine, and sulphur in the fly ashes in the presence of three different additives: kaolin, clinochlore ($(Mg,Al,Fe)_6[(Si,Al)_4O_{10}](OH)_8$), and ankerite ($Ca(Mg,Fe,Mn)(CO_3)_2$)(Figure 2.16)(Vamvuka et al., 2008).

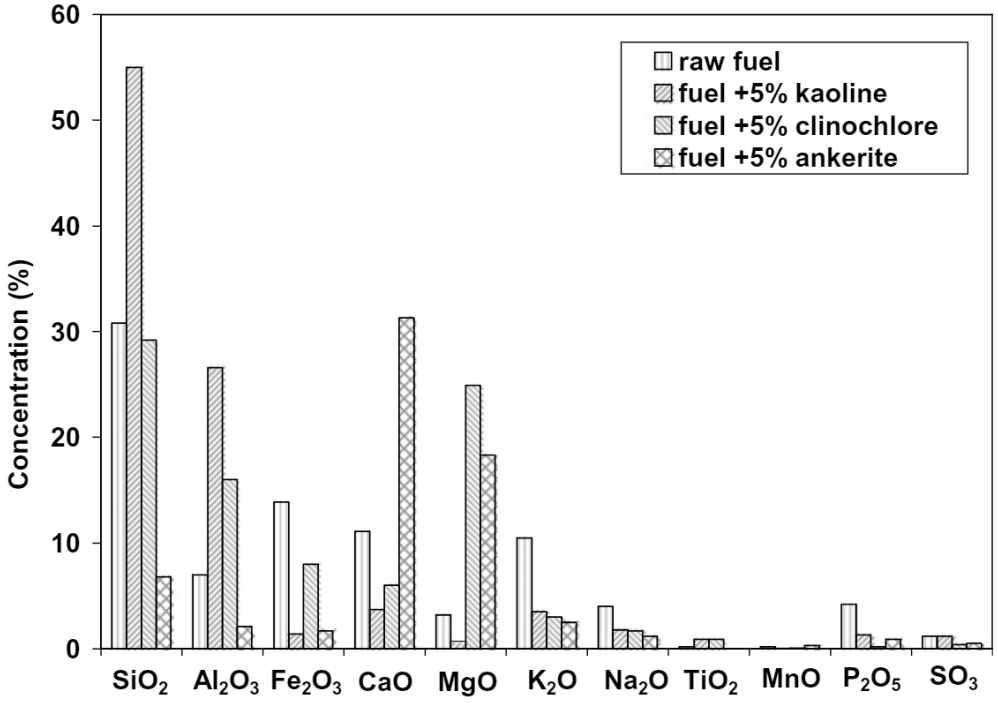

Figure 2.16. Main Components (Represented as Oxides) of Fly Ashes of Olive Kernal used with Additives (Vamvuka et al., 2008)

2.7.3 Industrial use of additives

The use of additives in industry to mitigate the slagging and fouling issues found in boilers is increasing. It is common practice in fact to use magnesia-additives in oil-fired boilers to dry up the oil ash deposits on boiler surfaces and reduce surface corrosion (Livingston, 2016). In particular, it is increasingly common to use additives in fluidised bed systems to reduce bed agglomeration problems. Vattenfall have developed a liquid fireside additive "ChlorOut" for this purpose and it has proved effective at the removal of KCl from flue gases. 1000 hour corrosion tests have been conducted in a 100 MWth bubbling fluidised bed boiler firing various wood biomass and coal which showed significant reductions in corrosion rates when ChlorOut was used (Broström et al., 2007).

There has also been some use of aluminosilicate additives in pulverised fuel boilers in the form of coal fly ash. Drax Power have patented this process (Straker et al., 2016) and are using it at their plant in Yorkshire for the combustion of wood chips. It is clear that the use of fuel additives can be of value, particularly in pulverised coal boilers with high final steam temperatures which have been converted to dedicated biomass firing (Livingston, 2016).

2.8 Ash Characterisation and Analysis

The formation and composition of ash products from combustion has a direct impact on slag formation (Vassilev et al., 2014). A comprehensive understanding of the composition of ash can give information about its formation that should allow for the mitigation of ash-related issues.

2.8.1 Current Characterisation Methods

There are a number of techniques that can be employed to learn about the chemical structure of ashes.

- Thermal Mechanical Analysis (TMA): Measure of the change in height of a sample of ash while heated at a constant rate to determine the sample sintering temperature (Tortosa Masiá et al., 2007)
- Simultaneous Thermal Analysis (STA): Combination of TGA and Differential Scanning Calorimetry (DSC) (Tortosa Masiá et al., 2007)
- Chemical fractionation: successive leaching by purified water, ammonium acetate, and hydrochloric acid (Nutalapati et al., 2007)
- Scanning Electron Microscopy (SEM) with Energy Dispersive X-ray spectroscopy (EDX)
    - Computer Controlled Scanning Electron Microscopy (CCSEM): Automation increases speed and objectivity of results. CCSEM collects high count X-ray spectra for each identified mineral particle
    - Quantitative Evaluation of Minerals by Scanning electron microscopy (QEMSCAN)
    - Mineral Liberation Analysis (MLA): Quantitative X-ray mineral analysis technique

2.8.2 SEM-EDX

Possibly the best, and one of the most widely used, ash characterisation tools is scanning electron microscopy (SEM) (Vassilev and Tascón, 2003; Vassilev and

Vassileva, 2005). There are three common modes of operation of SEM: back scattered electron imaging (BSE), secondary electron imaging (SEI), and energy dispersive x-ray spectroscopy (EDX). SEI is the most common (standard) SEM mode and provides information on the topology and morphology of the surface of a sample by the detection of low energy secondary electrons that have been released from the sample surface by the incident electron beam. BSE imaging involves the detection of high energy incident electrons that have been elastically back scattered by repulsion from the electromagnetic field of the sample nuclei. The quantity of back scattered electrons correlates with the atomic number. EDX analysis detects photons emitted by the dropping of electrons from a higher energy level to a lower energy level. The energy of the detected x-rays is unique to each element and so EDX analysis gives information on the chemical composition of a sample. The intensity of the peaks found on an EDX spectrum also gives some idea as to the elemental concentration of the sample although this cannot be used quantitatively. The use of these techniques allows the user access to information on the shape, morphology and chemical composition of a sample.

The characterisation of particles in coal fly ashes by SEM-EDX can be seen in the figure below (Figure 2.17). The samples were found to consist predominantly of amorphous aluminosilicate spheres, accounting for over 50% of the composition. Also present were iron-rich spheres which, for the majority, consisted of two phases mixed together: iron oxide and amorphous aluminosilicate (Kutchko and Kim, 2006).

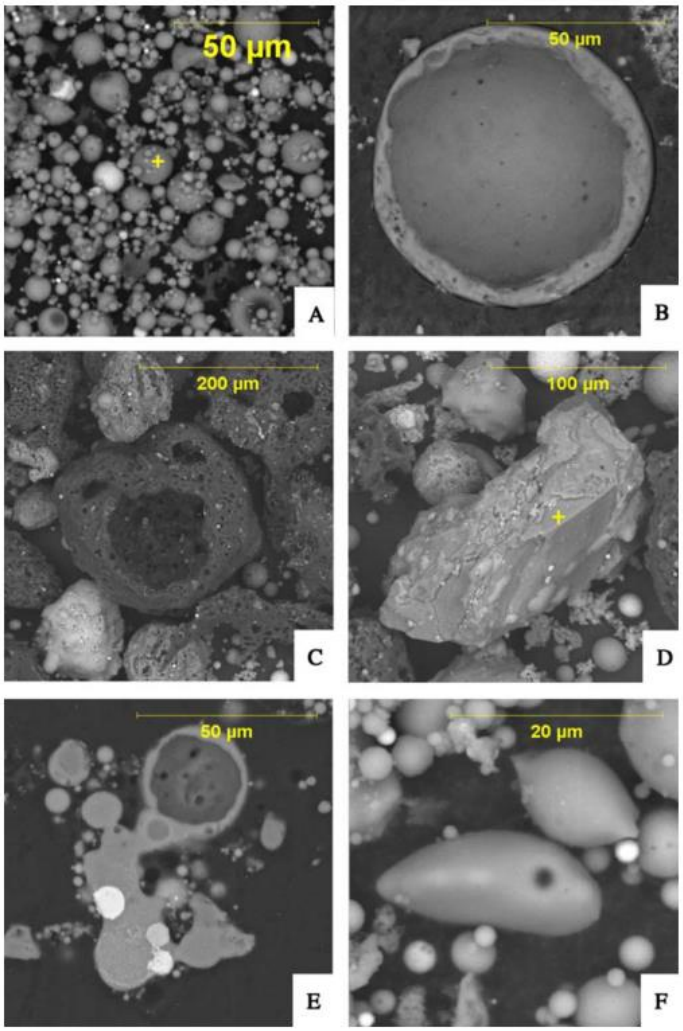

Figure 2.17. BSE Images of (A) typical fly ash spheres; (B) hollow cenosphere in cross-section; (C) unburned carbon particle; (D) mineral aggregate (quartz); (E) agglomerated particles in cross-section; (F) irregularly shaped amorphous particles (Kutchko and Kim, 2006)

2.8.3 Automated SEM-EDX

2.8.3.1 CCSEM

The manual analysis of sufficient particles for statistically significant data is very labour intensive and time consuming. The development of computer-controlled SEM (CCSEM) means that far more data can be collected more quickly and efficiently. Automation also increases objectivity and repeatability of results. CCSEM works by the programmed scanning of preselected areas of a polished sample surface. The capture of BSE signals above a pre-set value

prompts the subsequent detection of minerals and information on their size and chemical composition to be determined by a particle recognition and characterisation programme. The centre, approximate dimensions (average and maximum diameter across 8 axes), and area are also measured. For each particle an EDX spectrum is acquired and a chemical type is then assigned (Benson et al., 2012; Gupta et al., 1998).

2.8.3.2 QEMSCAN

Quantitative evaluation of minerals by scanning electron microscopy, or QEMSCAN, is another analytical technique that can be used for the characterisation of mineral matter. Also using a combination of BSE and EDX signals from SEM, QEMSCAN creates a digital image where mineral species appear as pixels. Once an individual mineral grain is identified from the BSE signals, a grid is superimposed over the particle and from each grid point, an EDX spectrum is obtained. Each mineral species can be classified by comparing EDX data with that from the species identification programme (SIP), an online look-up table (Liu et al., 2005). Using this data, an image of the mineral grain can be constructed, point by point, with different pixels corresponding to each mineral species present (Liu et al., 2007). QEMSCAN has the ability to manage a wide variety of mineral types by the use of a number of modes of analysis. These include bulk mineralogical analysis, particle mineralogical analysis, specific mineral search, and trace mineral search (Goodall et al., 2005).

2.8.3.3 MLA

Mineral liberation analysis is another analytical technique for the automated processing of SEM data. It is similar to the QEMSCAN method but uses a different approach to define the mineral grain boundaries. While there are several different modes of operation (listed below), generally with MLA, rather than using BSE merely to identify particles of interest before the using X-ray data to determine the particle shape, the BSE signals are used to define this first (Fandrich et al., 2007). Once the grain boundary is defined, EDX analysis is then applied.

2.8.4 Relevant applications of automated SEM-EDX

In spite of its clear advantages, there has been very limited reported research on biomass ashes and slags by the use of automated SEM-EDX. This is likely – at least in part – due to a lack of availability of automated SEM-EDX systems which are still relatively uncommon. Where such systems do exist, they are predominantly used for the geological analysis of mining minerals (Fandrich et al., 2007). MLA in particular is most commonly used for this purpose and – as its name suggests – serves primarily to offer information to researchers on which minerals can be liberated from coals or other ores (Fu et al., 2019; Li et al., 2018). Where MLA systems have been used for the analysis of solid fuels, focus has been on coal rather than biomass. These include the evaluation of coal component liberation upon impact breakage (Fu et al., 2019) and the use of MLA to adjust proximate and ultimate analysis data for coals with a high kaolinite content (Gräbner and Lester, 2016).

2.9 Conclusions

The release of gaseous potassium during the combustion of biomass is a significant problem in large-scale boilers. There are several strategies of mitigating the slagging and fouling effects of this, including boiler design, fuel selection, and pre-treatment methods such as fuel leaching. However, biomass combustion is frequently attempted in coal boilers which have undergone conversion, limiting the possibility for extensive redesigns. Also, the availability of specific biomass sources is variable, this is magnified by the need to minimise the associate carbon costs with its transport and storage. While fuel pre-treatments have been proven to be highly effective in improving the combustion properties of biomasses in terms of the ash characteristics, these methods often have a high economic cost. The use of additives during combustion appears to offer substantial promise of improved ash behaviour. When such additives can be sourced from waste products such as spent bleaching earth or coal fly ash, their use becomes very attractive, economically. Various studies have been conducted with sorbents but the knowledge of mechanisms, required injection rates and optimal temperatures is far from complete, particularly in PF systems.

The use of pure minerals for the purpose of defining optimal additive ratios and reaction temperatures, in a PF combustion system would appear to contribute to the knowledge of potassium migration during combustion in the presence of the active ingredients of popular additives. Mineral liberation analysis software used in conjunction with SEM-EDX is a powerful tool. By the rapid

characterisation of different phases within single particles across a sample of $>10^4$ particles, the location of potassium species in ashes could rapidly be defined across different additive experiments.

3 Materials and Methodology

3.1 Materials

3.1.1 Biomass Samples

Three different biomass fuels were used in this research: olive cake, miscanthus and wood pellets. Spanish olive cake (Olea europaea) was used for the majority of the experiments conducted. Olive cake is a solid biomass and is a waste product from the olive oil industry. The olive cake used in this research was provided by EDF Energy plc. The olive cake was stored indoors at room temperature and was milled and sieved prior to combustion. One size fraction (150-300 µm) of olive cake was used for all of the testing in this study and was chosen for being the largest size possible to be used in the drop tube furnace. Miscanthus is a type of grass that is grown as an energy crop. The miscanthus used in this research was provided by E.ON UK plc. and was in pellet form. The miscanthus pellets were stored indoors at room temperature prior to milling and sieving. The same size fraction of 150-300 µm was used for all miscanthus samples. The wood used in this research was purchased from Brites and is commercially available in the UK. The wood was in pellet form and was also stored indoors at room temperature prior to milling and sieving. The low ash content of the wood meant that very large amounts of the raw fuel had to be used to produce the necessary quantity of 550°C ash. As a result, fewer experiments were conducted with wood. However, its use does offer a useful comparison to the results obtained for the high ash olive cake. It is also widely used in industry.

3.1.2 Additives

Two different aluminosilicate-based additives were used in this research, kaolin clay and coal fly ash. The use of kaolin should give "ideal scenario" results as it consists of a single mineral which is composed almost exclusively of aluminosilicate. The majority of experiments conducted in this research focused on the use of kaolin for this reason. A comparison with coal fly ash was made, however. This is due to the convenience of fly ash as an additive for industry.

The kaolin clay used in this research was purchased from Sigma-Aldrich (K7375). The primary component of kaolin is the mineral kaolinite, $Al_2Si_2O_5(OH)_4$. The kaolin was used in all experiments in the condition which it was received. There is some entrained moisture which is lost when the kaolin is heated to 815°C. The mass yield for kaolin after heating to 815°C was 87.1%.

The elemental analysis of kaolin (determined by XRF) is shown in Table 3.1.

Table 3.1. Elemental analysis of kaolin and coal fly ash

	Kaolin	Coal fly ash
Al_2O_3	30.4	22.8
CaO	0.2	2.55
Fe_2O_3	0.9	10.3
K_2O	0.2	2.7
NiO	0.0	<0.1
P_2O_5	0.2	0.2
SiO_2	35.2	48.8
TiO_2	1.5	1.0

Units: wt%

The coal fly ash used in this study was sourced from Uniper Technologies and was collected from a UK power station. The coal fly ash was wet when received

and prior to use was dried in a drying oven at 105°C for 24 hours. Further mass loss was measured when the coal fly ash was heated to 815°C in the muffle furnace. The mass yield after heating to 815°C was 92.9%.

The elemental analysis of the coal fly ash used (as provided by Uniper) is shown in Table 3.1.

3.2 Sample Preparation

3.2.1 Milling

All biomass samples used were milled with a Retsch PM100 planetary ball mill as seen in Figure 3.1. This reduces the particle size of samples by crushing.

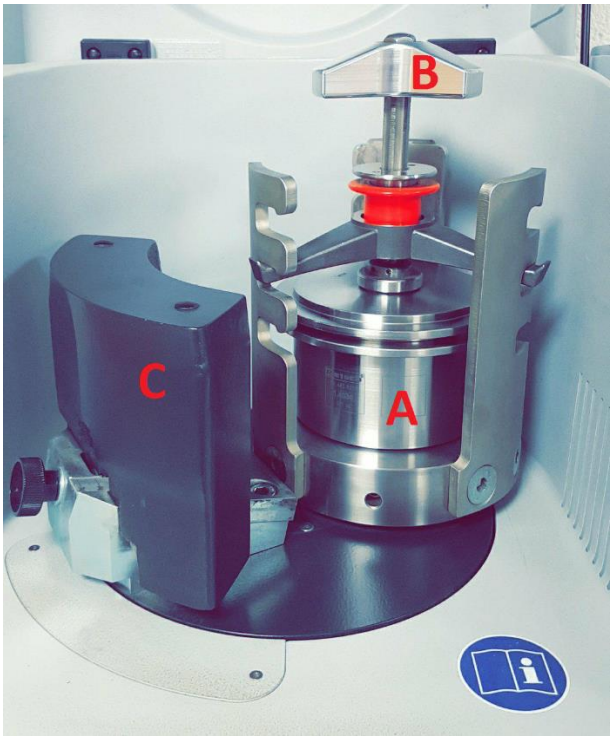

Figure 3.1. Rotary ball mill. A: mill chamber, B: screw clamp, C: counterweight

Approximately 200 ml of sample is placed into the chamber Figure 3.1,A with 8 grinding balls (Figure 3.2).The lid is then replaced and locked into position using a screw clamp with safety latch (Figure 3.1,B). The steel vessel is then spun at a

pre-determined speed both on a central axis and on an offset axis – balanced by a counterweight (Figure 3.1,C).

Figure 3.2. Grinding balls

The speed used was typically around 300 rpm and the vessel was spun for 2-3 minutes. If spun at greater speeds and/or for a longer duration then the vessel and sample within begin to heat up. Care was taken to mitigate this whenever possible by not running the mill for more than a few minutes at a time and by allowing the vessel to cool between runs to prevent any thermal degradation of the material.

3.2.2 Sieving

After milling, the biomass samples were sieved to obtain samples of specific size fractions. Sieves of different sizes were used and arranged in descending size fractions from top to bottom. The sample size fractions taken were 75-150 µm and 150-300 µm. In addition to the sieves required to obtain the size fractions desired, extra sieves were used above and below the range to allow better transport of materials through the sieve set.To allow thorough mixing,

the assembled sieve set and pan are placed on a shaker (Figure 3.3) and left for up to 30 minutes at a particle amplitude of 3 mm.

Figure 3.3. Sieve set and shaker

3.3 Thermogravimetric Analysis and Ultimate Analysis

Thermogravimetric analysis (TGA) was used in this research for the purpose of determining moisture, volatile matter and fixed carbon contents for sample proximate analysis. The thermogravimetric analyser that was used was a TA Instruments Q500. The procedure for TGA that was used is described below and was completed in triplicate for each sample:

- Establish a nitrogen atmosphere
- Increase temperature to 105˚C at 50˚C/minute

- Isothermal for 10 minutes to remove the moisture content
- Increase temperature to 700˚C at 50˚C/minute
- Isothermal for 10 minutes to remove volatile matter
- Introduce air
- Isothermal for 10 minutes to burn the fixed carbon and leave the ash behind
- Cool to room temperature

This procedure was used as it is the standard TGA procedure used within the research group. However, for the determination of ash content, the British Standard procedure for the determination of ash content of solid biofuels (BS EN ISO 18122:2015) was used. This involved the use of the muffle furnace and is described in the section below. The reasons for this were that for ash determination, 550°C must be used to prevent loss of alkali/alkaline earth metals and due to the low ash content of the samples, it was necessary to use a larger sample size for accuracy.

Ultimate analysis was conducted using a LECO CHN 628 elemental analyser. The solid samples were approximately 50 mg. Prior to analysis, the analyser was calibrated. This was done by first conducting a blank test to establish zero values. Five samples of 2,5-(Bis(5-tert-butyl-2-benzo-oxazol-2-yl) thiophene (BBOT) were then analysed, designated as “drift standards”. Once this was complete, the analyser was programmed to drift calibrate. The experimental samples were then analysed in triplicate.

Proximate and ultimate analyses for the biomass samples are shown in Table 3.2. Proximate analysis data was determined by a combination of thermogravimetric analysis and muffle furnace

Table 3.2. TGA proximate and ultimate analyses of olive cake, miscanthus and wood

	Olive cake	Miscanthus	Wood
Moisture	8.0	6.0	7.5
Volatiles	62.6	69.5	74.5
Ash	7.5	3.5	0.4
Fixed carbon	21.9	21.0	17.6
C	44.1	48.0	48.0
H	6.3	6.5	6.6
N	1.5	0.5	0.2
O	48.1	45.0	45.2

Moisture, volatiles, ash and fixed carbon determined an as received basis
C, H, N, O determined on a dry ash free basis
Units: wt. %

3.4 Muffle Furnace

3.4.1 Overview of Muffle Furnace

The muffle furnace provides a way of releasing volatiles and char from samples at a range of temperatures under slow heating rates.

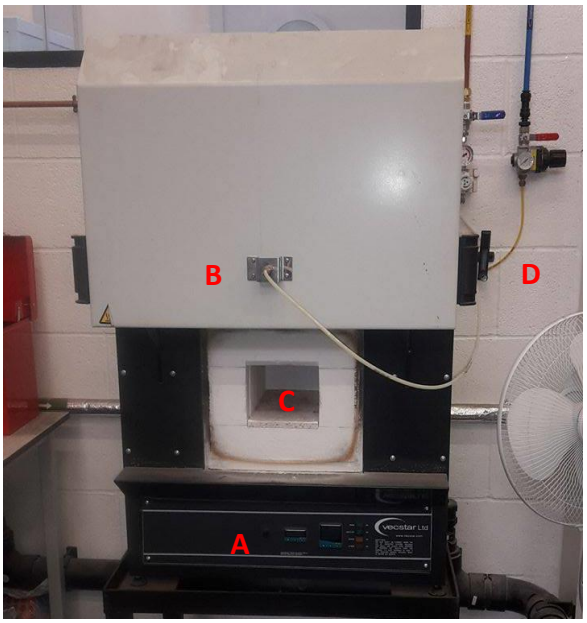

Figure 3.4. Figure showing the ashing oven used in slow-heating rate ashing experiments. (A) Control panel, (B) Gas feed-in, (C) Oven chamber, (D) Compressed air flow meter

The furnace can be programmed to ramp at specific ramp rates to specified temperatures and to soak for predetermined periods. The air composition in the chamber can be maintained by the input of either nitrogen or compressed air at variable flow rates. The muffle furnace used for the slow heating rate experiments can be seen in Figure 3.4 above.

3.4.2 Ashing Procedure

3.4.2.1 Determination of Moisture Content

Prior to ashing, the moisture content of samples may be determined. The procedure for this is described below and was adapted from the British Standard procedure for the determination of moisture in solid biofuels (BS EN ISO 18134-3:2015).

A clean porcelain crucible was heated to 105°C, maintained at this temperature for 15 min and then allowed to cool to room temperature in a desiccator. The dish was then weighed and approximately 1 g of sample was added. The sample and crucible were then heated to 105°C and maintained at this temperature for approximately 3 h. On removal from the oven the crucible was placed in a desiccator and allowed to cool to room temperature prior to weighing.

3.4.2.2 550°C Ashing Standard Procedure

Described below is the standard procedure for ashing experiments conducted at 550°C. This procedure was adapted from the British Standard procedure for the determination of ash content of solid biofuels (BS EN ISO 18122:2015).

Figure 3.5. Crucibles Used for Ash Content Determination and Small-Scale Ash Production

A clean porcelain crucible (Figure 3.5) was heated to 550°C for at least 60 minutes and then transferred to a desiccator and allowed to cool to room temperature. The crucible was then weighed and approximately 1 g of sample

added in an even layer over the bottom surface of the crucible. The crucible and sample were weighed and the mass recorded. The sample was then placed into the cold furnace and heated to 250°C over a period of 30 min to 50 min where it was held for approximately 1 h to allow the release of volatile material prior to char oxidation. The furnace was then heated to 550°C over a period of 30 min and then maintained at this temperature for at least 2 h in an air atmosphere. The British Standard method dictates that ashing should be continued until there is no further reduction in mass of the sample. For these first, small-scale (~1 g) "determination of ash content" muffle furnace runs, the samples were kept at 550°C for the minimum duration prescribed by the standard method (2 hours). It was found that not all samples ashed to completion. This was identified both by the visual presence of black/grey char particles and by higher mass yields. The standard method states that ashing is complete once no more reduction in mass is measured. However, to weigh the samples they had to be cool. It was impractical to weigh every sample numerous times and would result in the samples being exposed to multiple heating cycles. To overcome this issue, the samples were ashed for twice the minimum duration suggested in the standard method. These samples were found to have no visible char particles and consistent mass yields. To ensure no further ashing was possible, small samples were retained in the muffle furnace for excessive durations (>15 hours) to identify the maximum mass losses. For these samples there was no decrease in the mass yield.

3.4.2.3 815°C Ashing Standard Procedure

Described below is the standard procedure for ashing experiments conducted at 815°C. This procedure was adapted from the British Standard procedure for the determination of ash content of solid mineral fuels (BS 1016-104.4:1998).

A clean porcelain crucible (Figure 3.5) was heated to 815°C, maintained at this temperature for 15 min and then cooled to room temperature. It was then weighed to the nearest 0.1 mg and approximately 1 g of sample was spread evenly in the dish. The dish was reweighed with the sample and then inserted into the furnace at room temperature. The furnace temperature was then evenly raised to 500°C over a period of 60 min and held at this temperature for 45 min. The temperature was then raised further to 815°C and maintained at this temperature for at least 60 min in air. Once incineration was complete the sample was removed from the furnace and allowed to cool to room temperature in air before weighing.

3.4.2.4 Larger Scale Ash Production

The procedures above were modified for some experiments where greater sample masses were used to produce more ash for analysis. While following the same principle as the standard ashing experiments, the procedure for larger scale ash production involved the use of larger crucibles (seen below in Figure 3.6). These crucibles may be used with sample sizes of up to 25 g.

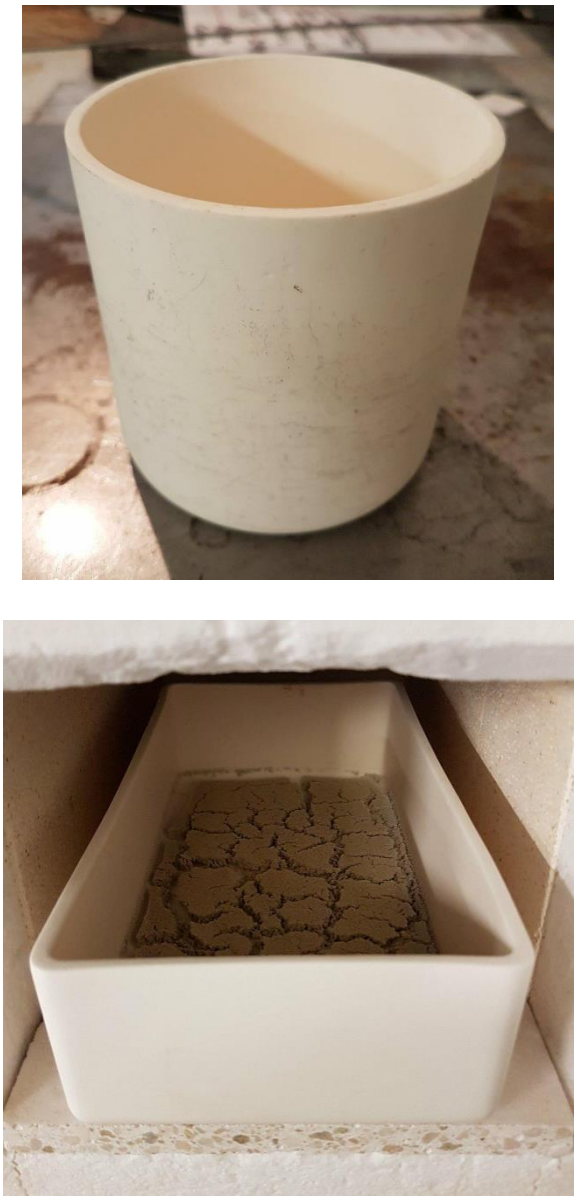

Figure 3.6. Larger Crucibles used for Larger Scale Ash Production

Once the correct values for ash content had been determined on the 1g scale, those values were used to ensure the larger scale ash production ran to completion. Any large-scale samples that gave mass yields above what was expected were returned to the muffle furnace for further ashing.

3.5 Drop Tube Furnace Experiments

3.5.1 Overview of Drop Tube Furnace

The drop tube furnace used in this research was commissioned by Severn Thermal Furnaces for E.ON Energy Ltd. in 1989 before being relocated to the University of Nottingham and extensively overhauled in 2007 (Le Manquais, 2011). The drop tube furnace allows the combustion of samples at high heating rates which approximately replicate those found in large scale boilers for power generation. This is achieved by feeding the sample through a cooled feed-in probe by gravity. From here, the particles fall through the furnace in a controlled atmosphere at a temperature up to 1450°C. A cooled collector probe is placed below the feed-in probe at a distance chosen by the operator. The distance between the feed-in probe and the collector probe and the gas flow define the residence time of the particles in the main section of the furnace. While they are in this area the particles are exposed to the full temperature of the furnace on all sides and should be fed in a laminar flow as facilitated by a carrier gas. The drop tube furnace can be seen below in Figure 3.7.

Figure 3.7. Top and Bottom of Drop Tube Furnace showing: (A) Screw Feeder, (B) Feed-in Probe, (C) Collector Probe, (D) Collector Pot, (E) Exhaust Filter, (F) Vacuum Pump

The drop tube furnace is, in essence, a vertical tube furnace with controllable residence time and controllable gas flow and composition in which samples can be heated to produce char and ash. It consists of a central, aluminosilicate work tube with an internal diameter of 50 mm (Figure 3.8). It is heated by a proximal main heater, comprising four vertical silicon carbide elements. The maximum temperature which the main heater can reach is 1600°C. A feed in probe is fitted into to the top of the work tube. It is through this which the solid sample and combustion gases can be fed. The feed in probe comprises a water-cooled, steel probe with an internal diameter of 3 mm. The fuel is fed through this probe which ensures the sample does not significantly increase in temperature until it reaches the combustion chamber. The gases are fed into the work tube around the outside of this feeder probe. A preheater element is situated around the insulated feeder probe to pre-heat the incoming gases to temperature near that found in the main furnace zone. To reduce the

turbulence of flow, a flow straightener is positioned just above the end of the feeder probe at the point where the gases first meet the fuel sample. Through the base of the work tube is the collector probe. Much like the feeder probe, this consists of a water-cooled steel probe, through which the sample particles fall after passing through the combustion zone. To compensate for heat loss resulting from the presence of the cooled probe, two trim heaters are situated near the base of the work tube. The height of the collector probe within the furnace can be changed depending on the desired residence time of the particles in the combustion zone. To encourage the passage of sample particles through the collector probe, a vacuum pump pulls the gas through the probe and through the cyclone under the probe, complete with dust collector pot. It is here that char/ash particles are collected in a cyclone.

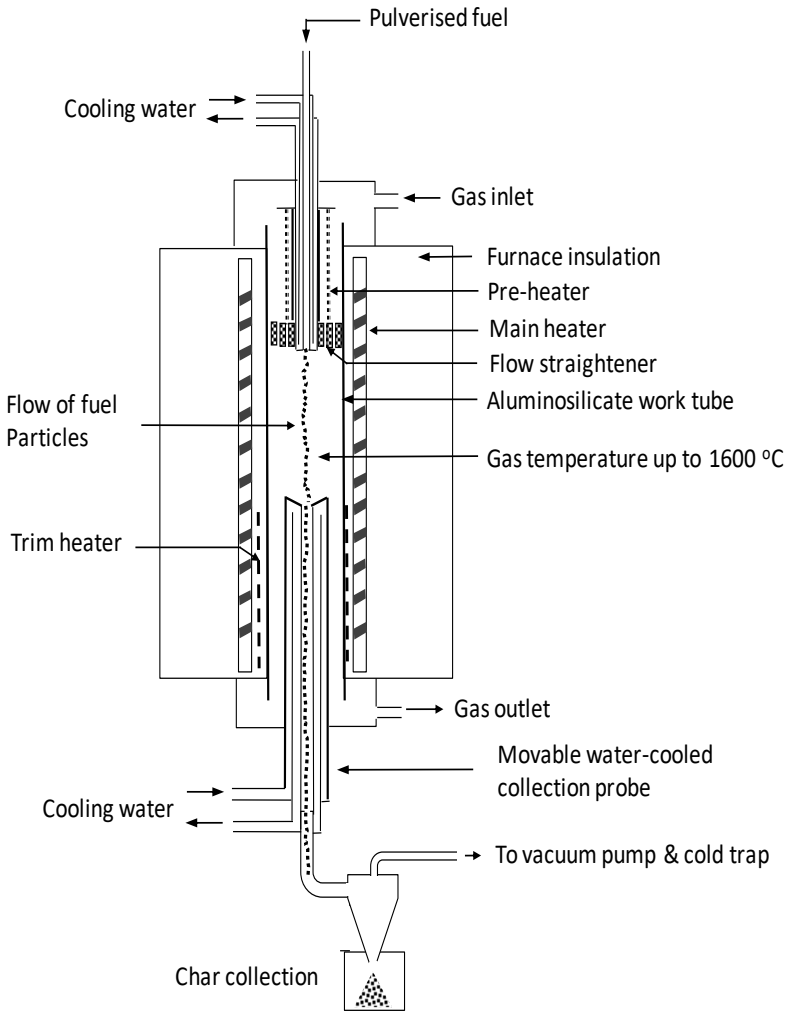

Figure 3.8. Diagram of the drop tube furnace (Farrow, 2013)

It is necessary for the flow of sample and carrier gases to be laminar to ensure the particles fall down the centre of the work tube and therefore directly into the collector probe. This is achieved by maintaining a low enough flow rate to yield a sufficiently low Reynolds Number. The temperature within the furnace is controlled by changing the temperature of the main heater – the pre and trim heaters are programmed to follow this. The gas composition is defined by adjusting flows from cylinders of N_2 and O_2. The flow rates of individual gases and of the cooling water are regulated by flow meters.

3.5.2 Programmable heater controls

The different three heaters within the furnace: the pre-heater, the main heater and the trim heaters, can be programmed individually by separate 2404 Eurotherm digital controllers. These controllers respond to eight type B thermocouples positioned at various locations along the length of the work tube within the furnace and allow the programming of multiple sequential stages to different temperatures and at different ramp rates.

3.5.3 Internal temperature profile

While the programmable heater controllers afford the DTF user with accurate control over the heater elements within the furnace body, the temperatures of the elements do not precisely correspond with the temperature experienced by a particle which travels through the middle of the furnace. To ensure that the desired combustion temperatures can be accurately reached, the temperature profile through the centre of the furnace was measured. This was done using an independent type B thermocouple which was lowered through the DTF one centimetre at a time. It was determined that depending on the residence time (defined by the probe separation and gas flow), the furnace controllers should be programmed to a temperature between 25°C and 100°C higher than the required temperature in order to produce an acceptable profile in the centre of the gas stream (Le Manquais, 2011). Figure 3.9 shows the

temperature profile when the controller temperature is set at 1325°C and with a residence time of 600 ms (probe separation 65 cm).

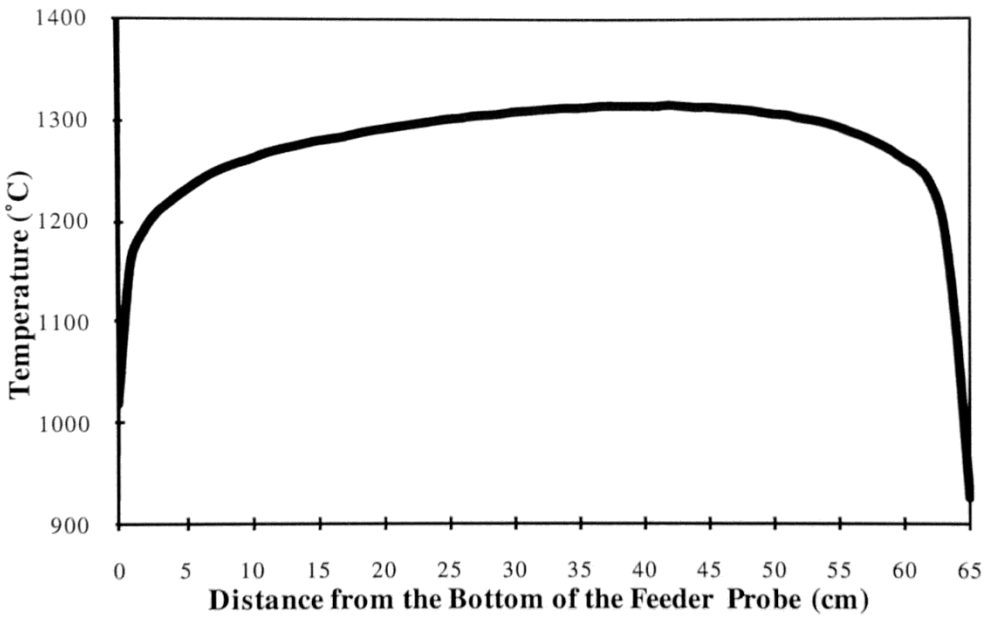

Figure 3.9. An example DTF temperature profile, generated at the main controller set point of 1325°C and a residence time of 600 ms (Le Manquais, 2011).

3.5.4 Gas supply

The drop tube furnace can be supplied with a selection of gases in a mixture as chosen by the user. These include compressed air, N_2, O_2 and CO_2. The gas supply is controlled by a flow meter for each gas, from which the gas is fed directly into the top of the furnace. For all of the experiments conducted in this study a gas composition of 90% N_2 and 10% O_2 (molar) was used. This was chosen so as to provide sufficient oxygen to yield complete char burnout. To ensure an accurate gas composition was maintained, a digital oxygen analyser was used to monitor the gas mix entering the furnace. To assist sample feeding, a carrier gas was used. This was simply a low-flowrate supply of N_2 which was

fed into the top of the feeder probe during manual feeding to assist the passage of the sample.

3.5.5 Sample feeding

While automatic sample feeders are available for the drop tube furnace, it has been found that these tend to clog when used with fibrous biomass samples. Additionally, where kaolin was used it was found that the tendency of the clay to stick to itself resulted in clumps of material forming and causing blockages. It was therefore decided that the samples should be fed by hand via a funnel into the top of the furnace.

3.5.6 Ash collection

The solid ash particles that are created in the combustion zone of the furnace come out via the collector probe assembly. This consists of a water-cooled collection probe which is insulated from the furnace by cylindrical ceramic fire bricks. The insulation is to protect the probe and reduce the cooling effect of the probe on the furnace temperature – the trim heaters also work towards this aim. The collector probe requires regular cleaning to remove deposits of tar and other particles. At its base, the collector probe is connected to a cyclone which has a dust collector. This feeds a collection pot where ash samples are deposited. A clean collector pot was used for each run. From the top of the cyclone a vacuum pump draws the remaining gas through glass fibre situated in a clear plastic tube to filter tar and entrained ash particles. This glass fibre was replaced when deemed necessary due to being visibly blackened by tar. There is also a filter on the vacuum pump.

3.5.7 Residence time calculation

The residence time is defined as the duration in which sample particles travel through the work tube. That is to say the time from leaving the feeder probe, to entering the collector probe. This can be changed by changing the distance the particles have to travel. To calculate the residence time, it must be assumed that the flow of particles within the work tube is laminar and that the gas velocity at any given point must therefore be a function of its radial position. With that assumption in place it is possible to apply the equation below.

$$\frac{V_r}{V} = 2\left(1 - \frac{r^2}{R^2}\right) \qquad (3.1)$$

Where V is the average fluid velocity through the tube across its entire radius (R), and V_r is the specific velocity at any given radius (r) from the centre. From this equation we can deduce that in the centre of the tube (V_0), where (r = 0), the velocity will be twice that of the overall average across the tube. As it is assumed that the particle stream will be in the centre of the flow, it will be this velocity which will be used to calculate residence time.

$$V = \frac{1}{2}V_0 \qquad (3.2)$$

It is now possible to derive the speed of the particle from the residence time (t) and the distance the particle travels in the furnace, L. This distance is defined by the separation of feeder and collector probes.

$$V = \frac{L}{2t} \qquad (3.3)$$

The velocity can also be expressed in terms of the volumetric flow rate of the gas (Q) through the furnace as shown below:

$$V = \frac{Q}{A} = \frac{Q}{\pi R^2} \quad (3.4)$$

Where A is the cross-sectional area of the tube. These equations can then be combined to yield the following equation with respect to the residence time, t.

$$t = \frac{L\pi R^2}{2Q} \quad (3.5)$$

To solve this for t, Q must be calculated as there is no means of measuring the volumetric flow rate within the DTF. This can be achieved by using the ideal gas equation:

$$\frac{Q_1}{Q_2} = \frac{T_1}{T_2} \quad (3.6)$$

Where 1 refers to the gas flow rate and temperature of gas flowing into the furnace at standard temperature and pressure, and 2 refers to the flow rate and temperature within the furnace. An example calculation is shown below:

$$Q_2 = 2.02 \times 10^{-4} \times \frac{1573}{298} = 1.06 \times 10^{-3}\ m^3 s^{-1} \quad (3.7)$$

In the example above, the following parameters are used. Incoming gas flow rate: 12.1 L min^{-1} (2.02x10^{-4} m^3 s^{-1}). Incoming gas temperature: 25°C (298K). Internal furnace temperature: 1300°C (1573K). Once Q_2 is known, t can be calculated using equation. In this case the probe separation is set at 65 cm (0.65 m)

$$t = 0.65 \times \frac{\pi(25\times10^{-3})^2}{2\times1.06\times10^{-3}} = 0.600\ s \quad (3.8)$$

As seen above, the residence time for this example is 600 ms.

3.5.8 Drop Tube Furnace Procedure

For the experiments conducted on the drop tube furnace the following procedure was applied. Care was taken to ensure the feed-in probe, collector probe, collector pots, and glass fibre exhaust filter were all clean. The furnace was turned on and programmed to ramp to 300°C at a rate of 1° min^{-1} then ramp further to 600°C at 3°min^{-1}, and then finally to the target temperature at a rate of 5°min^{-1}. To accurately reach the correct internal gas temperature, the furnace thermostat had to be set at a higher temperature (approximately 25°C more). The desired residence time was achieved by selecting the correct height in the furnace of the collector probe – adjusting the height of the probe defines the duration each particle is exposed to the furnace. Once the furnace was at temperature, the input gas balance was set.

The vacuum pump was also turned on and adjusted to the correct exhaust flow rate. The clean collector pot was then weighed and screwed onto the bottom of the collector probe. The sample was accurately weighed and its weight recorded. The sample was fed into the furnace slowly to ensure adequate exposure to heat of all particles and to prevent blocking of the feed-in probe and at the top of the collector probe. After all of each sample had been put into the furnace, the collector pot was retrieved and weighed to find the mass of the sample collected.

3.6 X-Ray Fluorescence Spectroscopy (XRF)

X-ray fluorescence spectroscopy (XRF) is an analytical tool that provides the relative quantities of elements in a sample within a range from sodium to

uranium on the periodic table. The use of XRF in this research should allow the alkali and alkaline earth metal retention of additives during biomass combustion to be measured quantitatively. XRF analysis has been conducted both at the University of Birmingham and at the University of Nottingham. All samples were run as a loose powder. The samples were analysed in plastic sample holders fitted with mylar film.

The instrument used at the University of Birmingham was a wavelength dispersive XRF spectrometer, a Bruker S8 Tiger. The instrument used at the University of Nottingham was an energy dispersive XRF, a PANalytical Epsilon 3 XL. For all experimental samples, results were obtained on an oxide basis.

The full compositions of the low temperature (550°C) ash of the three biomasses used in this study are shown below in Table 3.3. It should be noted that only elements more massive than Na are reliably detected by the XRF.

Table 3.3. Compositions of biomass ashes prepared at 550°C

	Olive cake	Miscanthus	Wood
Al_2O_3	1.6	1.0	0.0
CaO	10.9	5.3	36.8
Cl	2.4	2.4	0.0
Cu	0.0	0.0	0.0
Fe_2O_3	1.4	0.8	1.2
K_2O	28.9	10.5	17.0
MgO	5.3	2.3	5.1
Mn	0.0	0.0	2.4
Na_2O	0.1	30.7	0.0
P_2O_5	3.5	1.7	3.9
SiO_2	7.5	18.6	0.0
SO_3	1.5	2.2	1.9
Ti	0.1	0.0	0.0
Zn	0.0	0.0	0.2

Results obtained and presented as measured from XRF spectrometer at UoN
Units: wt. %

3.6.1 XRF Calibration

Due to using two XRF spectrometers at different institutions, it was imperative to ensure that both instruments provided reliable data. To verify the accuracy of both instruments, a standard reference material of certified composition was used.

In the first instance, the standard reference material that was used was NIST SRM 2690 coal fly ash and was purchased from Sigma-Aldrich. The material was tested both at the University of Birmingham (UoB) and at the University of Nottingham (UoN). The results for both are shown below in Table 3.4 with the certified values for each element.

Table 3.4. Comparison between values as measured by XRF at UoB and UoN against certified values for a sample of standard fly ash

	UoB	UoN	Certified Values
Al	9.5%	12.6%	12.4%
Ca	7.9%	5.6%	5.7%
Fe	5.6%	3.9%	3.6%
K	1.3%	0.9%	1.0%
Mg	1.2%	1.4%	1.5%
Na	0.2%	0.3%	0.2%
P	0.7%	0.4%	0.5%
S	0.3%	0.2%	0.2%
Si	21.5%	24.7%	25.9%
Ti	0.7%	0.6%	0.5%

It can clearly be seen that there are differences between all three sets of values. It was therefore necessary to account for these differences when interpreting experimental results conducted at each institution. Initially it was hoped that the percentage differences from the certified result for each element could be extrapolated and applied. However, when this was attempted for an olive cake

sample (with a potassium oxide content of around 30%) which was run on both instruments it was found that the correction was unsatisfactory. The reason for this is most likely that the level of potassium in the reference material is quite low. It was therefore decided that a correction factor would be determined based on the potassium oxide level in the sample run on both instruments while using the results for the standard reference material to scale the correction. To calculate this, first the bias from the certified value was determined as a decimal. The certified value for the potassium level in the reference material is 1.04%. The value as recorded at UoN is 0.89%. The value as recorded at UoB is 1.32%. The difference from the certified value is -0.15 percentage points for UoN and +0.28 percentage points at UoB. The bias from the reference for each is therefore:

$$15/(15 + 28) = 0.35$$

$$28/(15 + 28) = 0.65$$

Next, the potassium content in a sample of 550°C olive cake was determined by both instruments. The value as recorded at UoN was 29.58% and the value as recorded at UoB was 35.75%. The difference between the two values is 6.17. This was multiplied by 0.35 to give 2.16, and 0.65 to give 4.01. 2.16 was then added to the value determined at UoN and 4.01 was subtracted from the value measured at UoB. This gave a value of 31.74% for the level of potassium oxide in the sample. A correction factor for each instrument can then be calculated by dividing the actual level of potassium by the recorded level. This gave a correction factor of 1.073 for the XRF at UoN and 0.888 for the XRF at UoB. This

whole process was repeated for another sample of olive cake ash prepared at 550°C and two more correction factors were determined. The mean of the correction factors were 1.072 for the XRF at UoN and 0.888 for the XRF at UoB.

3.6.2 XRF Calibration Series

To further verify the validity of the correction factors as described above, a calibration series was devised. Here, a series of mixtures with known K_2O content were used. The source of K_2O was KNO_3 (99.999%, trace metals basis) and was obtained from Sigma Aldrich. KNO_3 has a relative K_2O content of 46.6%. This KNO_3 was analysed with the XRF at UoN and the raw results can be seen in Table 3.5 below.

Table 3.5. Measured and corrected values of K_2O in five repeat samples of KNO_3

Sample	Measured value for K_2O	Corrected value for K_2O
1	44.1%	**47.3%**
2	47.9%	**51.4%**
3	43.7%	**46.9%**
4	44.1%	**47.3%**
5	44.1%	**47.3%**
		Correction factor: 107.25%

The mean value for K_2O as measured by the instrument at UoN was 46.6%. When the UoN correction factor (as derived above) was applied, it gave a value of 48.0% K_2O in the sample of KNO_3. This test was repeated for mixtures of KNO_3 and aluminium oxide to give a range of K_2O contents. This series covers the full range of values measured within this research: 40%, 35%, 30%, 25%, 20%, 15%, 10%. In Table 3.6 below, the measured and corrected values for K_2O are shown for the sample of KNO_3 and for each mixture.

Table 3.6. Measured and corrected values of K_2O in samples of KNO_3 and Al_2O_3

K_2O in sample	Measured value for K_2O	Corrected value for K_2O
**46.6%	**44.8%	**48.0%
40.0%	38.1%	40.8%
*35.0%	*32.6%	*34.9%
30.0%	28.0%	30.1%
25.0%	22.7%	24.3%
20.0%	18.1%	19.4%
15.0%	13.6%	14.6%
10.0%	9.5%	10.1%

Correction factor: 107.25%
** Mean of 5 runs, standard deviation = 1.67
* Mean of 3 runs, standard deviation = 0.71

These results are also shown graphically in Figure 3.10 below:

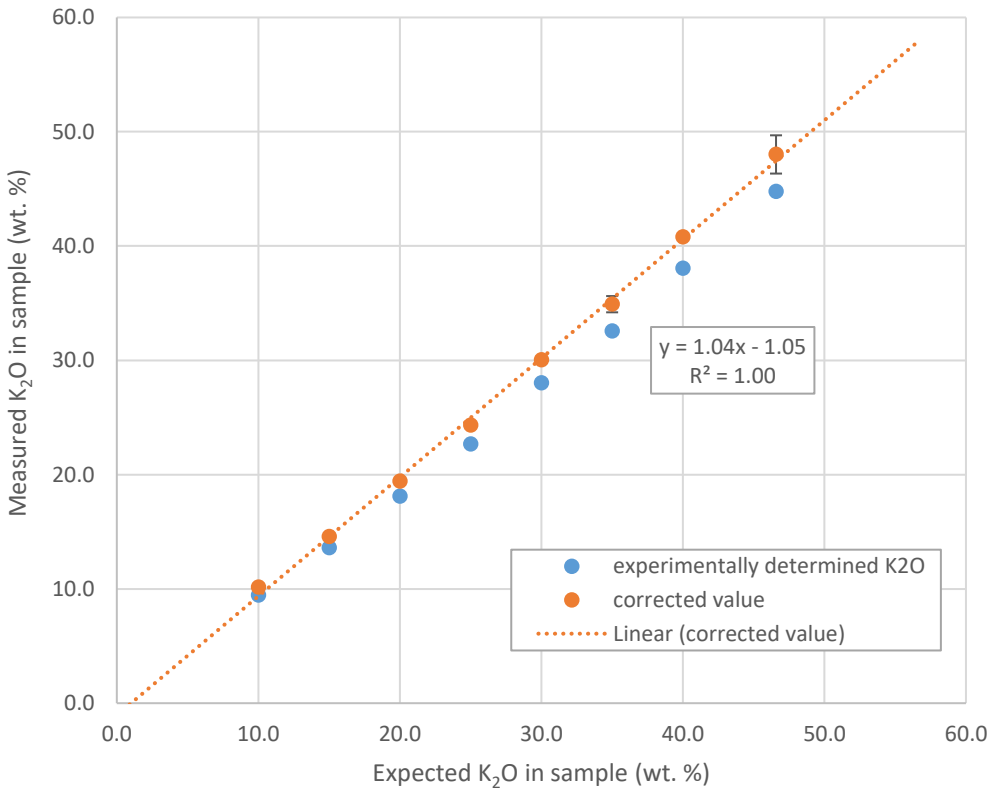

Figure 3.10. K_2O calibration series

The data in the graph above shows clearly that the corrected values for K_2O for each mixture fit very closely to those expected. This is evidenced by the r^2 value of 1.00 and the gradient of the trend line which is 1.04. Furthermore, the 35% K_2O sample was repeated in triplicate: the mean, corrected value was 34.9%

and the standard deviation 0.71. This therefore proves that the correction factor for the UoN instrument can be reliably applied across the full range of values in this research. By applying this correction factor, the inherent systematic bias associated with this instrument can be accounted for to give quantitative results – within the range of 10-40% K_2O.

In the case of the results from the instrument at the University of Birmingham, a systematic bias resulting in the values being too high was observed. An empirically derived correction factor (as determined using samples run on both instruments and described in the section above) was used to align the results obtained from UoB with those measured at UoN.

It was not possible to run a calibration series to independently prove this correction factor as it was for the UoN instrument due to the instrument being unavailable. However, it is possible to use the corrected UoN data to determine the accuracy of the UoB correction factor. If this is proven at points across a range, then it can be assumed that the UoB correction factor is sound. To do this, two sets of triplicate samples which were previously run at UoB, were repeated at UoN. The results for this are shown in Table 3.7. Also shown in the table are the K_2O values for the coal fly ash standard reference material (SRM) and the two samples of 550°C olive cake ash which were used to determine the correction factors for the two instruments.

Table 3.7. Percentage K_2O content in samples analysed both at UoB and UoN

	SRM	**50% kaolin 1300°C**			**30% kaolin 1150°C**			**550°C Olive**	
	Mean	1	2	3	1	2	3	1	2
UoB uncorrected	1.6	17.6	18.2	19.5	26.6	26.7	26.9	35.8	36.1
UoB corrected	**1.4**	**15.6**	**16.2**	**17.3**	**23.6**	**23.7**	**23.9**	**31.8**	**32.0**

UoN uncorrected	1.1	15.5	16.5	16.4	21.5	22.1	22.3	29.6	29.9
UoN corrected	**1.1**	**16.8**	**17.7**	**17.8**	**23.1**	**23.8**	**23.9**	**31.7**	**32.1**

In Figure 3.11, the XRF values from Table 3.7 above, as measured on both instruments and as corrected by the two correction factors, are plotted with respect to the calibrated UoN data. This means it is possible to determine the deviations of the uncorrected results from both instruments and the "corrected" (but uncalibrated) UoB values. The respective biases of the two instruments are immediately clear. What is also immediately clear is that for almost all values, the correction factor applied to the values from the UoB instrument align the results very closely with the corrected values from the UoN instrument. A linear trendline has been used to demonstrate this: the UoB corrected values fit this linear trendline with an r^2 value of 0.99 and the gradient is 1.01. At the extreme low end, it can be seen that the line deviates to give an intercept for the trendline of -0.52. However, as the lowest experimental value measured at UoB was greater than 10% K_2O and the vast majority were all above 15% K_2O, the inaccuracy found at 1% K_2O is of no concern to the results in this thesis.

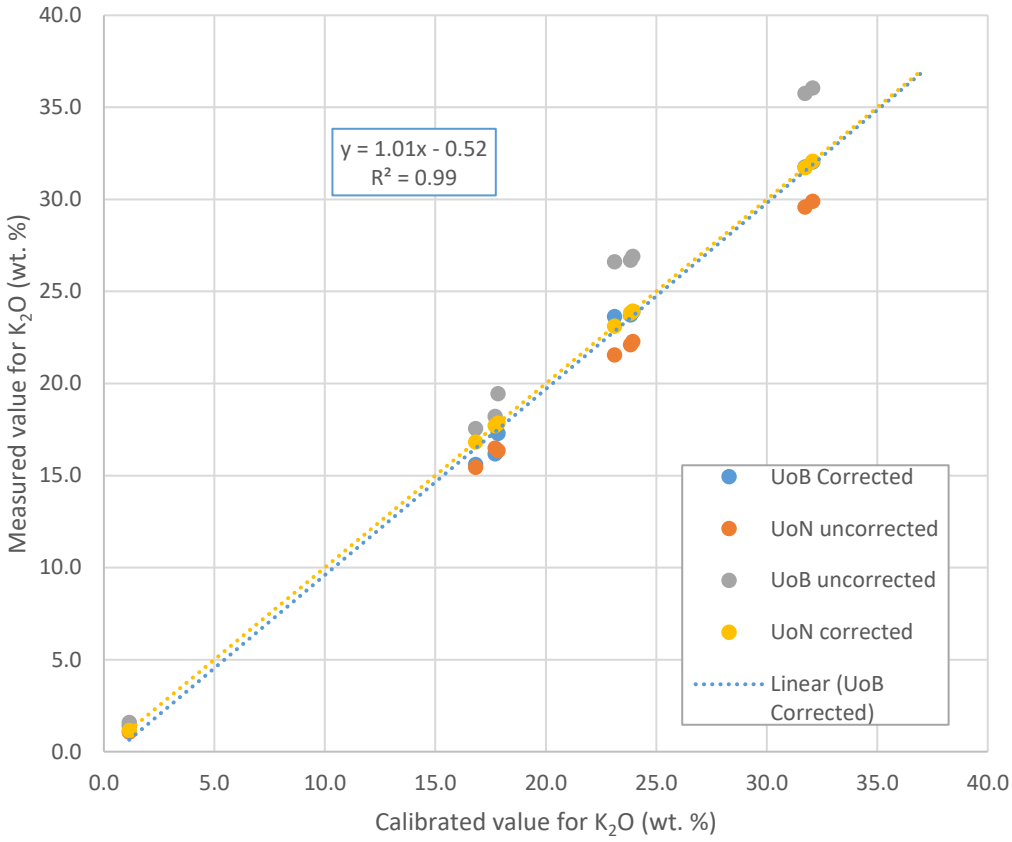

Figure 3.11. K_2O content of different samples measured at both UoB and UoN plotted with respect to calibrated UoN values

In conclusion, by the use of a calibration series covering the range 10-40% K_2O, corrected values taken from the instrument at UoN have been proven to be accurate across the entire range of relevant values for K_2O content. It can therefore be accepted that these values can be reliably used for quantitative analysis. There can be less confidence in the corrected values taken from the instrument at UoB as it has not been possible to run a calibration series. However, it has been shown that across the relevant range of values, the UoB correction factor aligns the results with the calibrated UoN values. There is some observable error in the UoB results from the UoN results in the middle of the range of K_2O content measured, but this was found to be within a

reasonable error to still have confidence in the assertions later made in this thesis.

3.6.3 XRF Results Interpretation

The raw data obtained from the XRF analysis provides the weight percentages of elements with masses between those of sodium and uranium. The software used offers a conversion calculation which predicts the most common oxide for each element and can therefore provide composition data in either elemental or oxide form. The use of XRF in this study is to find the comparative levels of elements, particularly potassium, in biomass samples post combustion, with and without the use of additives. A fundamental issue with using this approach however, is that by the addition of an additive such as kaolin, the composition of the biomass sample is changed. To get interpretable results it is therefore necessary to "subtract" the contribution of the additive (for each element) to the mixture. Where the contribution of an element from the additive in a 50:50 mixture is zero, this simply means doubling the reported concentration of that element in the mixture. This is true for potassium in kaolin but a small quantity of potassium is found in coal fly ash. As this was used as an additive in some experiments, it was necessary to account for and remove the potassium present from the additive.

Another issue that must be accounted for is the loss of sample mass during the combustion process. Both the additive and fuel have moisture associated with them when received. Kaolin has additional, entrained, chemically-bound moisture that is lost at a temperature of around 400-600°C. In addition to this,

the biomasses will of course lose mass during combustion. The amount of mass that is lost and the identity of the species that are leaving the sample will have a significant impact on the relative quantities of remaining elements in the sample and may potentially significantly mask the reactions occurring. For interpretable data to be obtained it is therefore necessary to consider carefully the ways in which the XRF data is adjusted to account for variables such as moisture content. A clear solution is to run blank tests where the constituent parts of the mixtures are combusted individually, under the same conditions. This will give information on the relative quantities of elements prior to, and subsequent to, exposure to combustion conditions. It should also give information on the mass yields of the starting materials. This information can then be used to calculate the expected concentrations of elements in the sample for comparison with the experimental data.

3.6.4 Analysis of 550°C olive cake ash

To measure the consistency of results obtained by both the ashing method and XRF analysis, a test of the potassium oxide content of olive cake ash produced at 550°C was conducted. In the experiment, 42 samples of olive cake were ashed in the muffle furnace and then analysed by XRF. Samples were either tested at UoN or UoB. The results were then corrected using the adjustment factor as described in the section above. The mean value for potassium oxide content in the ash was determined to be 33.05% with a standard deviation of 1.78%. A histogram with normal distribution curve is shown in Figure 3.12.

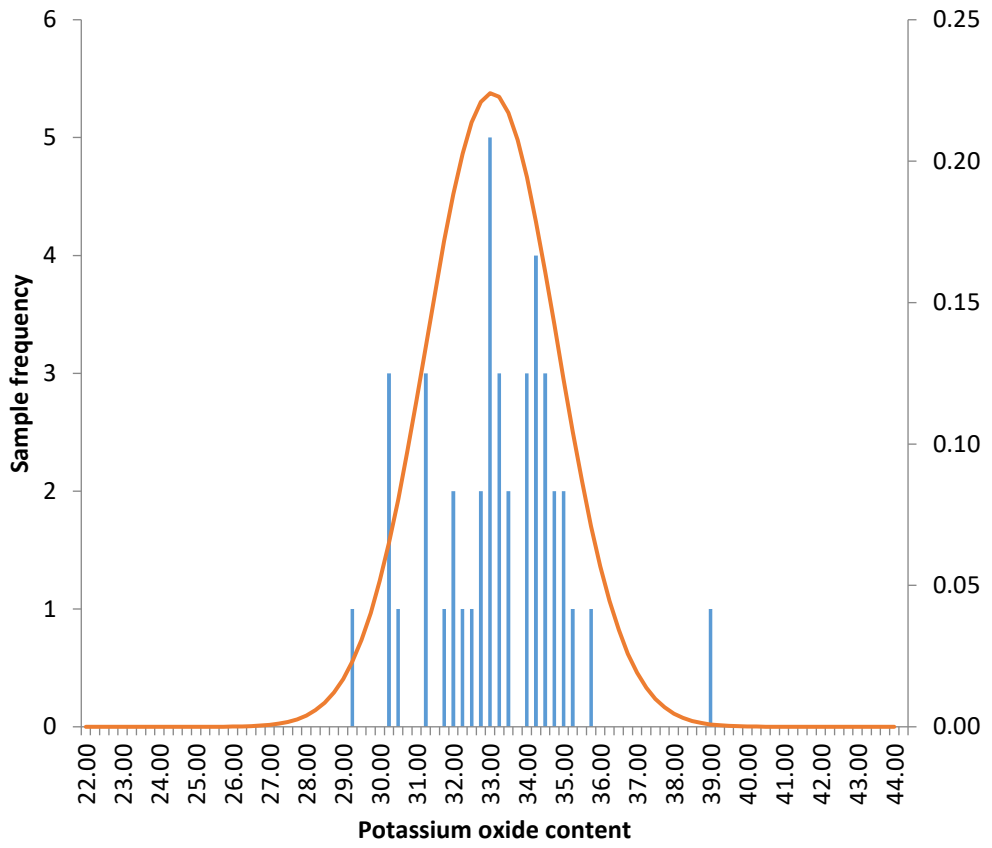

Figure 3.12. Histogram with normal distribution curve of potassium oxide content in 42 samples of olive cake ash

3.7 Scanning Electron Microscopy

3.7.1 Sample Preparation

To observe particles under a scanning electron microscope they must be fixed in the plane of an entirely smooth surface which is coated in carbon. To achieve this the samples to be analysed are set in resin blocks which are then polished. The first stage of this process is to create the blocks. 15 parts of EpoFix Resin should be mixed with 2 parts of EpoFix Hardener in a plastic pot and stirred vigorously for several minutes. Once well mixed, resin should be poured (to a depth of 3-4 mm) into plastic moulds (Figure 3.13) that have been greased with high-vacuum grease. The sample to be analysed should be put onto the liquid resin and mixed thoroughly. The samples in their moulds should then be placed

into a vacuum oven/pressure chamber at room temperature and placed under vacuum to draw out air bubbles. The resin should then be allowed to harden for several hours. Labels can subsequently be placed on top of the partially hard resin blocks and more resin should be added to a total block thickness of approximately 15-25 mm.

Figure 3.13. Preparation resin sample blocks using moulds

Once again, the bubbles should be removed in the vacuum oven and then the resin should be left to harden for at least 24 h. After hardening, the blocks should be removed from the moulds. The blocks will then require cleaning and sometimes sanding to remove the grease and any sharp edges or excess resin. The blocks should then resemble those shown in Figure 3.14.

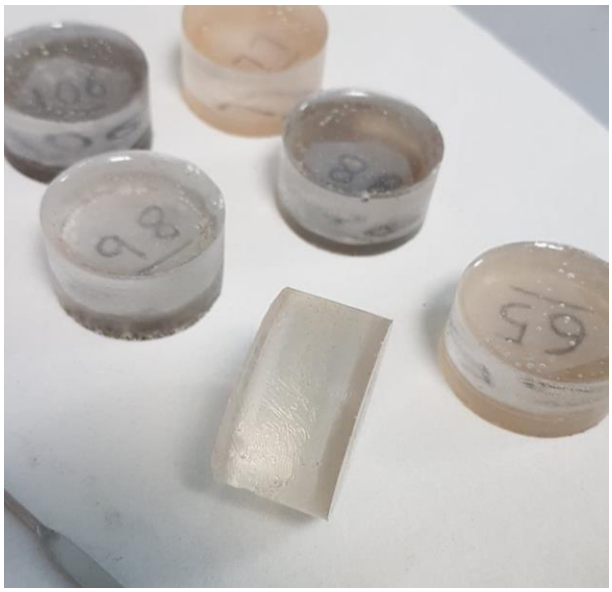

Figure 3.14. Hardened resin moulds

The next stage is to grind the blocks until the embedded sample particles are exposed and the sample surface is flat. A Struers Tegramin-25 automatic grinding and polishing machine was used for this (Figure 3.15). The blocks are placed in the sample holder and are polished sequentially. Firstly with diamond embedded grinding pads of decreasing grain size – lubricated with water – and then with diamond suspensions of decreasing grain size used with polishing pads. Between each polish it is imperative to ensure the sample is thoroughly and entirely cleaned of any residue that might contaminate the sample or the grinding/polishing pads.

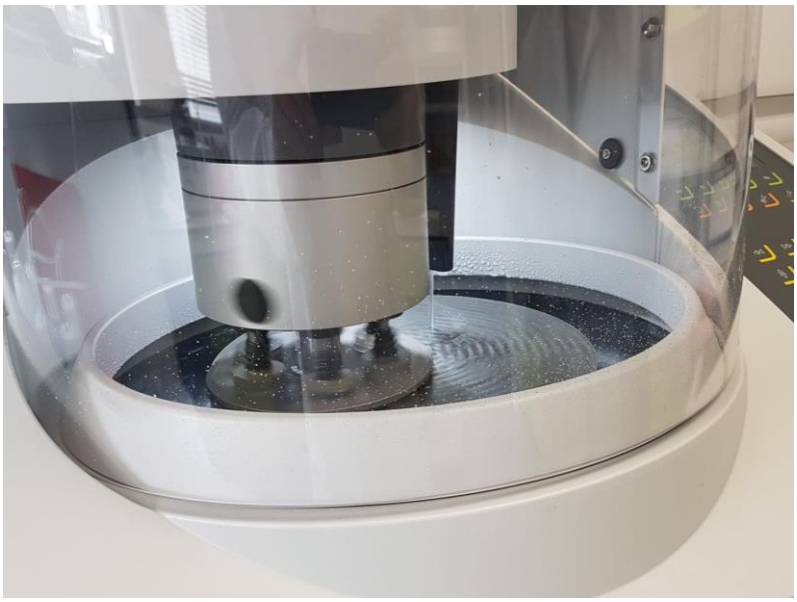

Figure 3.15. Sample polisher

With each lower grain size, the grooves in the resin should reduce in size until, after polishing at 1 µm, they should have disappeared entirely. This can be checked under an optical microscope. Once the sample surfaces have been polished they must be coated in carbon. This was done using a Quorum Q150R ES rotary pumped carbon evaporator. Three sample blocks can be placed into the instrument and carbon is evaporated from a cord onto the sample in short pulses. The thickness can be measured and typically should be around 10 nm. Once the samples in their blocks have been polished and carbon coated they are ready for analysis.

3.7.2 Sample Analysis

Once the samples had been prepared, they can be analysed by the SEM-EDX (Figure 3.16). The samples were placed into a sample holder and then attached to the inside of the sample chamber (Figure 3.17). The chamber was then placed under vacuum and the electron beam was turned on. The samples were run overnight.

Figure 3.16. SEM-EDX with MLA

Figure 3.17. SEM-EDX instrument sample chamber

3.7.3 MLA

For semi-quantitative analysis by the use of MLA, several stages of operation are employed. These procedures are outlined in the sections below.

3.7.3.1 Particle De-agglomeration

When using BSE to define the particle boundaries, problems may arise where particles in the sample touch each other. If this was not addressed, then it would effectively result in separate particles being treated as one. To avoid this, the MLA system has an automated de-agglomeration function. This recognises and separates agglomerated particles. An example of this, shown in Figure 3.18(a) (Gu, 2003) shows the original image prior to de-agglomeration. In (b), the background has been removed leaving several particles with apparent agglomeration. A single, agglomerated particle is shown in (c). Finally, after de-agglomeration, the particle is split into the six constituent particles, one of which is highlighted in (d).

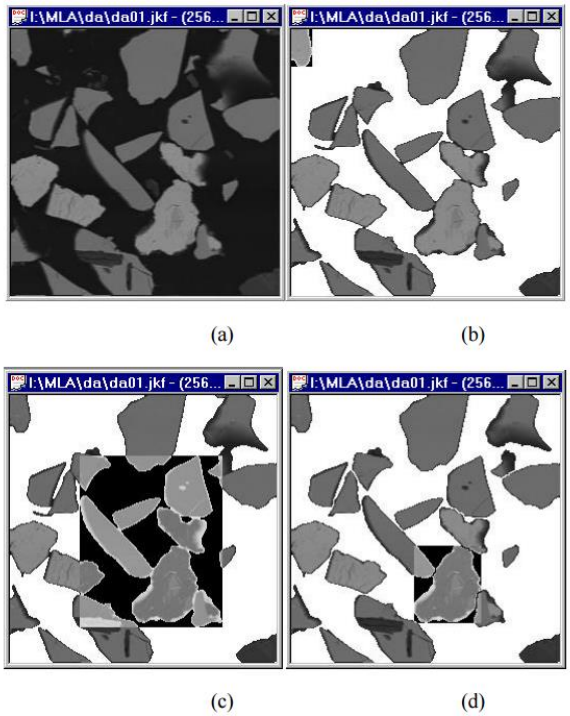

Figure 3.18. The De-agglomeration Process (Gu, 2003)

3.7.3.2 Image Segmentation

Image segmentation is the most common method of identifying mineral phases and determining their boundaries within a particle. An example of this can be seen in Figure 3.19 by the adoption of different colours for each grain (Gu, 2003). The different colours are not necessarily all of different mineral identities.

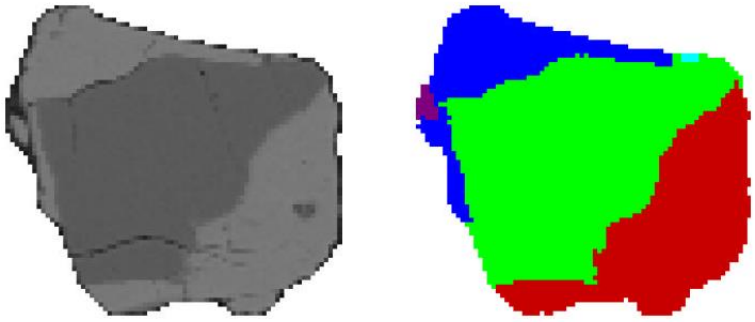

Figure 3.19. Grey Level and Segmented Particle Image (Gu, 2003)

This process works by segmenting regions of roughly homogeneous BSE grey level. As previously mentioned, BSE correlates with the atomic number of the

species (for minerals this is in the form of a unique average atomic number - AAN). The value and distribution of grey level signals can be plotted on a graph to give quantitative information on the minerals present. This method of characterising minerals is unreliable however due to grey level variation over the time of analysis, and also due to minerals having similar AAN values. To overcome this, the BSE data are generally used just to identify mineral boundaries and then x-ray data can be obtained for mineral identification.

3.7.3.3 X-ray Analysis

For fast identification of mineral species, X-ray analysis is used. This can be applied in a number of ways depending on the type of sample and the needs of the operator. These are combined with BSE to give a number of available measurement modes.

3.7.3.4 Measurement Modes

There are several modes of operation of MLA for different sample types as listed below (Fandrich et al., 2007):

- Standard BSE Liberation Analysis (BSE)

  The most basic method, the standard technique discriminates between minerals based purely on the BSE grey level distribution. Being reliant only on image analysis, it is only suitable for mineral samples that have sufficient BSE grey level contrast.

- Extended BSE Liberation Analysis (XBSE)

The extended liberation analysis involves the X-ray analysis of the mineral grain subsequent to the determination of the grain boundaries by BSE. This is done with one X-ray beam focussed on the centre of each particle.

- Ford Analysis or Grain-Based X-Ray Mapping (GXMAP)

GXMAP uses X-ray mapping on phases which cannot be segmented by BSE grey levels alone and faster X-ray analysis which can. The grains to be mapped are selected by the operator through a BSE or specific X-ray standard trigger. This means that all grains of interest can are mapped while saving valuable time. For rapid, comprehensive coverage, this method would appear to be the most relevant for this study.

- Sparse Phase Liberation Analysis (SPL)

This method targets specific particles of interest based on BSE data and then performs XBSE analysis on them. This uses the same methodology as the two previous modes but does not give bulk mineralogy information as it is selective in the particles it chooses.

- Particle X-ray Mapping (PXMAP)

Suitable for the differentiation of minerals with a very similar grey level, PXMAP relies more on X-ray than BSE data. Particle mineral maps are generated using X-ray dot mapping. After using BSE just to discriminate particles from the epoxy resin background, each grain is mapped and an X-ray spectrum is obtained. These data are then used to classify the identity

of each mineral. Due to the large number of X-ray analyses to be to be acquired this method is relatively time consuming.

- Selected Particle X-ray Mapping (SXMAP)

To maximise efficiency by combining the XBSE and PXMAP modes, PXMAP is used on selected particles and XBSE is performed on the rest. This saves time by only running the X-ray mapping on particles with similar grey levels. A BSE threshold can be applied by the operator to select which particles will be mapped by PXMAP.

- X-ray Modal Analysis (XMOD)

This mode uses a point counting system. BSE data defines particle matter and X-ray analysis is undertaken on each point that falls on a particle. As the name suggests, this method only provides modal mineralogy information. Modal mineralogy gives the relative quantities (by weight and area) of each measured mineral species.

- Rare Phase Search (RPS)

This method uses BSE data to find mineral phases of particular interest before collecting X-ray spectra on them. An image of each phase, in addition to its stage location and X-ray spectrum is recorded. This technique is useful when looking for minor components.

The measurement mode used to collect the MLA data was GXMAP. This mode identifies different mineral phases by BSE initially and then uses X-ray

spectroscopy to analyse grains of interest more thoroughly. Further details of the methodology used are explained in chapter 6.

4 An investigation into the Effect of Additive Ratio on Potassium Retention at 815°C in a Muffle Furnace

4.1 Summary

In this chapter, the effect of the presence of kaolin as an additive to fix potassium in olive cake combustion ashes by muffle furnace firing is investigated. It is expected that potassium in the biomass will bond with the aluminosilicate minerals from the kaolin to form high melting temperature mineral species instead of remaining as a vapour. This may be evidenced by determining the relative quantities of potassium by XRF before and after combustion and comparing with the same elemental balances where the additive is used. Mass balances should also provide evidence of any retention of inorganic matter. This experiment has been conducted across a range of different ratios of kaolin additive in the feedstock. This should provide an approximation for the optimal additive ratio in terms of potassium retention. The benefits of this experiment are that it is relatively simple to run and all solid mass is recovered in the ash.

4.2 Introduction

The biomass fuel used for this experiment was Spanish olive cake. This was chosen both for its high ash content and high potassium content. When ashed at 550°C in accordance with the British Standard procedure for the determination of ash content of solid biofuels (BS EN ISO 18122:2015), a value of 33.1% is measured for potassium oxide. The further heating of the 550°C ash to 815°C has a mass yield of 84.8%. To compare the K_2O values of both samples,

the 815°C ash value should be normalised to account for the extra mass loss. The un-normalised XRF value for K_2O in 815°C olive cake ash (corrected according to the K calibration) is 23.9%. This value is multiplied by 84.8% to give a normalised value for K_2O in the 815°C ash of 20.2%. This provides a number which is comparable with the value measured at 550°C and by finding the difference between the two values as a percentage we can see that approximately 40% of the potassium oxide is lost between 550°C and 815°C (as seen in Figure 4.1).

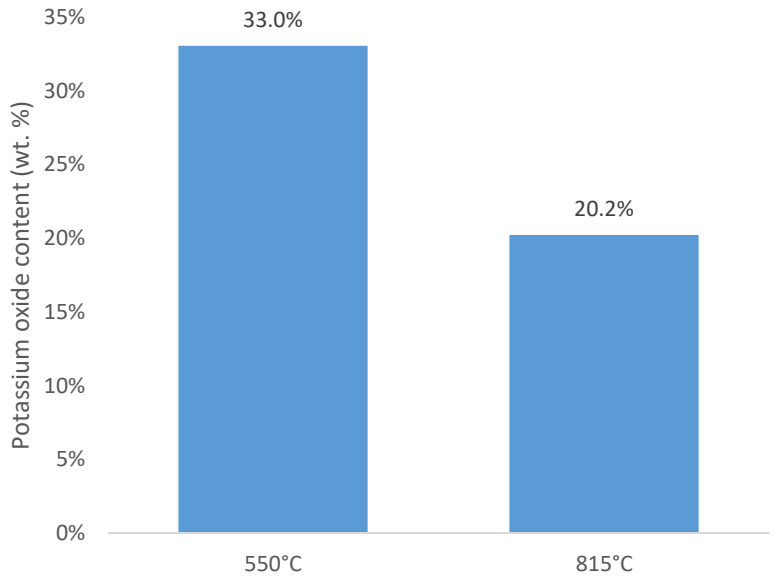

Figure 4.1. Weight percentage of potassium oxide in olive cake ash produced at 550°C and 815°C

This data is in agreement with values found in recent literature on the release of potassium from olive cake at similar temperatures (Clery et al., 2018). This volatile potassium which is lost from the biomass during the char combustion stage is the target of this investigation. The vaporisation of inorganic species, particularly alkali metal salts, during this stage of combustion is critical in terms of the ash properties and slagging and fouling behaviours of biomasses (Saidur

et al., 2011). The release of gaseous potassium as KCl and (in the absence of chlorine) as KOH is responsible for many detrimental corrosive effects in boilers and so mitigating its release is of great importance. The use of additives to fix the potassium in the combustion ashes in higher melting temperature mineral species has become an attractive option and one which numerous power companies have adopted in recent years. The aim of this investigation was to determine how the ratio of a single mineral additive to 550°C olive cake ash effects the release of gaseous potassium at the higher combustion temperature of 815°C. To determine the effect of additive ratio, tests were conducted with olive cake ash and kaolin in ratios of 5:1, 4:1, 3:1, 2:1, and 1:1 (by weight). As the ash mass yield of olive cake at 550°C is approximately 10%, these ratios translate to 2%, 2.5%, 3.3%, 5%, and 10% additive in the raw fuel. For each of these ratios, the olive cake and kaolin were thoroughly mixed prior to ashing at the higher temperature to give the greatest possible surface contact between fuel and additive. In addition, a test was conducted at a higher additive ratio of 1:2 (20% additive in raw fuel). In this experiment kaolin was added to the olive cake as a single layer. There was no pre-mixing of the fuel and additive. The purpose of this was to see if improved contact could be made between the potassium and the additive by forcing the vaporised gases to permeate through the layer of excess kaolin.

4.3 Experimental procedures

The first stage of the experiment was to ash the olive cake by heating to 550°C in air for several hours. The purpose of this was to release the volatile matter

and fully combust the volatile carbon while retaining the majority of volatile inorganics, particularly the volatile potassium. This would have the effect of significantly concentrating the potassium species. It is advantageous to do this as it allows greater opportunity for contact between fuel and additive, and it means that larger relative quantities of ash can be produced in the final, higher temperature combustion.

The additive used in this experiment was kaolin clay. After heating to 550°C, the olive cake samples were mixed with kaolin clay in different ratios of ash to kaolin by mass – 5:1, 4:1, 3:1, 2:1, 1:1. For each test, three separate crucibles were used simultaneously to provide results in triplicate. These mixtures were then heated to 815°C in air for a minimum of three hours. These conditions typically allow all volatile inorganics to be released. In addition, an experiment was conducted where an excess of kaolin was placed in a layer on top of the olive cake after 550°C ashing. The olive cake ash and kaolin were then taken to 815°C as with the other experiments but without any physical mixing. To provide baseline results, olive cake samples were run under the same conditions with no additive. The mass differences for all experiments were recorded and analysed and ash composition data was collected by x-ray fluorescence spectroscopy (XRF).

4.4 Mass balances

The masses of all samples were recorded prior to and following each test. The resultant mass balances are reported below in Table 4.1. The first aim of recording these mass balances is to identify any indicators of retention of

volatile matter by increased mass yields where additives are used. In addition, knowing the mass yields for each stage is important for accurate normalisation of XRF data. For each experiment, the ash yield at 815°C for each mixture is first provided. The total mass loss from the kaolin (13%) is then accounted for and the mass of the kaolin is removed to give the result for mass loss within just the olive cake. This is then shown for the overall mass loss of the ash.

Table 4.1. Mass balances for each experiment showing the ash yields for each stage

	Kaolin in mixture	Mixture mass (550-815°C)	OC mass yield (550-815°C)	OC mass yield (raw-815°C)
Baseline	0%	73.4%	73.4%	7.5%
5:1 Ratio	17%	82.1%	81.1%	8.6%
4:1 Ratio	20%	84.0%	83.3%	9.0%
3:1 Ratio	25%	77.7%	74.6%	8.6%
2:1 Ratio	33%	82.3%	79.9%	8.7%
1:1 Ratio	50%	81.3%	75.6%	6.7%
Kaolin layer	66%	84.1%	62.9%	6.2%

For the majority of additive experiments (all excepting the 1:1 ratio and kaolin layer test), increases in the muffle furnace mass yields were measured as a result of the presence of the additive. These increases were all of similar magnitude and so did not give an indication of any apparent trend as the amount of kaolin increases. The cause of these increases is expected to be in part due to an increase in the potassium in the high temperature ash as a result of adsorption to the kaolin. This cannot be confirmed without ash composition analysis, however.

4.5 XRF analysis and interpretation

To find the elemental composition of the ashes from the above experiments, each ash sample was analysed with X-ray fluorescence spectroscopy (XRF). The

results for potassium oxide concentration were corrected in accordance with the calibration procedure (described in chapter 3) and then adjusted to account for mass loss during combustion and the dilution effect caused by the addition of the kaolin. To adjust for mass loss, the specific mass yield obtained for the conversion of 550-815°C for each run was used to normalise the potassium level to align with that measured in the 550°C ash. For example, for the experiment with biomass to additive ratio of 5:1, the values for K_2O were measured on the XRF instrument at UoB as 24.7%, 25.0%, and 26.0%. These were corrected to 21.9%, 22.2%, and 23.1% using the 88.85% correction factor determined in chapter 3. These values were then multiplied by the individual mass yields recorded for each run: 82.4%, 81.0%, and 82.9% respectively. This gave values for K_2O of 18.1%, 18.0%, and 19.1%. Finally, they were normalised to account for the dilution factor of the additive. For this, the exact percentage of biomass which was weighed out was used. In the case of this example – with a target of 16.7% kaolin in 83.3% olive, the values were: 82.8%, 83.0%, and 83.3%. The mass-normalised K_2O values were multiplied by these percentages to give: 21.8%, 21.7%, and 23.0%. These results are now comparable with the K_2O values measured in the 550°C ash. The values for potassium oxide content in the experiment mixtures are shown in Table 4.2.

Table 4.2. Potassium oxide content in experimental mixtures as determined by XRF

	Fuel and additive mixed					Kaolin Layer
% kaolin	**17%**	**20%**	**25%**	**33%**	**50%**	**66%**
% K_2O	22.1%	21.8%	20.9%	22.0%	25.3%	20.5%
Error (2σ)	1.2%	2.4%	0.4%	1.2%	1.6%	3.6%

As the experiments were run in triplicate, the values in the table above are mean values. For each set of values, the standard deviation has been determined and doubled to give an error covering 95% certainty. It should be noted however that there were observable differences in the results between separate oven runs and that only one run (containing three repeat samples) was completed for each test. The values from Table 4.2 for potassium oxide in the olive cake ashes are represented graphically in Figure 4.2.

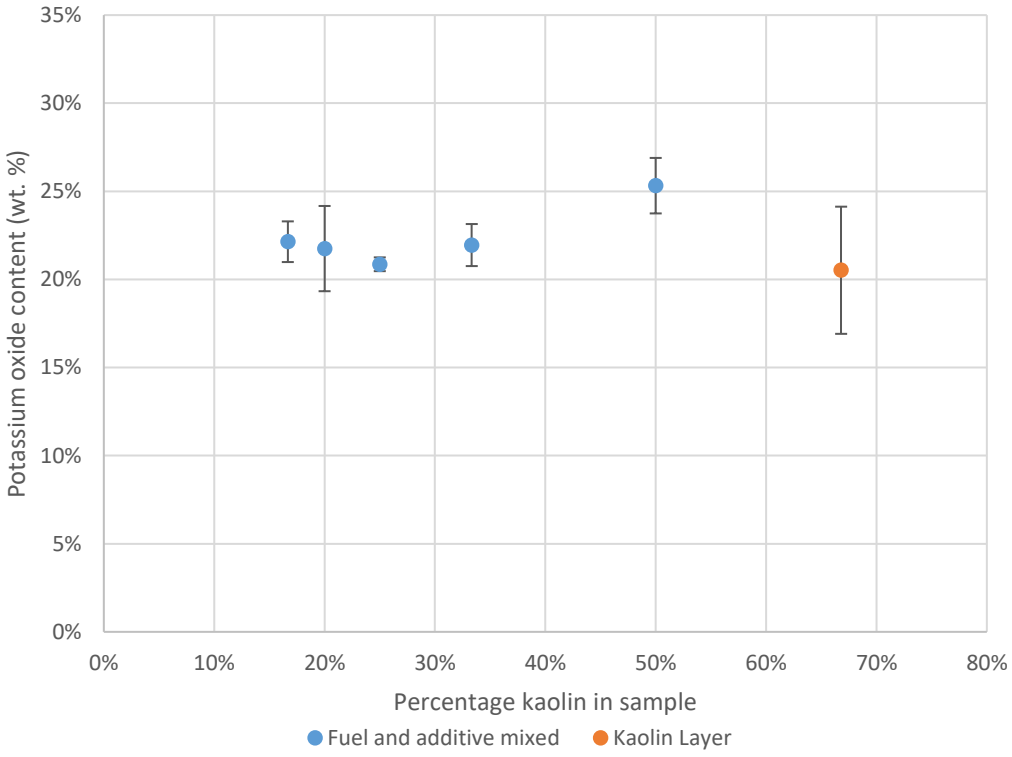

Figure 4.2. Potassium oxide content against additive ratio

In the graph it can be seen that the levels of potassium across the lower additive ratios are relatively similar to each other. An elevated level is seen for the highest level of additive – where the fuel and additives were pre-mixed. A lower level of potassium can be seen for the unmixed, kaolin layer experiment. To understand the extent to which the additive has made a difference, the level of

potassium in the ash can be expressed in terms of amount of volatile potassium that is retained.

4.6 Levels of retention of volatile potassium against additive ratio

As described in the introduction, the level of volatile potassium in this case is the potassium which is released from the olive cake between 550°C and 815°C. The level of this volatile potassium which is retained is shown in Table 4.3. As with the previous data, the error has been calculated as two standard deviations from the mean for each set of results.

Table 4.3. Retention of volatile potassium

	Fuel and additive mixed					Kaolin Layer
% kaolin	**17%**	**20%**	**25%**	**33%**	**50%**	**66%**
% K_2O	22.1%	21.8%	20.9%	22.0%	25.3%	20.5%
Error (2σ)	1.2%	2.4%	0.4%	1.2%	1.6%	3.6%
% retention of vol. K_2O	15.0%	11.9%	5.0%	13.5%	39.8%	2.3%
Error (2σ)	9.0%	18.9%	3.0%	9.3%	12.3%	28.1%

As can be seen from the results in the table above and in the graph below in Figure 4.3, some retention of potassium was found in all cases. The highest level of retention was seen with the greatest ratio of additive to olive cake tested in the pre-mixed series. It is also likely that the level of retention may be higher in this case. This is because the level of volatile potassium assumes the value for 100% retention to be at a level of 33.05% K_2O. For the case of the 1:1 additive ratio, a poor ash yield was achieved. It is expected that this would lead to there being less potassium being available to retain by the additive.

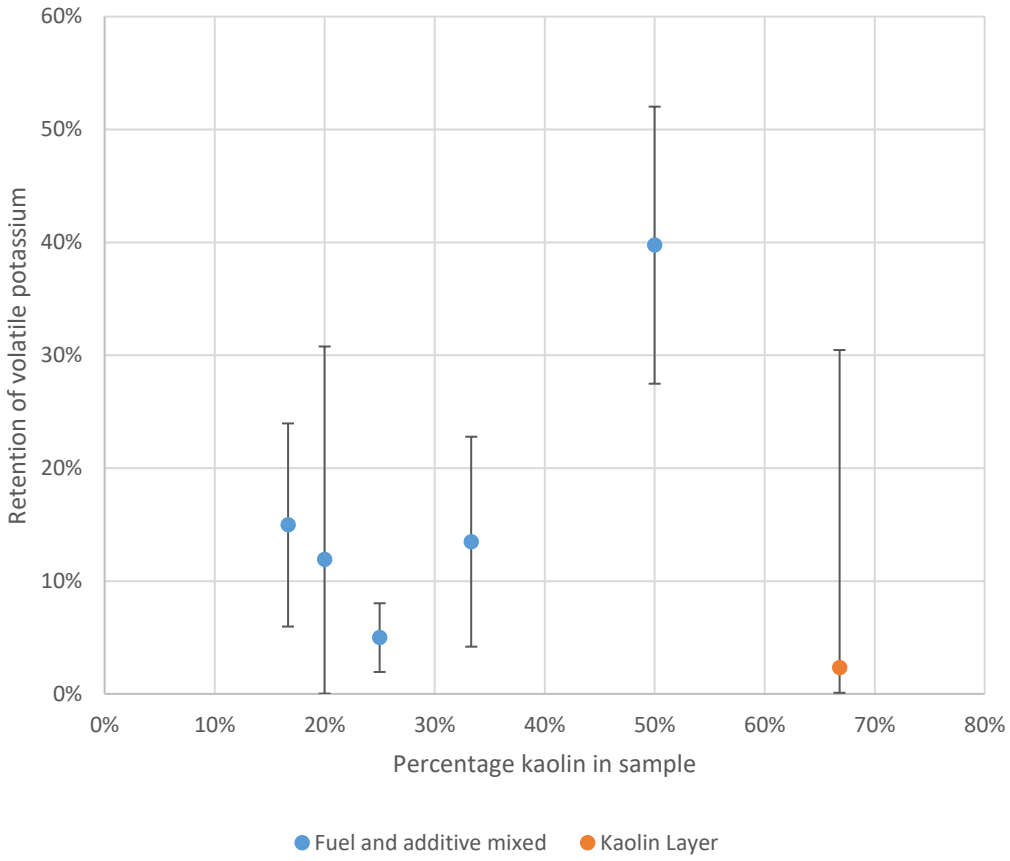

Figure 4.3. Retention of volatile potassium against additive ratio

It would therefore appear that substantial retention of potassium is achieved in the case of the 1:1 additive ratio (10% additive in raw fuel). It can also be said that significant retention was found for the lower additive ratios although to a lesser degree. Interestingly, for the kaolin layer experiment, there was little retention to be seen for the high level of additive used.

4.7 Conclusions

In general, it was found that where additives were used, a higher mass of ash was recovered. XRF was used to determine the K_2O level in each ash sample and was compared with the K_2O levels found in 550°C and 815°C olive cake ash that had not been exposed to the additive. It was found that the lower additive ratios (2-5% kaolin in olive cake) resulted in less than 20% potassium retention

in ash. Where the highest additive ratio was used however, a level of 40% retention was found. This is a significant level of potassium retention and provides good evidence to support the ability of kaolin in reducing gaseous potassium release. However, recent literature reports have demonstrated higher levels of retention for kaolin with olive cake (Clery et al., 2018). One reason for this could be the duration of the tests and the low heating rate. In this experiment the samples were held at 815°C for more than 3 h. It has been reported that kaolin can begin to degrade at high temperatures (over 950°C), converting into products with low potential to react with KCl (Zheng et al., 2008). However, once the potassium is bound in potassium aluminium silicates such as kalsilite and leucite, it should be expected that no further migration would occur due to their high melting temperatures (1500°C).

Another experiment was conducted where instead of pre-mixing kaolin with olive cake, a layer of kaolin was deposited over the top of the olive cake in the crucible. The reason for this would be to see how the results changed when volatile potassium species were encouraged to permeate through a layer of kaolin. This led to very low retention rates, suggesting that proper mixing prior to combustion yields much better interaction.

Of particular note should be that this experiment was conducted at a temperature lower than those found in conventional PF boilers and under slow heating rates. The next step would therefore be to conduct a similar experiment but under high heating rate conditions representative of PF firing.

5 An Investigation into the Effect of Aluminosilicate Additives on Potassium Retention in Pulverised Fuel Combustion

5.1 Summary

In this chapter, extensive use of the drop tube furnace provides an insight into how the alkali metal transfers in the presence of two aluminosilicate additives. A number of different experimental series are used to answer questions on the use of additives in pulverised fuel (PF) combustion of biomass. The first test series is an investigation into the effect of additive ratio on potassium retention in combustion at a temperature of 1300°C. This was designed as a progression from the research reported in the previous chapter where different additive ratios were investigated in a muffle furnace at 815°C. A streamlined version of this test is then repeated at 1150°C.

In the second test series, potassium retention is measured over a range of temperatures. The aim of this experiment was to profile the efficacy of kaolin as a function of temperature. This experiment was conducted at the highest ratio of additive to biomass to show the effect at the highest retention level.

The next experiment was to discover the relationship between potassium capture and combustion residence time. With all other drop tube furnace experiments conducted on the longest possible residence time of 600 ms to replicate PF conditions as closely as possible, an experiment was conducted at two shorter residence times: 200 ms and 100 ms. This test was devised to investigate the duration required for the reaction between the additive and biomass to occur or if it is instantaneous.

Following the completion of the above experiments with olive cake, two further biomasses were investigated: medium ash content miscanthus, and low ash content wood. The use of different biomasses broadens the scope of any findings and gives insight into how potassium retention in ash varies depending on its original source.

Finally, experiments were conducted with an alternative additive, coal fly ash. This is an area of significant interest due to the obvious economic benefits of using a waste product already associated with, and usually present at, power stations. These experiments were conducted with olive cake and wood to provide data on the two extreme ends of the scale in terms of ash content.

5.2 Introduction

Following on from the foundation of the previous chapter, the experimental work in this chapter begins by focusing on the same relationship between olive cake and kaolin in terms of the effect of additive ratio on potassium retention during combustion at high temperatures. However, by using a drop tube furnace, PF conditions, and particularly, particle heating rate, can be replicated. This is of great significance and should offer a greater insight into the behaviour and ability of kaolin to fix potassium in full scale power plants. As with other entrained flow reactors and vertical suspension furnaces, the use of the drop tube furnace offers something of an in-between scale to the researcher. This means it is possible to study effects that might only happen at very high heating rates and where particles flow in a suspension while avoiding the economic cost of running experiments on a commercially operating power plant. Possibly as a

result of this, there has been limited research on the intricacies of additive interactions during PF combustion (Clery et al., 2018; Yanqing; Niu et al., 2016; Paneru et al., 2016). The aim for the remainder of this research is to explore the retentive abilities of aluminosilicate additives and the fate of the retained potassium in combustion ashes under such conditions.

5.3 Interpretation of XRF data

Prior to any analysis, the values for potassium oxide were corrected as described in the calibration section in Chapter 3. As with the results in Chapter 4, to obtain data comparable with that for ashes produced at 550°C, it was necessary to normalise the values to account for mass loss during conversion. In Chapter 4, this was achieved by using the measured mass loss for each sample. However, recovery rates found when using the DTF are highly variable and often significantly lower than those achieved when using the muffle furnace. This renders the collection efficiency unreliable as a measure of mass loss during combustion. It should be possible in this case to use an ash tracer such as silicon. However, it was found that for repeat runs, silicon content varied significantly while the potassium contents were consistent. To therefore appropriately account for the loss of sample mass, an iterative calculation was derived. The first stage of this calculation was to normalise the K_2O value for each sample mixture against the mass losses found in the muffle furnace for its constituent parts. This was weighted to appropriately reflect the mixtures. The resultant ash from combustion at 1300°C of olive cake with 30% kaolin additive is used as an example:

815°C muffle furnace mass yield for olive cake: 84.8%

815°C muffle furnace mass yield for kaolin: 87.1%

$$\frac{(Additive\ mass\ yield \times 30) + (Biomass\ mass\ yield \times 70)}{100}$$

$$= mixture\ mass\ yield$$

$$\frac{(87.1\% \times 30) + (84.8\% \times 70)}{100} = 85.5\%$$

This value for mass yield can then be used to normalise the value of K_2O for the mixture. Once this has been done, the dilution effect of the additive is accounted for. To do this – in the case of a mixture with 30% kaolin – the K_2O value is divided by 0.7. This now leaves a value for K_2O which is measurable against those measured in the 550°C olive cake ash. However, this does not account for the effect that retention (due to the presence of the additive) might have on the mass yield of the ash: if K or any other major elements are retained in the ash due to the presence of the additive, the mass yield will be higher. To adjust for this, a second iteration is used. The K_2O value determined in the first iteration is compared with the K_2O content of the ash produced under the same conditions without additive.

Table 5.1. Iterative normalisation process

	0% kaolin	30% kaolin
First iteration		
Measured value	26.7	23.9
Corrected according to XRF calibration (UoB)	23.7	21.2
Normalised to muffle furnace mass yield	20.1	18.2
Adjusted for dilution due to additive	N/A	25.9
Second iteration		
Normalised to revised mass yield	N/A	19.4
Adjusted for dilution due to additive	N/A	27.7

This then informs on the level of retention found in the sample and the expected mass yields are adjusted and corrected (Table 5.1). For the same example of 30% kaolin in olive cake ash combusted at 1300°C, there was a difference in K_2O content of 6.5% (wt. % of mixture). There was also an increase in CaO content of 1.1%. These values were added to the 815°C biomass mass yield (84.8%) to give a revised mass yield for the biomass of 93.1%. The weighted average of the biomass and additive mass yields is then determined with the revised value for the biomass mass yield. s with the first iteration, the dilution effect of the additive is then accounted for.

5.4 The use of kaolin in olive cake combustion and the effect of additive ratio on potassium retention

For this experiment, kaolin clay was used in different quantities to determine the level at which the highest retention of potassium in the combustion ashes could be achieved. This was conducted first at 1300°C and then at 1150°C. The biomass used was olive cake which had been prepared by ashing at 550°C. The additive ratios used at 1300°C were: 17%, 20%, 25%, 30%, 33%, 40% and 50% by mass of kaolin in 550°C olive cake ash. Due to the ash yield of olive cake at 550°C being around 10%, these equate to amounts of 2%, 2.5%, 3.3%, 4.3%, 5%, 6.7% and 10% kaolin in the raw fuel. For the 1150°C tests, the additive ratios used were: 20%, 30%, 40% and 50% kaolin in 550°C olive cake ash (2.5%, 4.3%, 6.7% and 10% kaolin in raw olive cake).

Figure 5.1 shows the potassium oxide content of olive cake ash produced in the muffle furnace at 550°C and 815°C and at 1150°C and 1300°C in the drop tube

furnace. There is a loss of approximately 40% of the potassium oxide in the muffle furnace as the temperature is increased from 550°C to 815°C. When 550°C olive cake ash is put through the drop tube furnace it can be seen that the loss of potassium is very similar. When collecting ash from the drop tube furnace, variable yields – typically far lower yields – are found. This is because solid ash particles can be carried through the exhaust gas flow and bypass the ash collector pot. The results in Figure 5.1 show that the mean values for potassium content in the drop tube furnace ashes are very similar to those found at 815°C in the muffle furnace and therefore show that potassium retention can be reliably measured by analysing the ash collected. In all cases, error bars show two standard deviations from the mean value recorded over at least three runs.

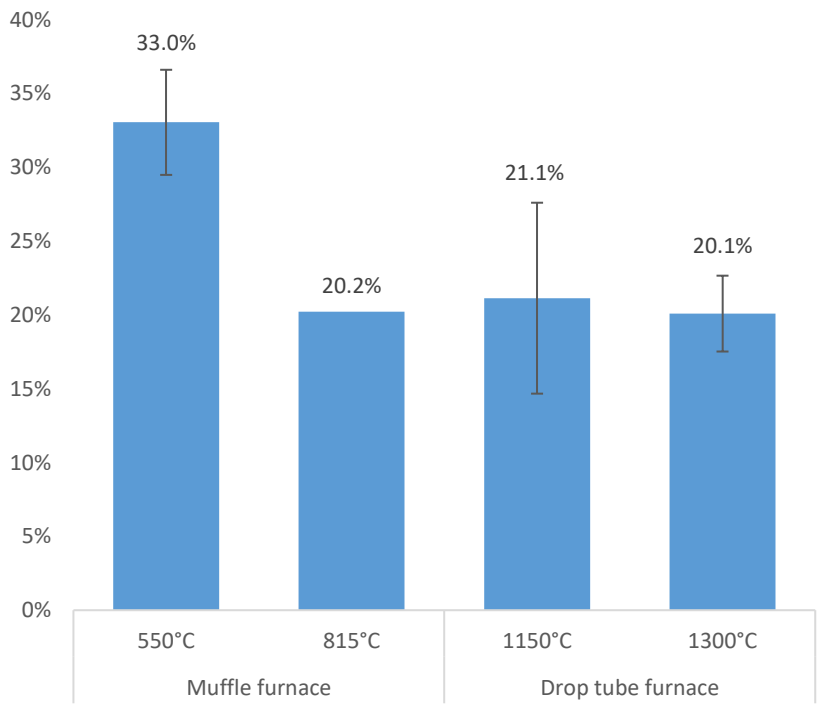

Figure 5.1. Potassium oxide content of olive cake ashes produced under different conditions

5.4.1 Experimental procedure

The experiments for the investigation at 1300°C were conducted over two phases. The first phase mirrored the muffle furnace experiment additive ratios. These were 5:1, 4:1, 3:1, 2:1 and 1:1 olive cake ash to kaolin ratio. This set of tests consisted of a single run at each temperature. The furnace heating temperature was set to 1325°C to provide an exposure temperature of 1300°C. The gas flow rate was set to 12.1 L/min and consisted of 10% O_2 in N_2. The exhaust flow rate was set to 14 L/min. The furnace residence time was set at 600 ms by using a probe separation of 65 cm. Solid ash was collected and analysed by XRF.

For the second phase, an adjusted set of ratios was used. These were: 20%, 30%, 40% and 50% kaolin in ash. This was selected to provide a linear series of ratios. All runs for this set were completed in triplicate. As with the first set of runs, for each sample the furnace was operating under the same parameters.

For the tests conducted at 1150°C, the second set of ratios was used (20%, 30%, 40%, 50% kaolin). All runs in this series were completed in triplicate. The furnace heating temperature was set to 1175°C to provide an exposure temperature of 1150°C. The gas flow rate was set to 13 L/min and consisted of 10% O_2 in N_2. The furnace residence time was set at 600 ms by using a probe separation of 65 cm.

5.4.2 XRF Analysis

The compositions of all ashes produced from drop tube furnace firing were analysed by XRF spectroscopy. The results for the first set of additive ratios are

shown below in Figure 5.2. It can clearly be seen that significant levels of retention were found across all additive ratios, ranging from 45-55%. Additionally, it appears that the level of retention increases as the amount of additive in the sample increases. Such a trend is to be expected so these initial results are encouraging.

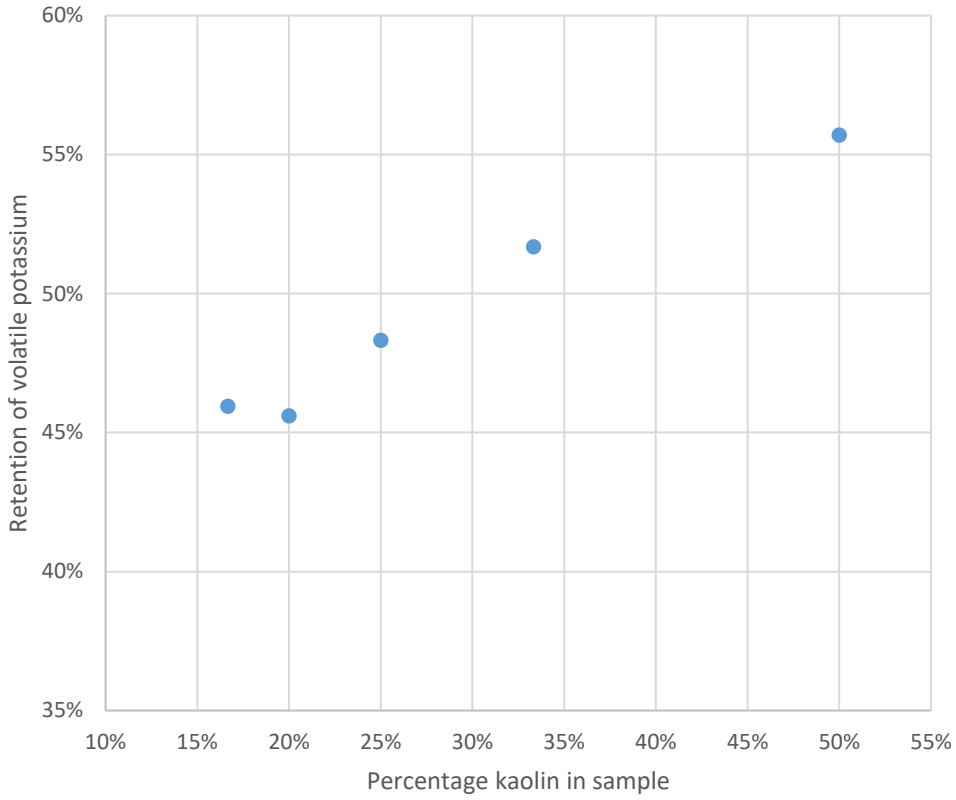

Figure 5.2. Retention of volatile potassium at 1300°C – additive ratio series 1

If the rate of increase were to be seen to plateau, then it could be concluded that a maximum effective limit of additive had been reached. At this point, no further addition would be successful in retaining more potassium. It is possible that such a trend could exist within the range of Figure 5.2 but with a gap in the results between the two higher ratios, and due to the results coming from only single runs, no such conclusion can be drawn. The results for the second set of

additive ratios can be seen in Figure 5.3. In this case, the results are mean values of triplicate runs.

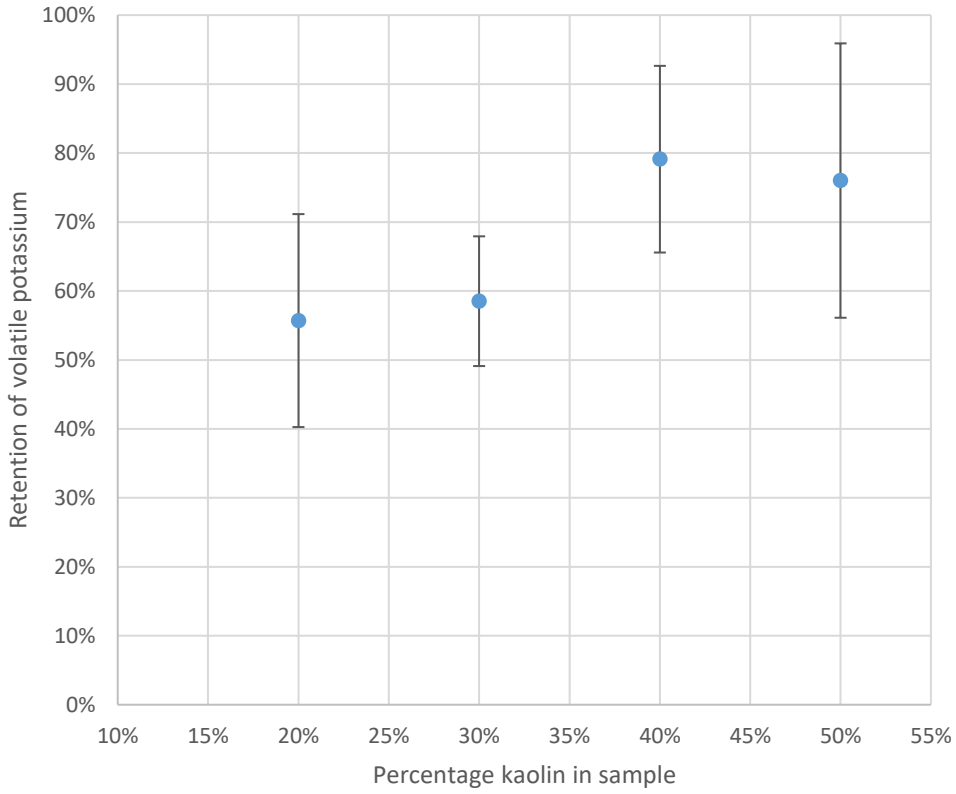

Figure 5.3. Retention of volatile potassium at 1300°C – additive ratio series 2

The standard deviation was calculated for each set of values and doubled to provide error bars covering 95% certainty. As with the first series it can be seen that there is an increase in retention of potassium where higher additive ratios are used. It appears that the value for retention at 40% kaolin is very similar to that achieved for 50%. It is unlikely that the retention would reduce so this may be evidence for reaching the equilibrium limit for the reaction. Following the completion of both sets of ratios, the results were combined to provide a dataset covering all mixtures. Where there were multiple results for one ratio, the mean is provided. The combined results are seen in Figure 5.4. The trend line on the graph represents the moving average. From this it can be seen that

at the lower additive ratios, retention rates of around 50% are found. The level of potassium retention then increases to over 70% for the highest levels of kaolin addition.

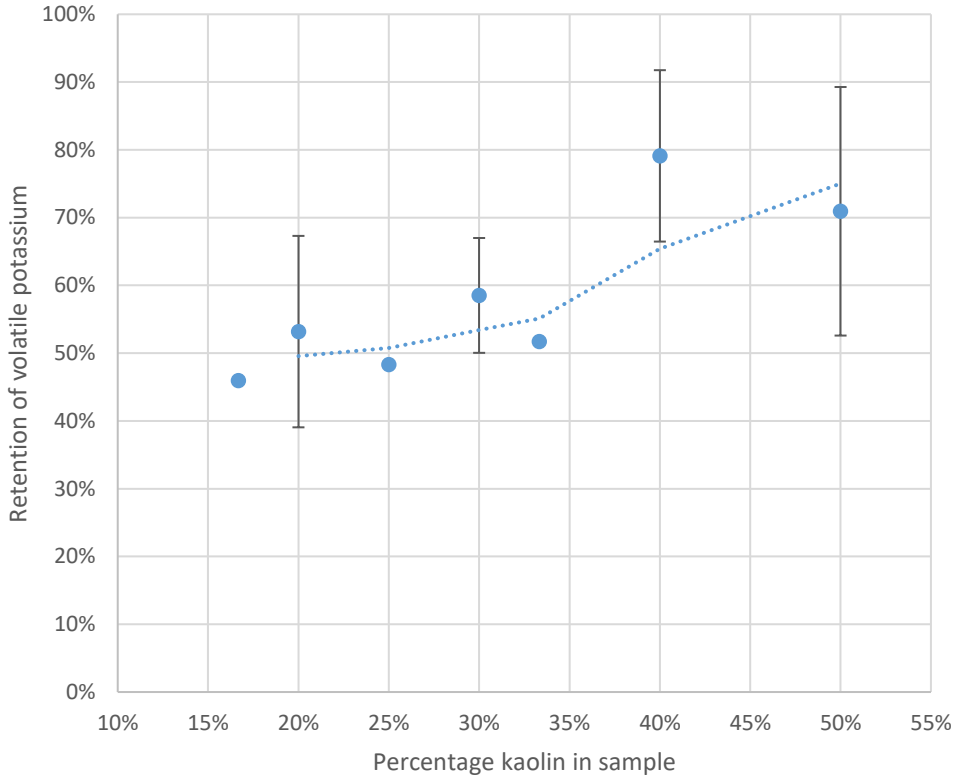

Figure 5.4. The effect of additive ratio on retention of volatile potassium by kaolin at 1300°C (series 1 & 2 combined)

The results for volatile potassium retention at 1150°C are shown in Figure 5.5. It can be seen that retention of over 80% was achieved for all additive ratios with two of the results being within 95% error of 100% retention.

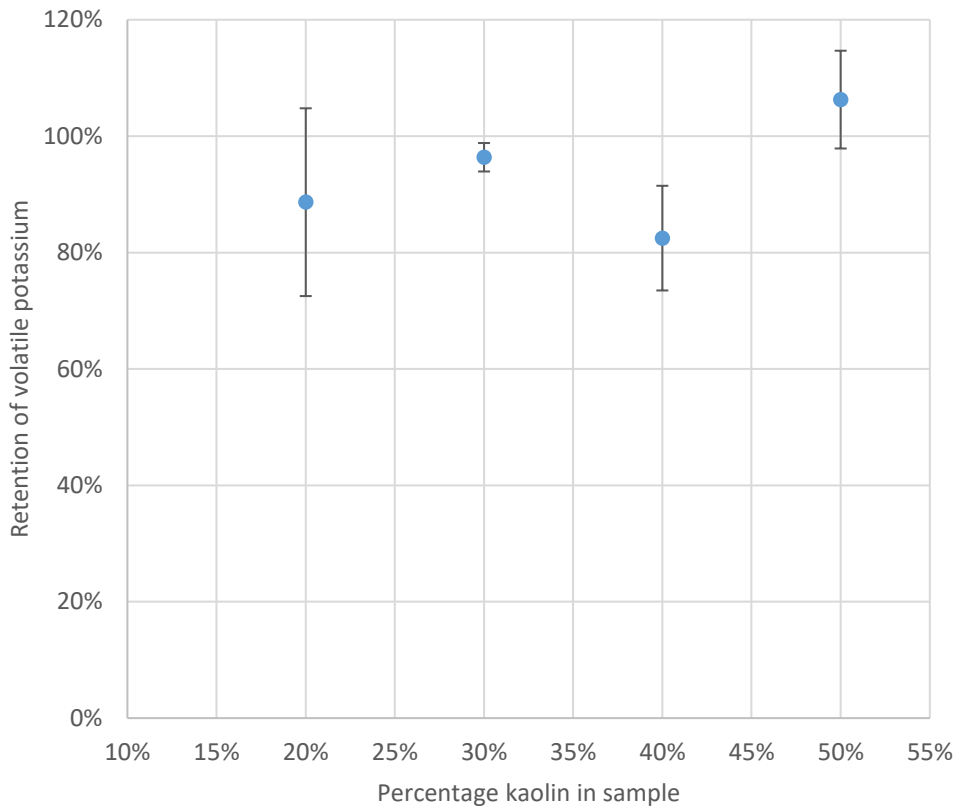

Figure 5.5. Retention of volatile potassium for different additive ratios at 1150°C

As all the results (including for the lowest additive ratio) are close to 100% retention, no significant trend would be expected or is apparent. The combined results of the experiments conducted at 1300°C and 1150°C are shown in Figure 5.6. The difference in retention caused by the effect of temperature can clearly be seen here.

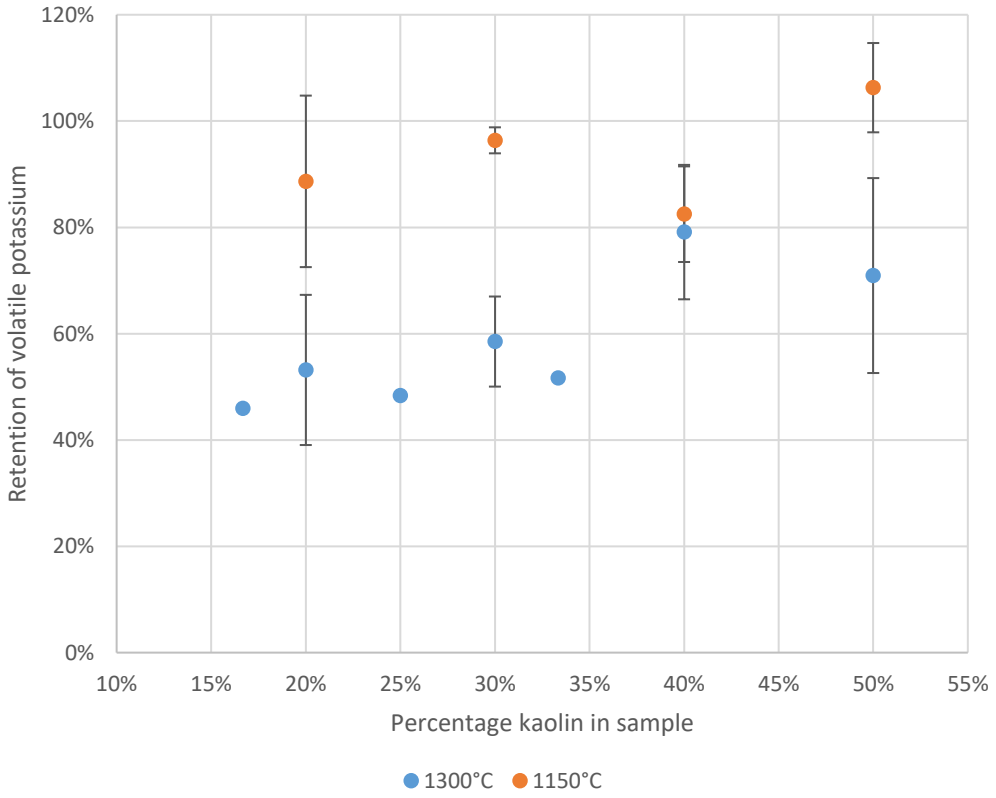

Figure 5.6. Retention of volatile potassium for different additive ratios at 1150°C and 1300°C

5.4.3 Conclusions

In the tests conducted at 1300°C, it was found that for the lower levels of kaolin addition (17-33%), retention of over 50% of volatile potassium can be achieved. For the higher ratios (40% & 50% kaolin), a retention rate of more than 70% was found. There was also some evidence to suggest that a plateau had been reached – indicating that the equilibrium limit for the reaction, or "threshold value" for the level of kaolin was found.

In the tests conducted at 1150°C, retention rates of between 80 and 100% were found, with two of the results within error of 100%. A significant trend caused by the amount of additive in the sample was not observed, likely due to the retention rates all being so high.

In general, higher rates of potassium retention were found at 1150°C than at 1300°C.

5.5 Effect of temperature on potassium retention

In this second test series, the effect of combustion temperature on the capture of potassium from the kaolin additive was investigated. To achieve this, the same conditions as before were used but with a fixed additive ratio of 50% kaolin in olive cake ash prepared at 550°C (10% additive in raw fuel). The temperature range covered four different temperatures: 1000°C, 1150°C, 1300°C, and 1450°C. Previous research (Zheng et al., 2008) into the effect of temperature on weight gain of several sorbent pellets when subjected to gaseous KCl has suggested that kaolin absorbs less potassium as temperatures increase from 900-1300°C and then more once temperatures rise from 1300-1500°C (Figure 5.7). This range spans temperatures critical in PF combustion and so it is therefore of significant relevance to understand if this holds true in such conditions as are found in PF boilers.

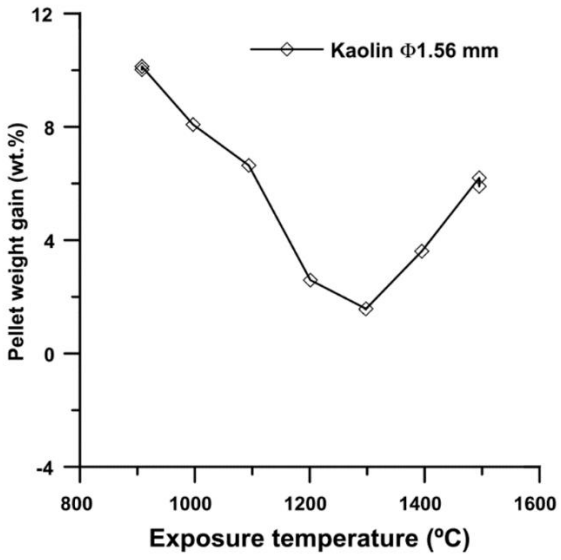

Figure 5.7. Effect of reaction temperature on potassium capture by different sorbent materials(Zheng et al., 2008)

The amount of potassium oxide found in olive cake ash produced at different temperatures in the drop tube furnace is shown below in Figure 5.8. It can be seen that the potassium levels at all drop tube furnace combustion temperatures are very similar to each other and to that of the ash produced at 815°C.

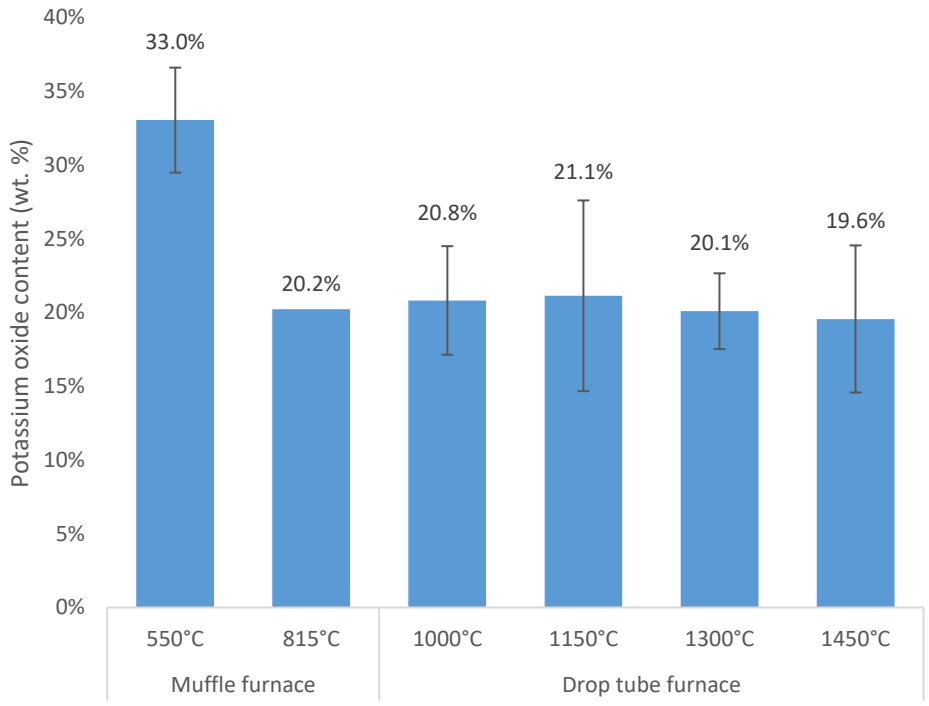

Figure 5.8. Potassium oxide content in olive cake ash produced at different temperatures

5.5.1 Experimental procedure

The experiment consisted of four drop tube furnace tests, each run in triplicate. All tests used the additive ratio of 50% kaolin in olive cake ash produced at 550°C, equivalent to a 10% kaolin content in the raw feedstock. Each test was conducted in a gas mixture of 10% O_2 and 90% N_2. For the 1000°C experiment, the furnace temperature was set to 1025°C with an overall gas flow rate of 15.05 L/min. For 1150°C, the furnace temperature was 1175°C and the gas flow rate was 13 L/min. The 1300°C test was conducted using the same parameters

as for the previous experiment: 1325°C furnace temperature and 12.1 L/min. Finally, for the 1450°Cruns, the temperature was set to 1480°C and the flow rate used was 11 L/min. For all temperatures, the probe separation was fixed at 65 cm to ensure a residence time of 600 ms.The solid ashes collected from the tests were analysed by XRF.

5.5.2 XRF Analysis

The potassium oxide content of all ashes produced in the drop tube furnace are shown in Figure 5.9. Error bars show two standard deviations to give 95% certainty of results. Across all temperatures, greater levels of potassium are found where kaolin was added. To determine the retention of volatile potassium for each temperature, the amount of volatile potassium was determined from the values shown in Figure 5.8.

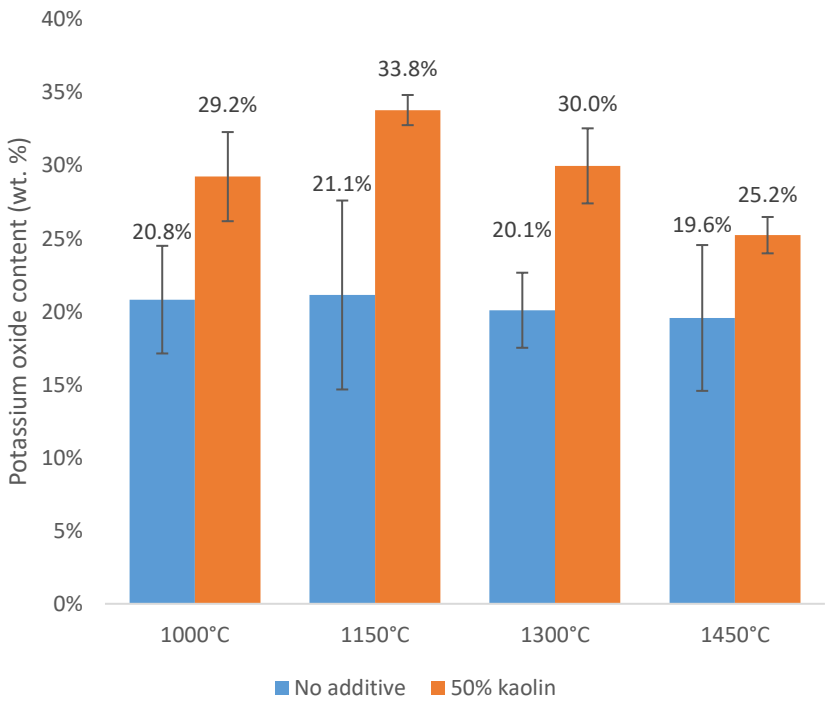

Figure 5.9. Potassium oxide content of olive cake ash produced at different temperatures with and without kaolin

The results for the retention of volatile potassium by the presence of the kaolin are shown in Figure 5.10. The values of 100% retention at 1150C and of 70% retention at 1300°C as seen in the previous, additive ratio, experiment indicate a decrease of retention as the combustion temperature increases. This trend continues up to 1450°C. However, there is also reduced retention as the temperature decreases from 1150°C.

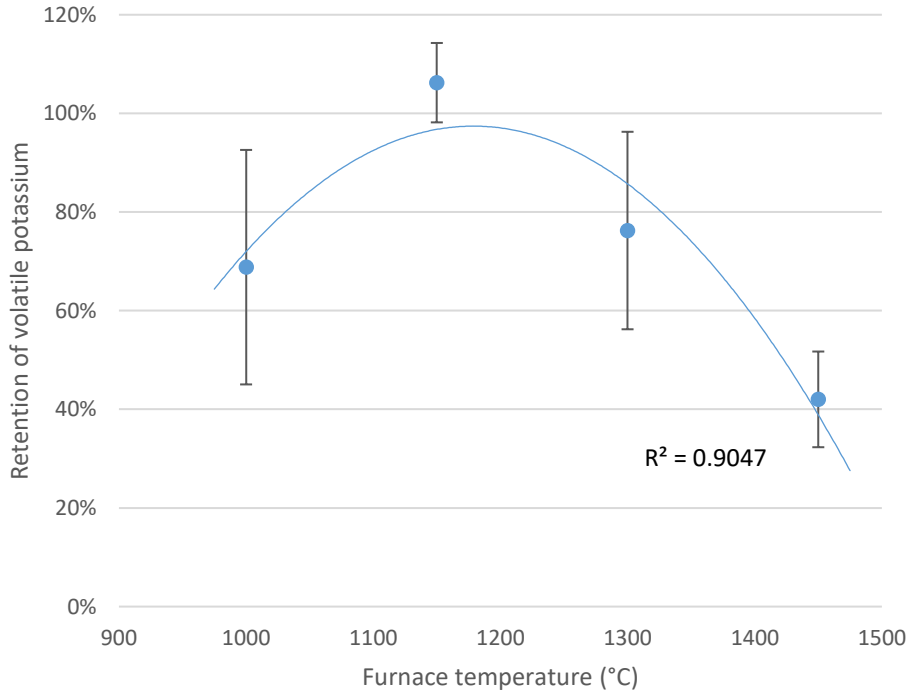

Figure 5.10. Retention of volatile potassium by kaolin over a range of temperatures

5.5.3 Conclusions

The results of this experiment showed that retention of potassium by the presence of kaolin increases from 1000°C to 1150°C but then decreases from 1150°C to 1450°C.The peak level of retention achieved was 100% of the volatile potassium in the olive cake. The reason for reduced retention at lower temperatures is that at high temperatures the reaction is likely to occur under thermodynamic control. However, as the temperature decreases, the reaction

will come under kinetic control. This is further evidenced by the experiments in the previous chapter in the muffle furnace at 815°C where minimal retention was found.

5.6 Effect of residence time on potassium retention

The purpose of this experiment is to discover how the duration at which the reaction between feedstock and additive is held at combustion temperature, affects its outcome. If the reaction takes place under thermodynamic control, it would be expected that the reaction should occur instantaneously. It should be possible to determine if this is the case by conducting an experiment with a high additive ratio at different residence times. To achieve this, olive cake ash prepared at 550°C was fired at 1300°C with 50% kaolin by mass at three residence times.

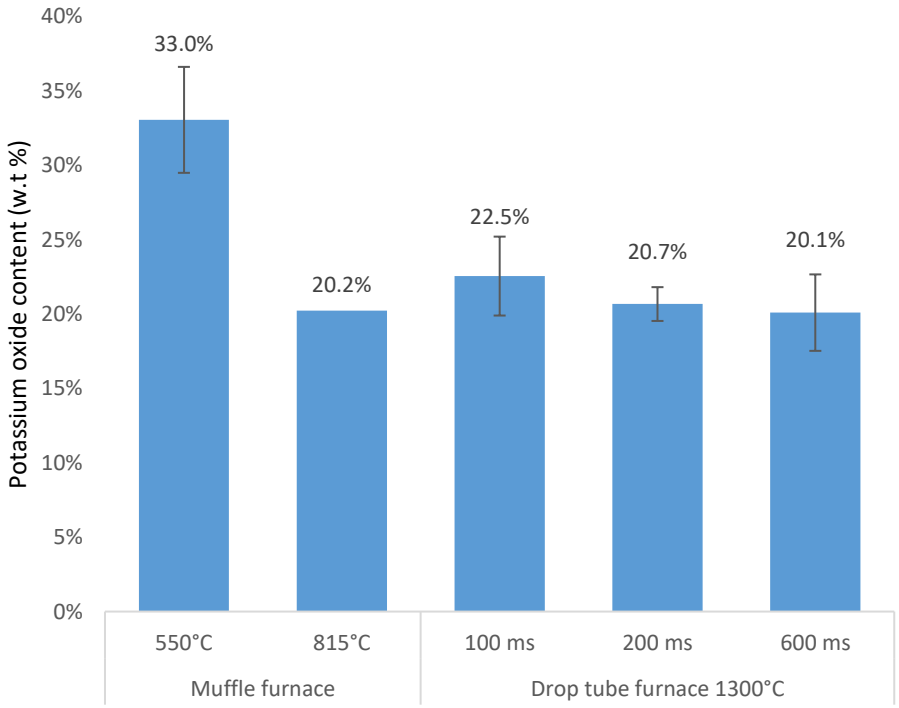

Figure 5.11. Potassium oxide content in olive cake ash produced at different residence times

The baseline levels of potassium oxide in olive cake ash produced under the conditions used in the experiment are shown in Figure 5.11. When compared to the level of potassium in ash produced at 815°C in the muffle furnace it can be seen that 600 ms firing results in a similar level of potassium loss. This decreases [slightly], however, as the residence time is reduced. This suggests that at shorter residence times, not all of the volatile potassium is released. This is accounted for when measuring the retention rates but it is an early indicator that there may be some variation in the results found when the kaolin additive is used.

5.6.1 Experimental procedure

For each of the three tests, a 1:1 ratio of olive cake ash (produced at 550°C) to kaolin clay was used. The samples were all pre-mixed prior to firing. The tests were all run in triplicate. The gas mixture for each run was 10% O_2 in N_2. The gas flow rate for the 600 ms run was 12.1 L/min and the probe separation was set at 65 cm. The furnace temperature was set at 1325°Cto give an exposure temperature of 1300°C. For the 200 ms run the overall gas flow rate was 12.3 L/min and the probe separation was 22 cm. The furnace temperature was set at 1400°C to provide the same exposure temperature of 1300°C to the particles in the stream. To achieve final residence time of 100 ms, the probe separation was 15 cm, with an overall gas flow rate of 16.7 L/min. The furnace was set to 1420°C to ensure the exposure temperature remained at 1300°C.

5.6.2 XRF Analysis

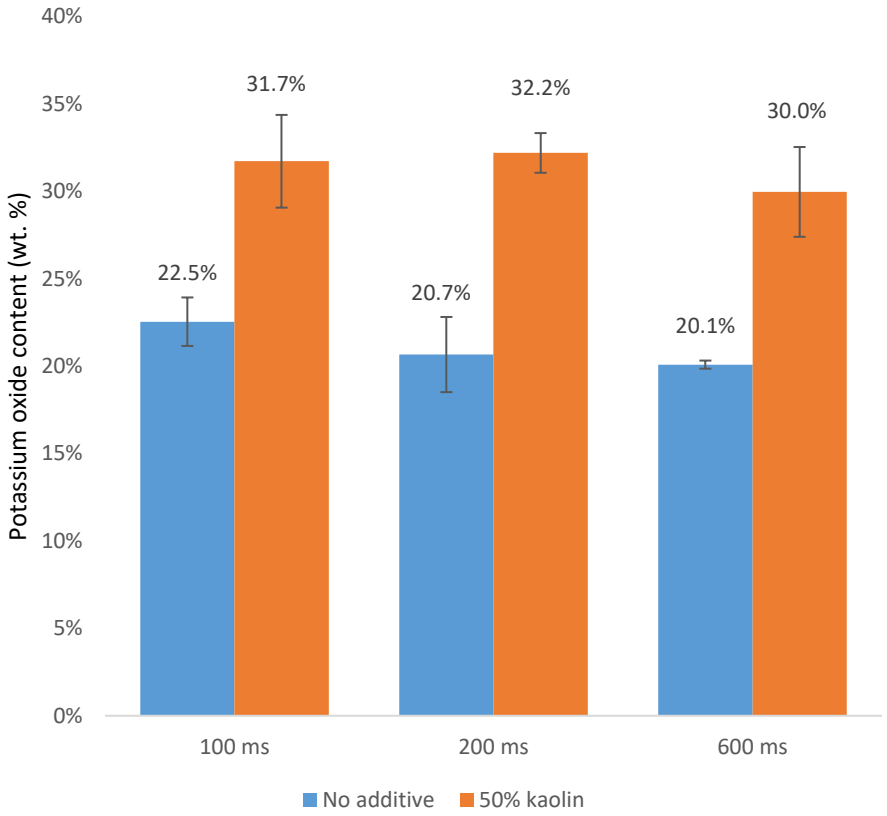

Figure 5.12. Potassium oxide content of olive cake ash produced at 1300°C for different residence times with and without kaolin

The results for volatile potassium oxide retention are shown in Figure 5.13. At the shortest residence time of 100 ms, the mean level for potassium retention was 87%. At 200 ms the mean retention rate was 93%. These were both higher that the retention found at 600 ms (76%). However, all of the results fall within experimental error and no clear trend can be seen.

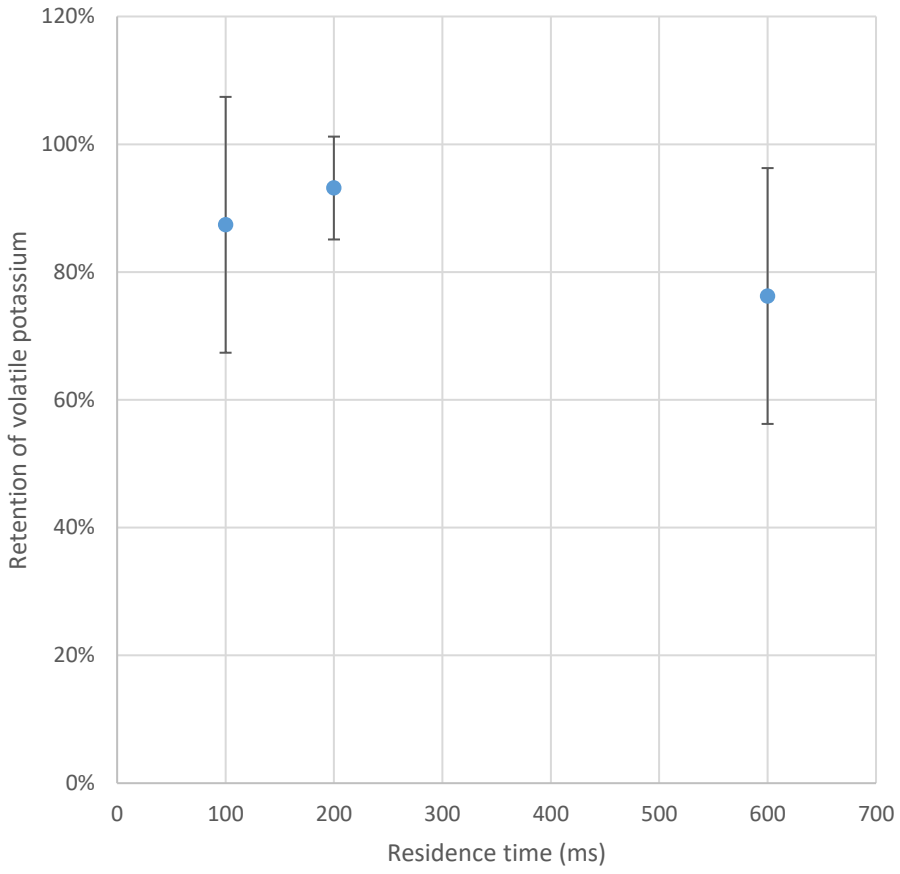

Figure 5.13. Retention of volatile potassium oxide at different residence times

5.6.3 Conclusions

High levels of retention of volatile potassium were found for all three residence times at 1300°C. The mean values found at the shorter residence times of 100 and 200 ms were slightly higher than the level of retention at 600 ms. However, the results for each residence time fall within experimental error of each other, and don't appear to describe a trend. Nonetheless, there is no evidence of a reduction in the completion of the reaction that occurs as a result of reducing the residence time.

5.7 Other feedstocks – miscanthus and wood

To get an understanding of how the reaction between potassium and kaolin might change with different biomasses, two further feedstocks were tested –

miscanthus and wood. Olive cake is a high ash, high alkali metal content biomass and sourced from the waste of an industrial process. Miscanthus was chosen as a biomass source with a medium ash content and medium alkali metal content. Tests were conducted on miscanthus at 1150°C and 1300°C in a one to one ratio by mass of kaolin to mass of 550°C ash. At 550°C the ash yield of miscanthus is 3.6%. This lower ash content of miscanthus means that the 1:1 additive ratio of ash to kaolin would equate to 3.6% kaolin when firing with the raw feedstock. After ashing at 550°C, the mean potassium oxide content of miscanthus ash is 10.9% (Figure 5.14).

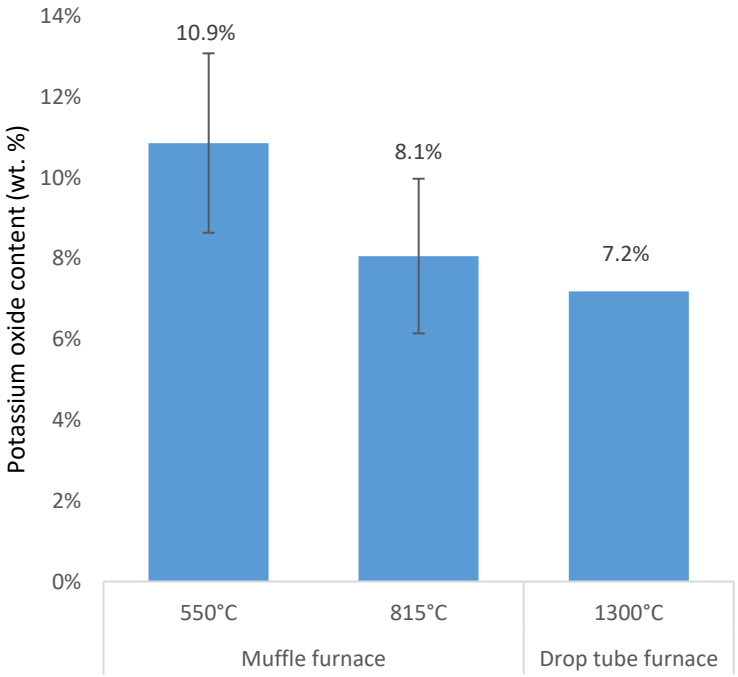

Figure 5.14. Graph to show the weight percentage of potassium oxide in miscanthus ash prepared at different temperatures

When comparing that with the remaining potassium after ashing at 815°C, there was a loss of 25.8% when going from 550°C to 815°C. A slightly lower potassium content was found after drop tube furnace combustion at 1300°C than was found after ashing at 815°C in the muffle furnace. It is possible that

this is because more potassium is volatilised at the higher temperature. However, this isn't the case with olive cake where both of the higher temperatures yielded similar losses of potassium. For the tests with olive cake it was determined that ashing at 815°C was sufficient to volatilise all available potassium. When also considering that the absolute values for potassium are significantly lower in miscanthus than in olive cake and that the relative error is greater, it was concluded that the same determination could be made.

Following the experiments with miscanthus, a single kaolin additive experiment was conducted with wood. As with the miscanthus tests, an ash/additive ratio of 1:1 was used. The ash yields of the wood used are 0.34% at 550°C and 0.26% at 815°C. The potassium oxide content of the wood ash produced at 550°C and 815°C are shown in Figure 5.15. The loss of potassium from 550°C to 815°C is 42%.

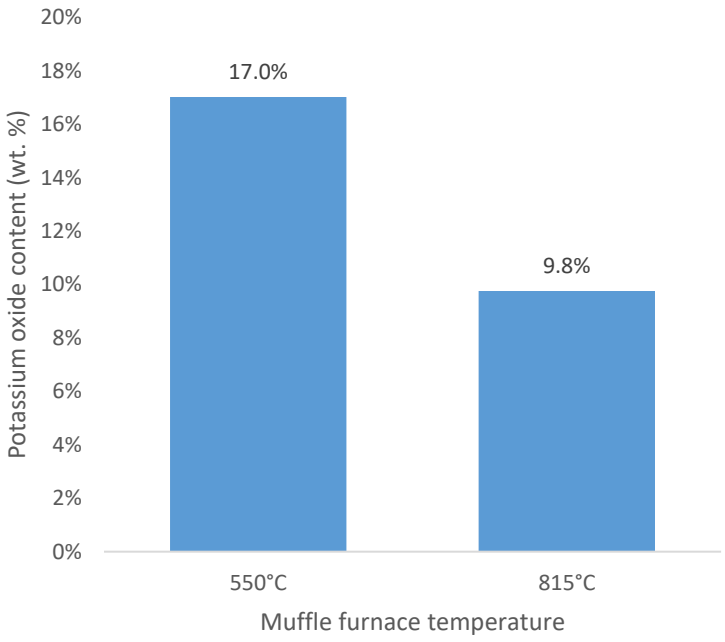

Figure 5.15. Graph to show the weight percentage of potassium oxide in wood ash prepared at different temperatures

5.7.1 Experimental procedure

Three runs were completed for miscanthus ash with kaolin in a 1:1 ratio at 1150°C in the drop tube furnace. The same parameters for temperature setting, gas content, gas flow rate and probe separation were used as for all other previous runs at that temperature. For the 1300°C test, six runs were completed, each on a 1:1 miscanthus ash to kaolin ratio.

For the wood ash test, a single run was completed at 1300°C in the drop tube furnace on a 1:1 wood ash to kaolin ratio. The ash collected for all experiments was analysed by XRF.

5.7.2 XRF Analysis

The XRF data for the experiments conducted with miscanthus are shown in Figure 5.16. It can be seen that there are high levels of potassium oxide in the drop tube furnace ashes of the miscanthus/kaolin mixtures with a higher measured value for 1150°C than 1300°C. This is as expected for the presence of kaolin at those temperatures and suggests a high level of potassium retention caused by the presence of the additive. However, such is the quantity of potassium oxide in the samples, it would appear that greater than 100% of potassium has been retained in both cases – 148% for the test at 1300°C and 190% for the test at 1150°C. However, it should be considered that the smaller absolute value for potassium (only 10.9% in the 550°C ash), combined with the lower level of volatile potassium, results in greater relative experimental error.

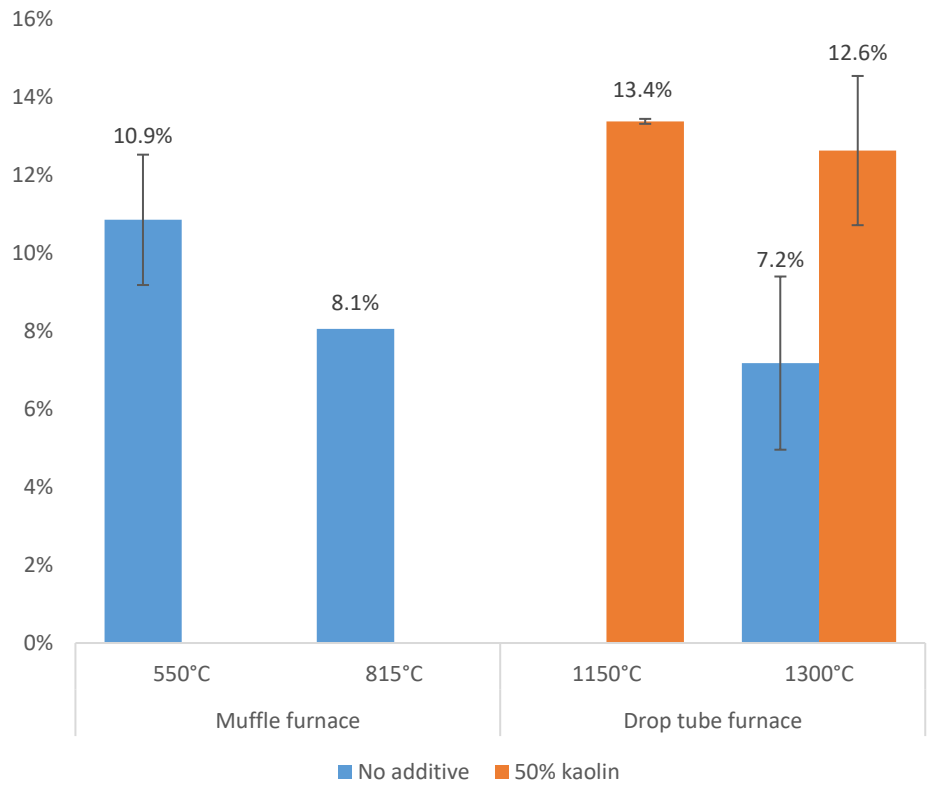

Figure 5.16. Potassium oxide content of miscanthus ash produced at different temperatures with and without kaolin

The potassium oxide content of the experiment undertaken with wood ash and kaolin are shown in Figure 5.17. It was found that in the presence of kaolin, 75.2% of the volatile potassium in the wood ash was retained at 1300°C. This is a high level of retention and is very close to the level of retention found at the same temperature when olive cake was used as the feedstock.

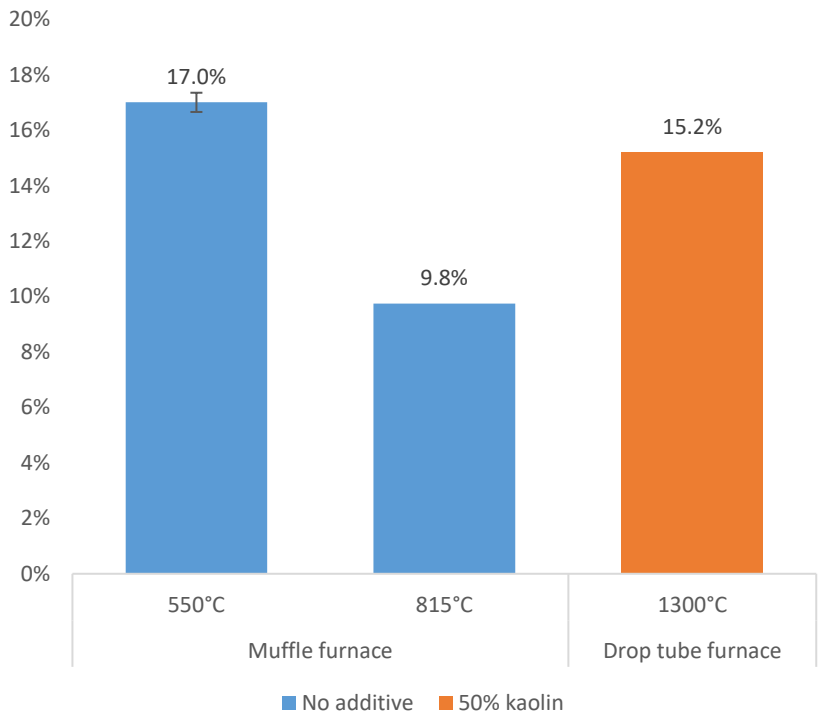

Figure 5.17. Potassium oxide content of wood ash produced at different temperatures with and without kaolin

5.7.3 Conclusions

Miscanthus ash has the lowest potassium content (10.9% in 550°C ash) of the three feedstocks tested in this research and only 25.8% of that potassium is volatile. This equates to only 2.8% of the mass of the 550°C ash – in 550°C olive cake ash, 12.8% of the mass is volatile potassium. With such small quantities of potassium to retain it is therefore more difficult to accurately measure the retention levels that occur due to the presence of the additive. However, for both additive experiments, higher levels of potassium were measured when kaolin was used. Additionally, a higher level of retention was found at 1150°C than at 1300°C, in keeping with the trend found for potassium retention in olive cake.

For the experiment with wood ash and kaolin, it was determined that 75% of the volatile potassium was retained by the presence of kaolin.

5.8 The use of coal fly ash as an additive

The final experiments conducted on the drop tube furnace were devised to compare the use of kaolin with that of coal fly ash. The use of coal fly ash as an aluminosilicate additive is an attractive option due to the significant economic benefits associated with its use as a waste product. The use of coal fly ash an additive has been studied under PF conditions for the combustion of wood and has proved successful in improving the properties of the ash melting temperatures and in reducing the release of gaseous potassium chloride (Wu et al., 2013). Coal fly ash is also used as a slagging and fouling mitigant for the combustion of wood biomass at Drax power plant in Yorkshire, UK (Livingston, 2016). Elemental composition of coal fly ash as provided by Uniper is provided below in Table 5.2. As can be seen from the table, the ash consists mostly of alumina and silica. It is on this basis that the use of coal fly ash is being used as a source of aluminosilicates for biomass addition. There are some key differences in the composition of the coal fly ash used and that of kaolin, however. Most notably, there is a significant level of Fe_2O_3 in the coal fly ash and the ratio of silica to alumina is approximately 2:1 (by wt. %) where in kaolin it is approximately 1:1.

Table 5.2. Elemental composition of coal fly ash

	Coal fly ash
Al_2O_3	22.8
CaO	2.55
Fe_2O_3	10.3

K_2O	2.69
Ni	160 mg/kg
P_2O_5	0.23
SiO_2	48.8
SrO	498 mg/kg
TiO_2	0.95
ZnO	295 mg/kg

Units: wt% (except where specified)

The use of coal fly ash as an additive to mitigate the adverse effects of potassium release during wood combustion is currently underway at Drax power station.

The experiments conducted with the coal fly ash were all in a 50% fly ash to biomass ash ratio. Tests were conducted in the drop tube furnace at 1150°C and 1300°C with olive cake and at 1300°C with wood.

5.8.1 Experimental procedure

For all experiments, a ratio of 1:1 for biomass ash to coal fly ash was used. This was chosen so that a direct comparison could be made between kaolin and coal fly ash on a mass of additive basis. All samples were pre-mixed and fired under the same conditions as those outlined above for the relevant temperatures in the drop tube furnace.

5.8.2 XRF Analysis

The mean results for the potassium oxide levels found in the ash of the experiments conducted with olive cake are shown in Figure 5.18. For the olive cake and coal fly ash test conducted at 1150°C, the mean value for potassium oxide is 27.4%. This equates to a volatile potassium retention of 52.8%. For the olive cake and fly ash test conducted at 1300°C, 21.2% potassium oxide was

measured, yielding a retention of 8.8%. When considering the error, it is not possible to conclude that the presence of the fly ash causes the retention of potassium under these parameters.

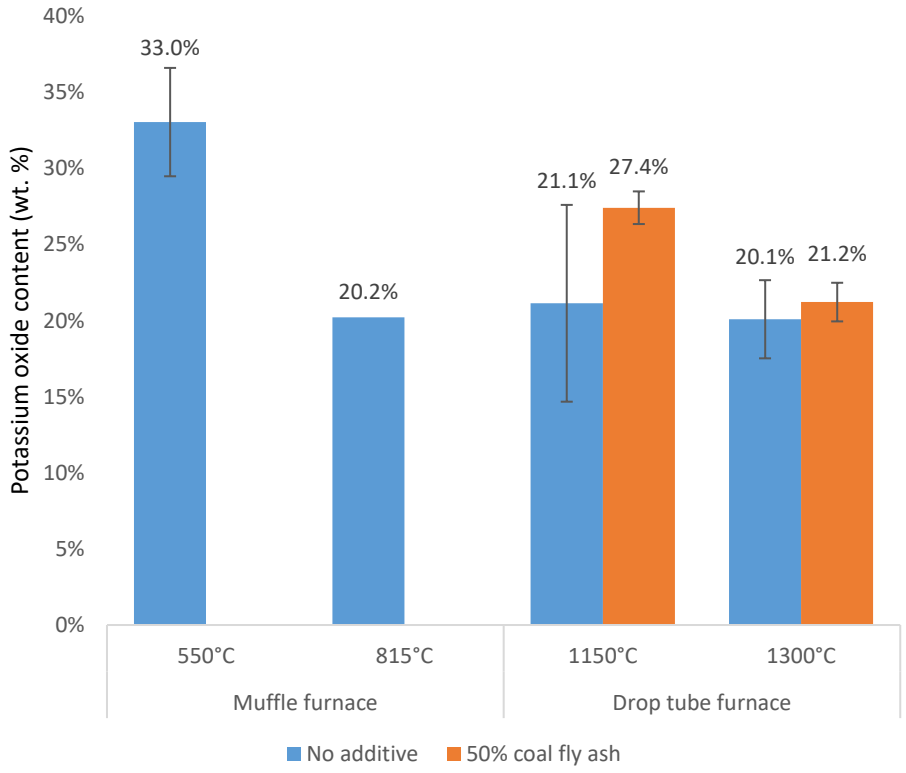

Figure 5.18. Potassium oxide content of olive cake ash produced at different temperatures with and without coal fly ash

The result for the experiment with wood ash and coal fly ash is shown in Figure 5.19. The value for potassium oxide in the ash produced in the drop tube furnace is very close to that for the potassium oxide in the 815°C ash indicating no significant retention as a result of the presence of the coal fly ash additive.

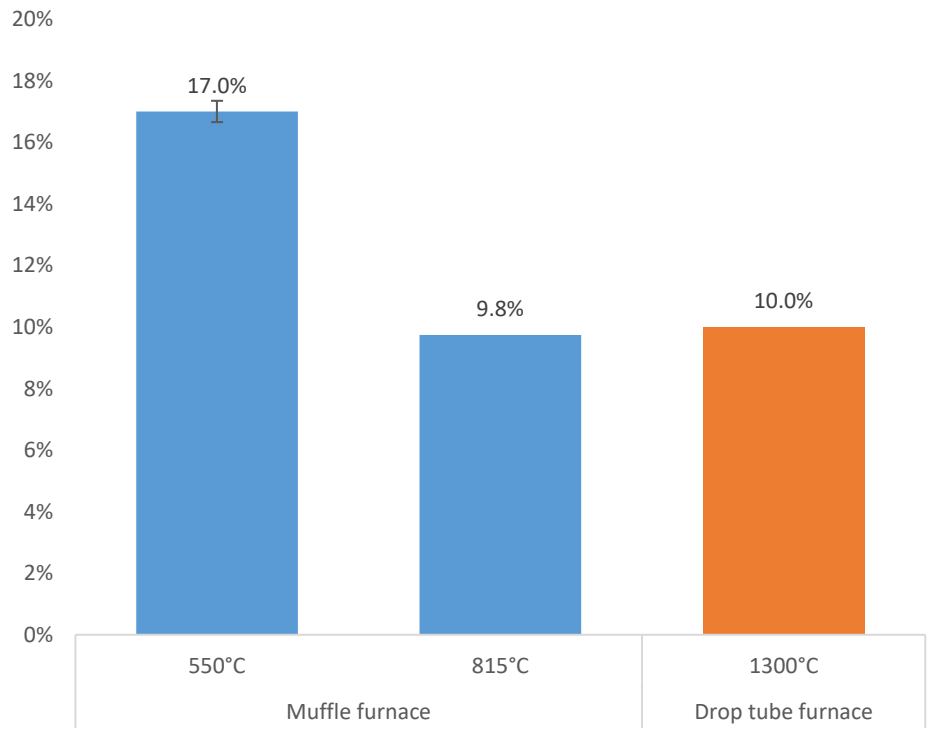

Figure 5.19. Potassium oxide content of wood ash produced at different temperatures in a muffle furnace without any additive and at 1300C in the drop tube furnace with coal fly ash additive

5.8.3 Conclusions

When fired at 1150°C with coal fly ash at a ratio of 1:1 with olive cake ash produced at 550°C, 52.8% of volatile potassium was retained. At this temperature and additive ratio, with kaolin additive instead of coal fly ash, 100% retention was achieved. At 1300°C with the same ratio of 1:1 for coal fly ash and olive cake ash, just 8.8% of potassium was retained. The retention found when kaolin was used under the same conditions was 76.3%.

For the wood ash experiment, with an increase in potassium oxide of only 2% for the single additive experiment, it can be said that no retention was found at 1300°C as a result of the presence of coal fly ash as an additive. When kaolin was used in the same 1:1 ratio with wood ash at 1300°C, 72% of the volatile potassium was retained in the ash.

It can therefore be concluded that when compared on an overall mass of additive basis, that coal fly ash is significantly less effective than kaolin for retaining volatile potassium under the conditions tested.

Where the use of coal fly ash has been reported in literature, higher quantities of additive have proved more effective. Significant improvements in the ash properties of wood have been reported where coal ash was injected at a level four times that of the ash content of the wood (Wu et al., 2013). The reason for this is the lower aluminosilicate content of coal fly ash when compared to kaolin.

6 Characterisation of Combustion Ashes by Mineral Liberation Analysis

6.1 Summary

In this chapter the use of scanning electron microscopy with energy dispersive x-ray spectroscopy is used in conjunction with mineral liberation analysis to characterise the ashes of six different experiments. The experiments tested include drop tube furnace ashes produced at 1150°C and 1300°C with and without kaolin. A sample of 550°C ash was analysed to provide baseline results. A list of mineral phases present within the ash samples has been created and the samples have been mapped. Potassium distribution across all mineral phases is analysed and potassium migration behaviour with and without additives is determined.

6.2 Introduction

The examination of ash particles by the use of scanning electron microscopy is a common method of characterisation. The detection of back-scattered electrons (BSE) provides a signal – the strength of which is determined by the atomic mass of the incident nucleus. This can be used to create a black and white image of the sample where brighter signals indicate the presence of heavier elements. Images produced by BSE detection can be used as a way of determining particle size, composition and shape. The shapes of ash particles can also offer insight into the process of their formation.

Where SEM is used in conjunction with energy dispersive x-ray spectroscopy (EDX), detailed composition data can be acquired. To obtain this, a high-energy

beam of electrons is used to stimulate the emission of characteristic x-rays. By combining both methods it is therefore possible to get a visual picture of the particles in the sample, and the elemental composition of those particles.

6.3 Mineral Liberation Analysis (MLA)

MLA is an analytical technique used for automated processing of SEM data. It allows the rapid identification and characterisation of a large number of particles (>10^4). The MLA software first defines the grain boundaries of particles in the sample by the use of BSE data. To do this a threshold backscatter value must be imposed by the operator. Once this has been applied, all particles detected are analysed by either BSE or EDX to determine the compositions. There are different measurement modes available when using MLA. The measurement mode used in this study was GXMAP (for further details, see section 3.7.3.4). The use of GXMAP allows the rapid characterisation of particle phases by the use of a single EDX point where the phases can be segmented by BSE data alone, but complete x-ray mapping where they cannot. The benefit of this mode is that all particles can accurately be mapped while drastically reducing measurement time.

Once the sample has been analysed, data can be extracted. To do this, the operator must create a mineral list. To acquire composition data from the sample, single spots can be selected and the x-ray spectrum showing the grain composition for that area is provided. The composition can be recorded, given a colour and added to the list. All other phases that match that composition will then be assumed to be the same and will appear in the same colour. Once a list

has been made that accounts for as many different mixtures that exist in the sample as possible, it is possible to group mineral identities together.

6.4 Samples analysed

In total, it was possible for only seven samples to be analysed by SEM-EDX and MLA. It was therefore necessary that the experiments selected for ash characterisation by this method should have the greatest opportunity to show the impact of potassium retention. As such, it was decided that the samples would all be from olive cake and would examine the results of drop tube furnace combustion at two different temperatures, in the presence of kaolin at two different additive ratios. These comprised 40% and 50% kaolin in 550°C olive cake ash fired at 1150°C and 1300°C. In addition, baseline samples of olive cake ash produced at 550°C in the muffle furnace, and 1150°C and 1300°C in the drop tube furnace in the absence of kaolin, were characterised. From the previous chapter, it was found from XRF data that the rate of retention of volatile potassium in ash after combustion at 1150°C was around 80% for the 40% kaolin ratio and 100% for the 50% kaolin ratio. For the same tests conducted at 1300°C, approximate retention rates of 80% and 70% respectively were achieved for the 40% and 50% kaolin tests.

6.5 Individual Mineral Species Analysis

A list of 18 mineral identities was created based on the compositions of the grains present across all the samples. This is not a list of specific compounds or minerals that all have easily definable formulae, rather it is a list of the mineral phases that were found to be present, as identified by their relative

compositions. In some cases, such as with quartz, calcite and kaolinite, specific minerals were clearly found and are listed. However, for many of the phases, due to their formation at high temperature, no appropriate specific minerals were expected to be found and so they are named with intentional ambiguity and identified simply by the elements that are present in the largest quantities. The complete list of mineral phases with their defining compositions are shown in Table 6.1 and the colours assigned to them are shown in the legend in Figure 6.1.

Table 6.1. Mineral list with elemental compositions

	Elemental composition (%)											
Mineral	Al	C	Ca	Cl	Fe	K	Mg	Na	O	P	Si	Ti
Quartz	0.0	0.0	0.0	0.0	0.0	0.0	0.0	0.0	53.3	0.0	46.7	0.0
Aluminium Silicate 6%K	22.6	0.0	0.0	0.0	2.0	6.1	1.3	0.5	37.6	0.0	29.1	0.8
CaMgK silicate mixture	4.0	0.0	20.1	0.0	2.2	12.4	9.3	0.3	34.7	2.5	14.4	0.0
Potassium calcium silicate	0.0	0.0	9.2	0.0	0.0	11.9	2.5	4.5	36.5	0.0	35.5	0.0
CaPK oxide	0.0	0.0	34.7	0.0	0.0	13.8	2.3	0.8	31.2	17.3	0.0	0.0
CaMg oxide	1.5	0.0	29.3	0.0	1.1	3.5	36.7	0.0	25.3	1.8	1.0	0.0
Kaolinite	30.2	0.0	0.0	0.0	0.8	0.0	0.0	0.0	39.1	0.0	28.9	1.0
Aluminium silicate 17%K	21.6	0.0	0.0	0.0	0.5	17.6	0.0	0.0	38.5	0.0	21.5	0.5
Carbon mixture	1.6	9.2	8.4	1.1	2.5	1.9	2.5	0.0	70.0	0.0	2.7	0.0
Calcite	0.0	12.0	40.0	0.0	0.0	0.0	0.0	0.0	48.0	0.0	0.0	0.0
K oxide	0.0	0.0	0.0	0.0	0.0	63.3	0.0	0.0	36.7	0.0	0.0	0.0
CaKAlSi oxide mix 1	13.8	0.0	26.0	0.0	0.0	12.5	0.1	0.3	33.6	1.5	12.3	0.0
KCaAlSi oxide mix 2	13.4	0.0	13.9	0.2	0.0	21.7	0.0	0.0	34.9	3.9	12.1	0.0
K-bearing Mg Silicate	0.0	0.0	0.0	0.0	0.0	5.4	21.0	0.0	40.7	0.0	32.9	0.0
KSiP mix	0.0	0.0	0.0	0.9	0.0	36.4	0.2	2.3	43.1	4.3	12.7	0.0
P containing K oxide	0.0	0.0	0.0	1.0	0.0	61.3	0.0	1.7	25.5	8.3	2.2	0.0
K chlorine mix	0.0	0.0	0.0	4.4	0.0	53.6	0.0	1.4	40.6	0.0	0.0	0.0
Labradorite	15.9	0.0	8.8	0.0	0.0	0.0	0.0	3.4	47.1	0.0	24.8	0.0

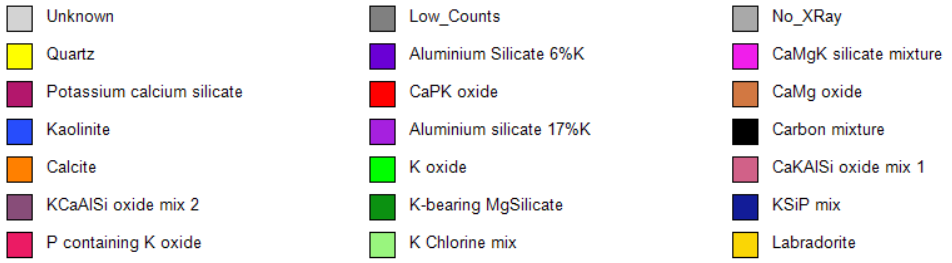

Figure 6.1. Legend of mineral colours used in MLA images

Sample BSE and MLA images of olive cake ash produced at 550°C in the muffle furnace, and 1150°C and 1300°C in the drop tube furnace are shown in Figures

6.2-4. Immediately clear in the images are the differences between the ash produced at low temperature in the muffle furnace and the ashes produced at high temperature in the drop tube furnace.

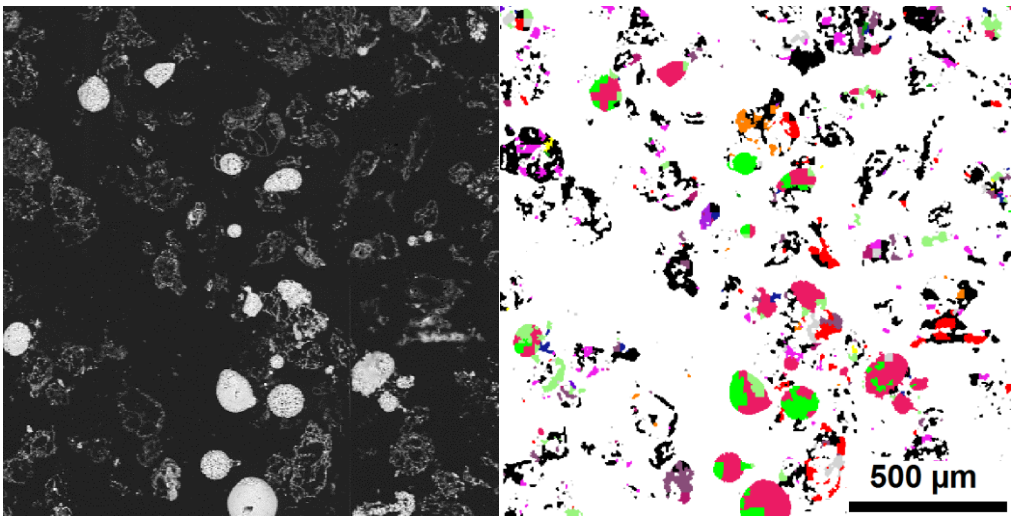

Figure 6.2. BSE image (left) and MLA image (right) of 550°C olive cake ash

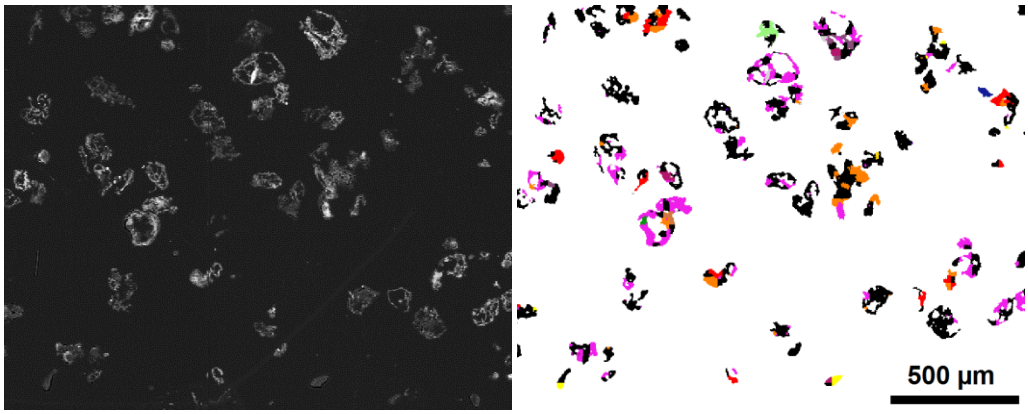

Figure 6.3. BSE image (left) and MLA image (right) of 1150°C olive cake ash

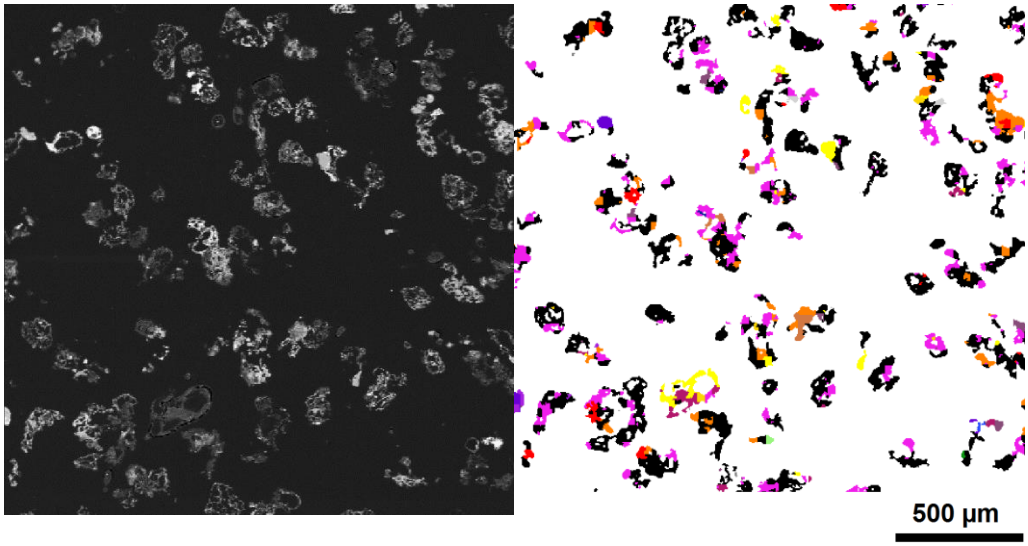

Figure 6.4. BSE image (left) and MLA image (right) of 1300°C olive cake ash

When initially assessing the images by eye, while the drop tube furnace ashes appear to consist of similar minerals, the lower temperature ash has a greater spread of colours, suggesting more diversity in its constituent mineral particles. Additionally, in the BSE image of the 550°C ash, there are several particles of high intensity which are absent in the drop tube furnace ash samples. These correspond with areas of bright green and magenta on the MLA image indicating that they are comprised primarily of potassium oxide. This is as expected and demonstrates the presence of volatile potassium in the 550°C which is lost at higher temperatures. It is this potassium that is expected to be present – bound to aluminosilicates – in the ashes produced at high temperatures with the kaolin additive.

With the MLA it is possible to approximately quantify the association between minerals and the distribution for each element across the mineral phases. In Table 6.2, the relative distribution of potassium across the full list of mineral phases in ash produced at the three different temperatures, without any additive, is shown. The list is in descending order of potassium content in 550°C ash. In the 550°C ash, the mineral phases containing the most potassium are as follows:

- "P containing K oxide". This consists of 61.3% K, 25.5% O, 8.3% P, 2.2% Si, 1.7% Na, and 1% Cl
- "K chlorine mix" containing 53.6% K, 40.6% O, 4.4% Cl and 1.4% Na
- K_2O

The quantities of all three of these phases reduce almost to zero after combustion in the drop tube furnace. It would therefore appear that most of the volatile potassium in the 550°C ash is lost from phases containing potassium oxide and potassium chloride. Meanwhile, the relative levels of potassium in silicate phases appears to remain level, or increase significantly, after drop tube furnace combustion.

Table 6.2. Potassium distribution across mineral phases in olive cake ash

Temperature	550°C	1150°C	1300°C
P containing K oxide	31.94	0.00	0.37
K Chlorine mix	19.36	0.92	1.32
K oxide	12.10	0.09	0.04
CaMgK silicate mixture	8.61	45.82	41.17
Carbon mixture	7.31	30.93	25.54
KCaAlSi oxide mix 2	7.18	6.19	8.44
CaPK oxide	5.47	7.88	10.63
KSiP mix	5.06	0.57	1.72
Potassium calcium silicate	1.32	1.28	4.03
Aluminium silicate 17%K	1.22	4.83	4.41
K-bearing Mg silicate	0.14	0.16	0.11
CaMg oxide	0.13	0.24	0.53
CaKAlSi oxide mix 1	0.09	0.36	0.60
Aluminium Silicate 6%K	0.07	0.73	1.10
Total	100.00	100.00	100.00

Mineral phases containing no potassium are not shown

These results have not been normalised in any way and so, as the absolute level of potassium decreases by around 40% at the two higher temperatures, the increases that are seen in the relative potassium content of some minerals can be attributed in part to this.

Figures 6.5 & 6.6 show the ash created from the combustion of olive cake at 1150°C in 40% kaolin and 50% kaolin respectively. The kaolin additive itself (blue in the MLA image) is very conspicuous in these samples. Also visible in

abundance are the purple potassium aluminium silicate species. The values for volatile potassium retention in these samples were measured by XRF as approximately 80% & 100% retention.

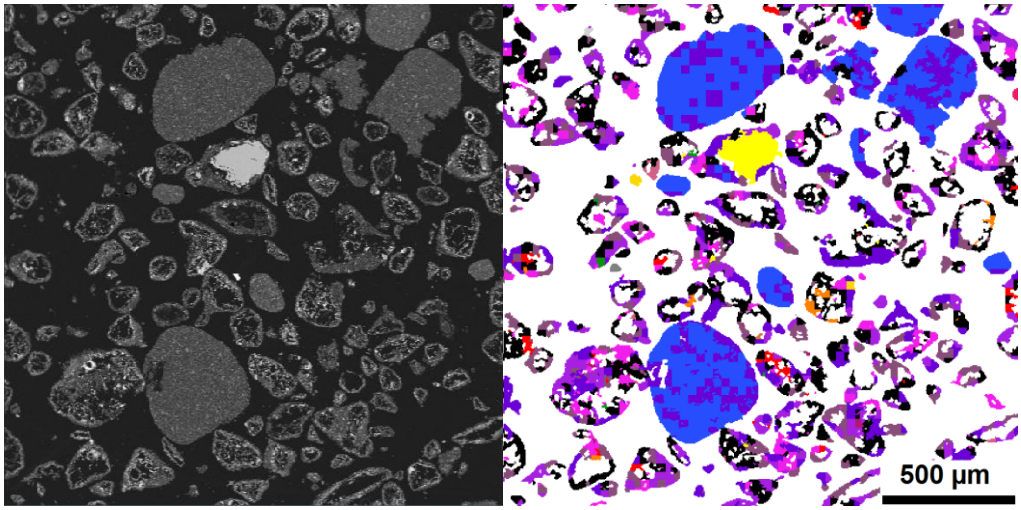

Figure 6.5. BSE image (left) and MLA image (right) for 1150°C olive cake ash with 40% kaolin

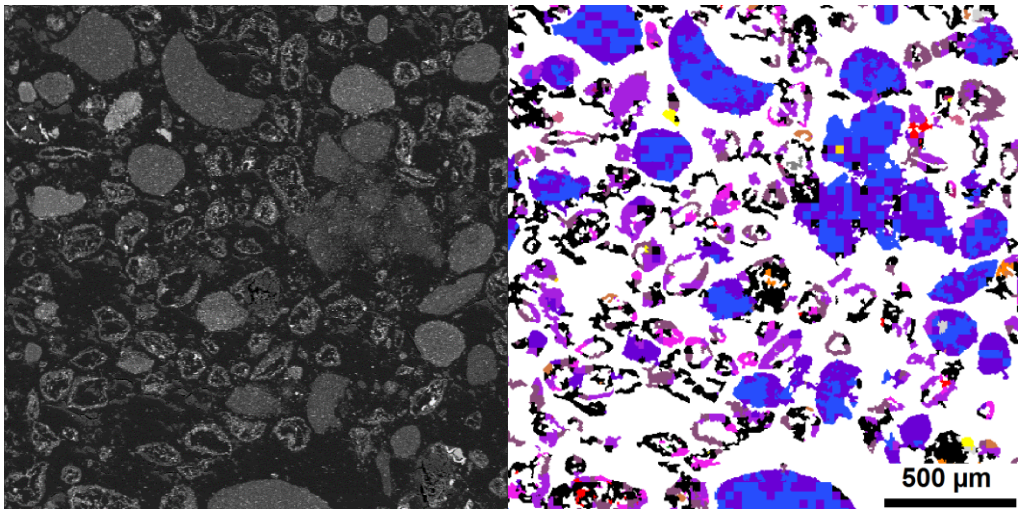

Figure 6.6. BSE image (left) and MLA image (right) for 1150°C olive cake ash with 50% kaolin

BSE and MLA images of the ashes created at 1300°C in 40% and 50% kaolin are shown in Figures 6.7 & 6.8. As with the 1150°C ashes, there is noticeably more purple in the MLA images where additive is used than in the sample of just olive cake ash (Figure 6.4). When compared with the 1150°C runs, it is expected that there should be less potassium in the form of potassium aluminium silicates in

the ash produced at 1300°C as volatile potassium retention was determined to be around 70% for these additive ratios.

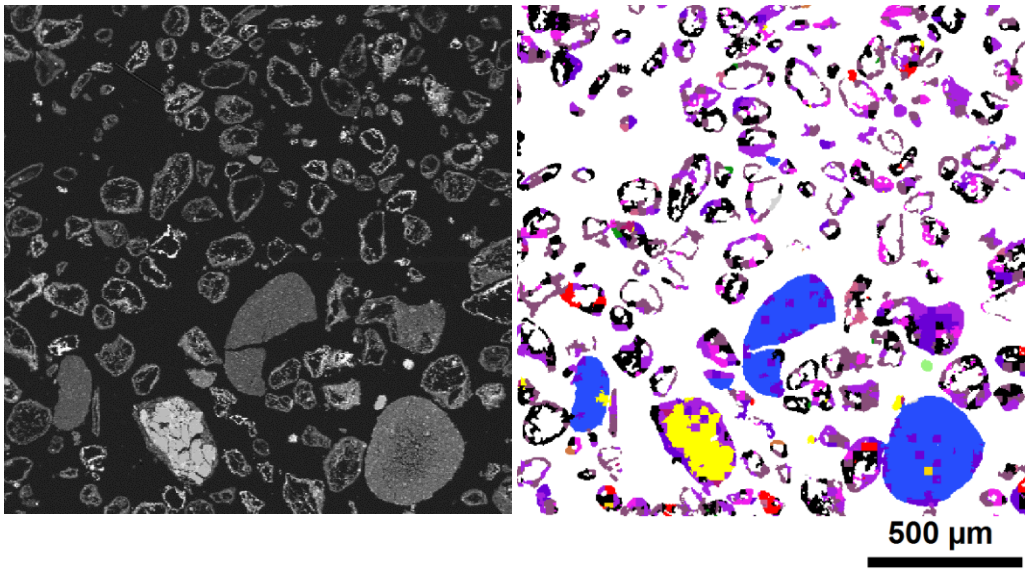

Figure 6.7. BSE image (left) and MLA image (right) for 1300°C olive cake ash with 40% kaolin

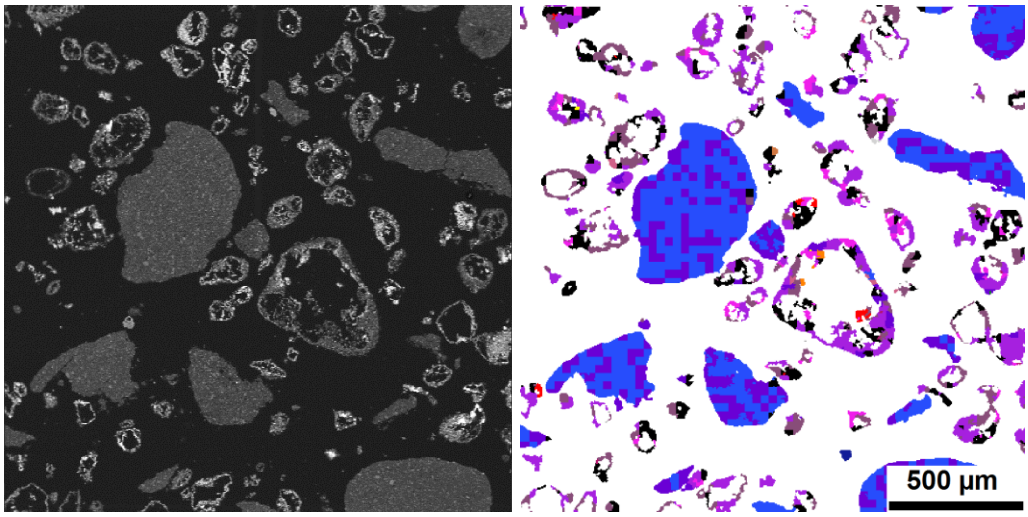

Figure 6.8. BSE image (left) and MLA image (right) for 1300°C olive cake ash with 50% kaolin

The results for potassium distribution across mineral phases in the samples combusted with kaolin are shown in Table 6.3. As with the previous table, the values are in descending order for the distribution of potassium in 550°C olive cake ash. Where the additive is used it can be seen that the distribution of potassium is split primarily between:

- "Aluminium silicate 17%K" (38.5% O, 21.6% Al, 21.5% Si, 17.6% K)

- "KCaAlSi oxide mix 2" (34.9% O, 21.7% K, 13.9% Ca, 13.4% Al, 12.1% Si, 3.9% P)
- "Aluminium silicate 6%K" (37.6% O, 29.1% Si, 22.6% Al, 6.1% K, 2.0% Fe)

Table 6.3. Potassium distribution across mineral phases in olive cake ash and kaolin mixtures

Temperature	550°C	1150°C		1300°C	
Kaolin	**0%**	**40%**	**50%**	**40%**	**50%**
P containing K oxide	31.9	0.1	0.0	<0.1	0.0
K Chlorine mix	19.4	0.1	0.1	0.1	<0.1
K oxide	12.1	0.0	0.0	<0.1	0.0
CaMgK silicate mixture	8.6	8.6	6.3	7.1	5.4
Carbon mixture	7.3	7.4	5.2	5.1	3.6
KCaAlSi oxide mix 2	7.2	30.8	31.9	43.0	36.9
CaPK oxide	5.5	2.3	2.4	2.1	1.5
KSiP mix	5.1	0.1	0.1	0.1	0.1
Potassium calcium silicate	1.3	0.7	0.4	0.4	0.3
Aluminium silicate 17%K	1.2	37.6	38.8	37.2	46.6
K-bearing Mg silicate	0.1	0.1	0.1	0.1	<0.1
CaMg oxide	0.1	0.1	0.1	0.1	0.1
CaKAlSi oxide mix 1	0.1	0.7	0.4	0.5	0.5
Aluminium Silicate 6%K	0.1	11.4	14.2	4.3	5.1
Total	100.0	100.0	100.0	100.0	100.0

This provides clear evidence of association between potassium and the kaolin additive. Interestingly, while there is a higher level of the aluminosilicate with 6% potassium at 1150°C than at 1300°C, there is a higher level of the aluminosilicate with 17% potassium at 1300°C. What is also noticeable is that minerals which are not expected to increase in the presence of the additive such as "carbon mixture" (70% O, 9.2% C, 8.4% Ca, 2.7% Si, 2.5% Fe, 2.5% Mg, 1.9% K, 1.6% Al, 1.1% Cl) and "CaMgK silicate mixture" (34.7% O, 20.1% Ca, 14.4% Si, 12.4% K, 9.3% Mg, 4.0% Al) were seen to remain fairly constant or even decrease, where without the additive they increased. To better understand this data it is possible to normalise the potassium distributions based on the level of retention of potassium as measured by the XRF data

obtained for these experiments. This was done relative to the potassium level in the 550°C ash. Relative to the measured value for potassium in 550°C ash (33.1%), ash produced in the drop tube furnace at 1150°C with no additive has a potassium yield of 63.8%. Therefore, to normalise to the level in 550°C ash, the potassium distribution values for the 1150°C ash was all multiplied by 63.8%. This gives a sum of all parts of 63.8% and is therefore a measure of potassium that is comparable with the starting material. This was repeated for 1150°C ash with 40% kaolin (potassium yield: 93.8%). At 1150°C with 50% kaolin, 100% of the K_2O was retained and so the value for potassium, relative to the 550°C, remains the same. The normalised values for 1150°C are seen in Table 6.4 and for 1300°C in Table 6.5.

Table 6.4. Potassium distribution across mineral phases for 1150°C experiments - normalised to potassium level in 550°C ash

Temperature	**550°C**	**1150°C**		
Kaolin addition	0%	0%	40%	50%
P containing K oxide	31.9	0.0	0.1	0.0
K Chlorine mix	19.4	0.6	0.2	0.1
K oxide	12.1	0.1	<0.1	0.0
CaMgK silicate mixture	8.6	29.3	8.1	6.3
Carbon mixture	7.3	19.8	7.0	5.2
KCaAlSi oxide mix 2	7.2	4.0	29.0	31.9
CaPK oxide	5.5	5.0	2.2	2.4
KSiP mix	5.1	0.4	0.1	0.1
Potassium calcium silicate	1.3	0.8	0.6	0.4
Aluminium silicate 17%K	1.2	3.1	35.2	38.8
K-bearing MgSilicate	0.1	0.1	0.1	0.1
CaMg oxide	0.1	0.2	<0.1	0.1
CaKAlSi oxide mix 1	0.1	0.2	0.7	0.4
Aluminium Silicate 6%K	0.1	0.5	10.7	14.2
Total	100.0	63.8	93.8	100.0

Table 6.5. Potassium distribution across mineral phases for 1300°C experiments - normalised to potassium level in 550°C ash

Temperature	550°C	1300°C		
Kaolin addition	0%	0%	40%	50%
P containing K oxide	31.9	0.2	<0.1	0.0
K Chlorine mix	19.4	0.8	0.1	<0.1
K oxide	12.1	0.0	<0.1	0.0
CaMgK silicate mixture	8.6	25.0	6.5	4.9
Carbon mixture	7.3	15.5	4.7	3.3
KCaAlSi oxide mix 2	7.2	5.1	39.5	33.5
CaPK oxide	5.5	6.5	1.9	1.3
KSiP mix	5.1	1.1	0.1	0.1
Potassium calcium silicate	1.3	2.5	0.4	0.3
Aluminium silicate 17%K	1.2	2.7	34.2	42.3
K-bearing MgSilicate	0.1	0.1	0.1	0.0
CaMg oxide	0.1	0.3	0.1	0.1
CaKAlSi oxide mix 1	0.1	0.4	0.4	0.4
Aluminium Silicate 6%K	0.1	0.7	4.0	4.6
Total	100.0	60.8	92.0	90.8

With these values normalised to the potassium yield for each sample - relative to the olive cake ash – it is possible to see potassium migration across phases. This can be represented graphically by finding the difference in relative potassium content between each experiment and the 550°C baseline (Figures 6.9 & 6.10).

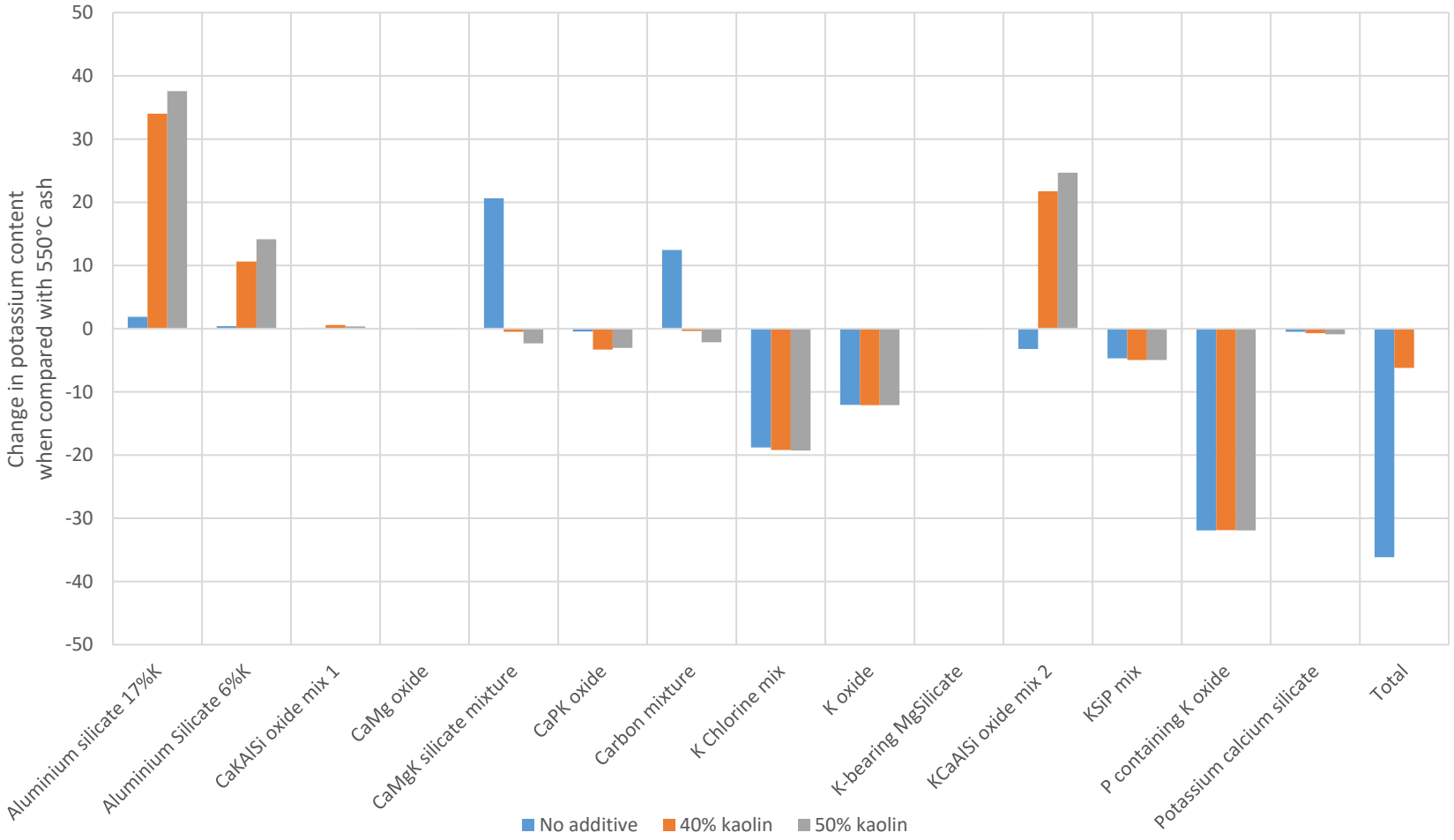

Figure 6.9. Change in potassium distribution from 550°C ash for experiments at 1150°C

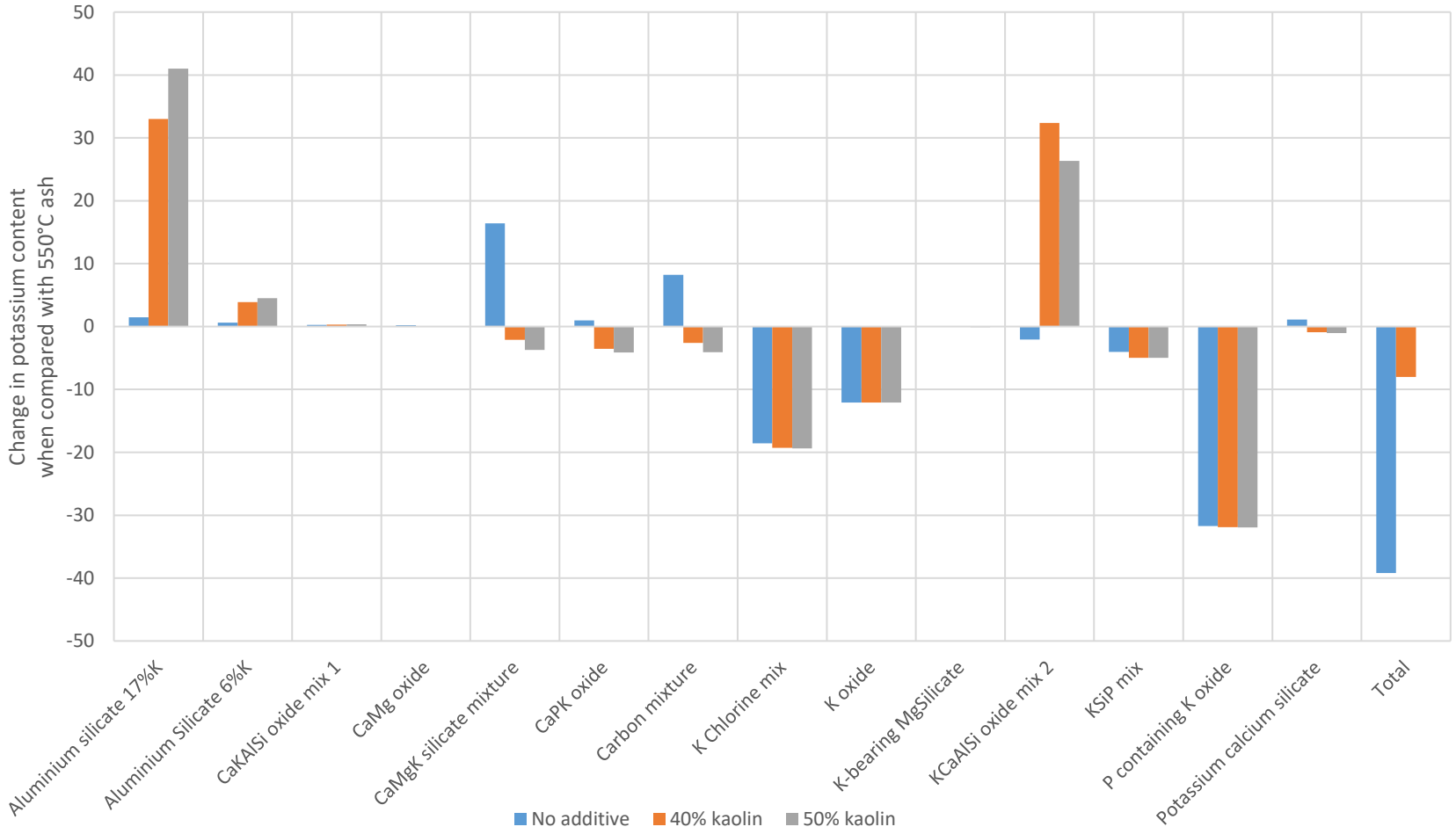

Figure 6.10. Change in potassium distribution from 550°C ash for experiments at 1300°C

In both graphs the loss of volatile potassium can be seen from the potassium oxide and chloride phases with and without additive. Where no additive is used, there is an increase in “CaMgK silicate mixture” and “carbon mixture”. This evidences migration of potassium during combustion. In the presence of kaolin it appears that this migrating potassium preferentially reacts with the additive to create potassium aluminium silicates.

6.6 Further Analysis and Interpretation of Identified Mineral Phases

The mineral phases found in combustion products are difficult to interpret fully as they are combustion products, not pure minerals. However, it is possible to speculate as to the likely formed compounds based on the elemental ratios present. To do this, the elemental ratios for each mineral phase should be represented on a molar basis rather than by weight percentage. The molar ratios of elements present in four different potassium containing mineral phases are shown with respect to the potassium content in Table 6.6. These four mineral phases were all shown (in Figure 6.9 and Figure 6.10) to be volatile during high temperature combustion.

Table 6.6. Elemental composition data of volatile potassium species on weight-percentage and molar basis

	Al	C	Ca	Cl	Fe	K	Mg	Na	O	P	Si
"K chlorine mix"											
Wt. %	0.0	0.0	0.0	4.4	0.0	53.6	0.0	1.4	40.6	0.0	0.0
Moles	0.0	0.0	0.0	0.1	0.0	1.4	0.0	0.1	2.5	0.0	0.0
Rel. to moles K	0.0	0.0	0.0	0.1	0.0	1.0	0.0	0.0	1.9	0.0	0.0
"K oxide"											
Wt. %	0.0	0.0	0.0	0.0	0.0	63.3	0.0	0.0	36.7	0.0	0.0
Moles	0.0	0.0	0.0	0.0	0.0	1.6	0.0	0.0	2.3	0.0	0.0
Rel. to moles K	0.0	0.0	0.0	0.0	0.0	1.0	0.0	0.0	1.4	0.0	0.0
"KSiP mix"											
Wt. %	0.0	0.0	0.0	0.9	0.0	36.4	0.2	2.3	43.1	4.3	12.7
Moles	0.0	0.0	0.0	0.0	0.0	0.9	0.0	0.1	2.7	0.1	0.5
Rel. to moles K	0.0	0.0	0.0	0.0	0.0	1.0	0.0	0.1	2.9	0.1	0.5
"P containing K oxide"											
Wt. %	0.0	0.0	0.0	1.0	0.0	61.3	0.0	1.7	25.5	8.3	2.2
Moles	0.0	0.0	0.0	0.0	0.0	1.6	0.0	0.1	1.6	0.3	0.1
Rel. to moles K	0.0	0.0	0.0	0.0	0.0	1.0	0.0	0.0	1.0	0.2	0.0

It can be seen from the above data that all four mixtures comprise primarily of potassium and oxygen. It is therefore reasonable to assume that all four mixtures contain large quantities of KOH as their principal constituent.

In Table 6.7, elemental compositions on a molar basis – relative to Si content – are shown for "CaMgK silicate mixture" and "carbon mixture". These two mineral phases are of interest because they both exhibited greater representation among the K containing mineral phases following high temperature combustion in the absence of additives. This suggests that where

no additive is used, some potassium (likely volatile KOH) is fixed to form these potassium-containing silicates.

Table 6.7. Elemental composition data of silicate-containing mineral species on weight-percentage and molar basis

	Al	C	Ca	Cl	Fe	K	Mg	Na	O	P	Si
"CaMgK silicate mixture"											
Wt. %	4.0	0.0	20.1	0.0	2.2	12.4	9.3	0.3	34.7	2.5	14.4
Moles	0.1	0.0	0.5	0.0	0.0	0.3	0.4	0.0	2.2	0.1	0.5
Rel. to moles Si	0.3	0.0	1.0	0.0	0.1	0.6	0.7	0.0	4.2	0.2	1.0
"Carbon mixture"											
Wt. %	1.6	9.2	8.4	1.1	2.5	1.9	2.5	0.0	70.0	0.0	2.7
Moles	0.1	0.8	0.2	0.0	0.0	0.0	0.1	0.0	4.4	0.0	0.1
Rel. to moles Si	0.6	8.0	2.2	0.3	0.5	0.5	1.1	0.0	45.5	0.0	1.0

When looking at the data in the table above, it is interesting to note that for both mineral phases, the K to Si ratio is approximately 1:2. The phase "carbon mixture" was named as such due to its high carbon content. When the presence of calcium and magnesium, and its strong abundance of oxygen, are also considered, it is probable that this identified phase contains carbonate compounds such as $CaCO_3$ and $MgCO_3$ (in a ratio of approximately 2:1).

In Table 6.8, the elemental compositions of potassium-aluminium-silicate phases formed during combustion in the presence of the kaolin additive are shown on a molar basis.

Table 6.8. Elemental composition data of potassium-aluminium-silicate mineral phases on weight-percentage and molar basis

	Al	C	Ca	Cl	Fe	K	Mg	Na	O	P	Si
"Aluminium Silicate 6%K"											
Wt. %	22.6	0.0	0.0	0.0	2.0	6.1	1.3	0.5	37.6	0.0	29.1
Moles	0.8	0.0	0.0	0.0	0.0	0.2	0.1	0.0	2.4	0.0	1.0
Rel. to moles Si	0.8	0.0	0.0	0.0	0.0	0.2	0.1	0.0	2.3	0.0	1.0
"Aluminium silicate 17%K"											
Wt. %	21.6	0.0	0.0	0.0	0.5	17.6	0.0	0.0	38.5	0.0	21.5
Moles	0.8	0.0	0.0	0.0	0.0	0.5	0.0	0.0	2.4	0.0	0.8
Rel. to moles Si	1.0	0.0	0.0	0.0	0.0	0.6	0.0	0.0	3.1	0.0	1.0
"KCaAlSi oxide mix 2"											
Wt. %	13.4	0.0	13.9	0.2	0.0	21.7	0.0	0.0	34.9	3.9	12.1
Moles	0.5	0.0	0.3	0.0	0.0	0.6	0.0	0.0	2.2	0.1	0.4
Rel. to moles Si	1.2	0.0	0.8	0.0	0.0	1.3	0.0	0.0	5.1	0.3	1.0

The expected products of the reaction between potassium and kaolin are kalsilite ($KAlSiO_4$) and leucite ($KAlSi_2O_6$). When attempting to identify the presence of either of these reaction products, the obvious starting point is to consider the ratio of Al to Si. In the first mixture: "Aluminium silicate 6%K" there is a ratio of 0.8:1. This could suggest that there is a mixture of both products with mostly kalsilite and some leucite. For "Aluminium silicate 17%K" there is an Al to Si ratio of 1:1, suggesting the presence of just kalsilite. Both of these identified mineral phases are short of the level of potassium that would be present in pure samples of kalsilite or leucite. This is expected to occur where the additive is used in excess. The K to Ca to Al to Si ratio in "KCaAlSi oxide" is 1.2:0.8:1.3:1. This strongly evidences that kalsilite is present in this mixture. It

also would give evidence that K_2CaSiO_4 is present – as reported by Vassilev et al. (Vassilev et al., 2014).

6.7 Grouped Analysis

When using the MLA software, it is possible to group mineral species together. By having only one colour per group in the MLA images, it affords striking visual evidence of mineral association at a glance. From the list of 18 minerals, four groups were created. The groups each consist of a list of identified elemental compositions. The first group was defined as being biomass ash species and consists of a number of potassium and calcium containing species. The list of compositions for this group is provided in Table 6.9.

Table 6.9. Mineral reference list for "biomass ash" group

Biomass ash	Element (%)										
Mineral	Al	C	Ca	Cl	Fe	K	Mg	Na	O	P	Si
CaMgK silicate mixture	4.0	0.0	20.1	0.0	2.2	12.4	9.3	0.3	34.7	2.5	14.4
Potassium calcium silicate	0.0	0.0	9.2	0.0	0.0	11.9	2.5	4.5	36.5	0.0	35.5
CaPK oxide	0.0	0.0	34.7	0.0	0.0	13.8	2.3	0.8	31.2	17.3	0.0
Carbon mixture	1.6	9.2	8.4	1.1	2.5	1.9	2.5	0.0	70.0	0.0	2.7
CaKAlSi oxide mix 1	13.8	0.0	26.0	0.0	0.0	12.5	0.1	0.3	33.6	1.5	12.3
KCaAlSi oxide mix 2	13.4	0.0	13.9	0.2	0.0	21.7	0.0	0.0	34.9	3.9	12.1
K-bearing MgSilicate	0.0	0.0	0.0	0.0	0.0	5.4	21.0	0.0	40.7	0.0	32.9
KSiP mix	0.0	0.0	0.0	0.9	0.0	36.4	0.2	2.3	43.1	4.3	12.7
P containing K oxide	0.0	0.0	0.0	1.0	0.0	61.3	0.0	1.7	25.5	8.3	2.2
K Chlorine mix	0.0	0.0	0.0	4.4	0.0	53.6	0.0	1.4	40.6	0.0	0.0
K oxide	0.0	0.0	0.0	0.0	0.0	63.3	0.0	0.0	36.7	0.0	0.0

For the MLA images this group was coloured red. The next group was defined as originating from the kaolin additive. This group consisted of only one mineral – kaolinite – and was coloured blue. The composition of kaolinite as defined in the mineral list is: Al, 30.2%; Fe, 0.8%; O, 39.1%; Si, 28.9%; Ti, 1.0%.

The third group consists of mixtures containing potassium, alumina and silica. The purpose of this group is to indicate areas of association between potassium

and aluminosilicates. The list of compositions for this group is shown below in Table 6.10. The colour chosen for this group was purple.

Table 6.10. Mineral reference list for "potassium aluminium silicates" group

K Al Silicate mixtures	Element (%)									
Mineral	Al	Ca	Cl	Fe	K	Mg	Na	O	Si	Ti
Aluminium Silicate 6%K	22.6	0.0	0.0	2.0	6.1	1.3	0.5	37.6	29.1	0.8
Aluminium silicate 17%K	21.6	0.0	0.0	0.5	17.6	0.0	0.0	38.5	21.5	0.5

The final group is made up of inert mineral species with no potassium or alumina silica in them. This group includes quartz and calcite and was coloured black. The mineral list for this group is shown in Table 6.11. Figure 6.11 shows the colours used for the grouped MLA images

Table 6.11. Mineral reference list for "biomass minerals" group

Biomass minerals	Element (%)										
Mineral	Al	C	Ca	Cl	Fe	K	Mg	Na	O	P	Si
Quartz	0.0	0.0	0.0	0.0	0.0	0.0	0.0	0.0	53.3	0.0	46.7
CaMg oxide	1.5	0.0	29.3	0.0	1.1	3.5	36.7	0.0	25.3	1.8	1.0
Calcite	0.0	12.0	40.0	0.0	0.0	0.0	0.0	0.0	48.0	0.0	0.0
Labradorite	15.9	0.0	8.8	0.0	0.0	0.0	0.0	3.4	47.1	0.0	24.8

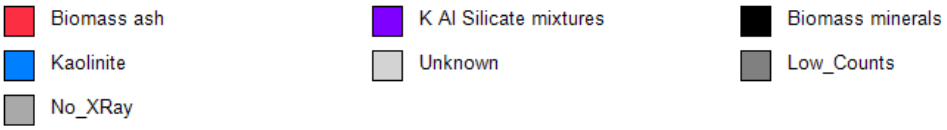

Figure 6.11. Legend of mineral group colours used in MLA images

Figures 6.12-14 shows sample screenshots of BSE images and MLA grouped images of olive cake ash produced at 550°C in the muffle furnace and 1150°C and 1300°C in the drop tube furnace. The MLA grouped images show that in the absence of any additive, the majority of all particles are red. This identifies them as having a composition that most closely matches with those listed in the first mineral list grouping, "biomass ash". This group consists primarily of potassium, calcium, magnesium and phosphorous containing species including silicates and carbonates.

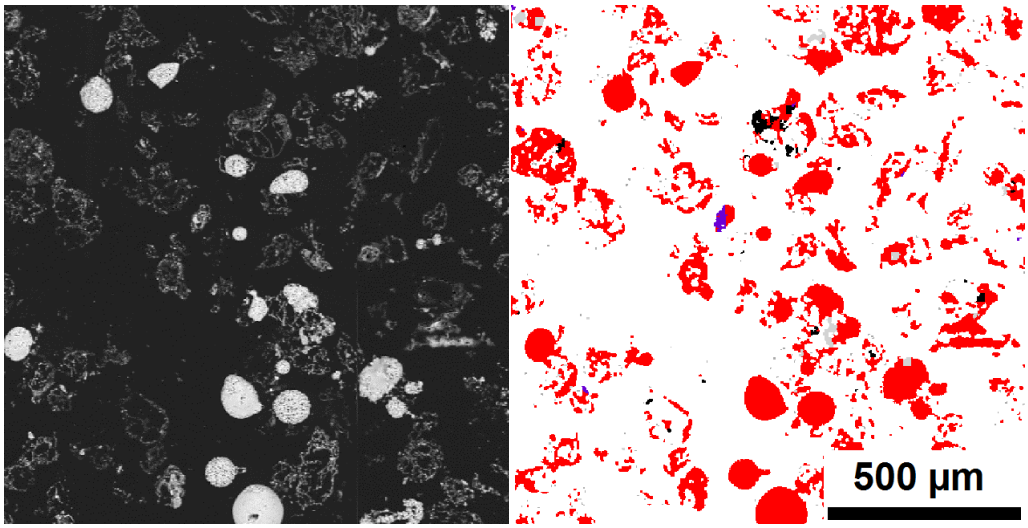

Figure 6.12. BSE image (left) and MLA image (right) of ash particles from the combustion of olive cake ash at 550°C with no additive

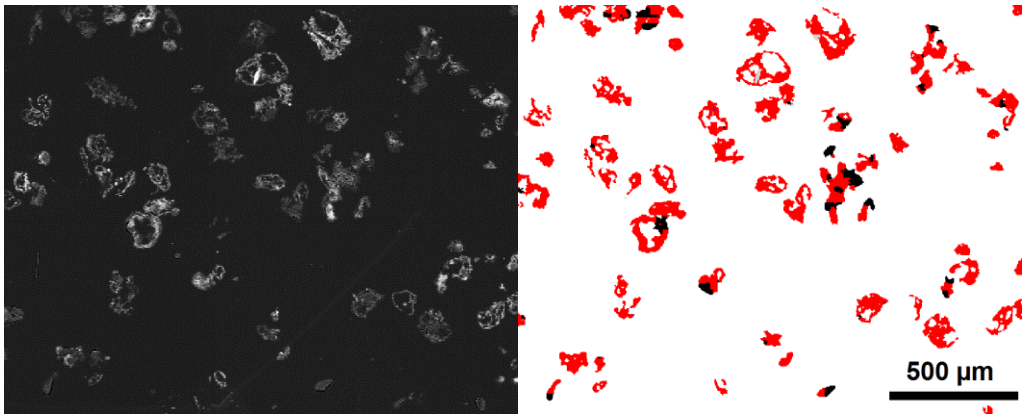

Figure 6.13. BSE image (left) and MLA image (right) of ash particles from the combustion of olive cake ash at 1150°C with no additive

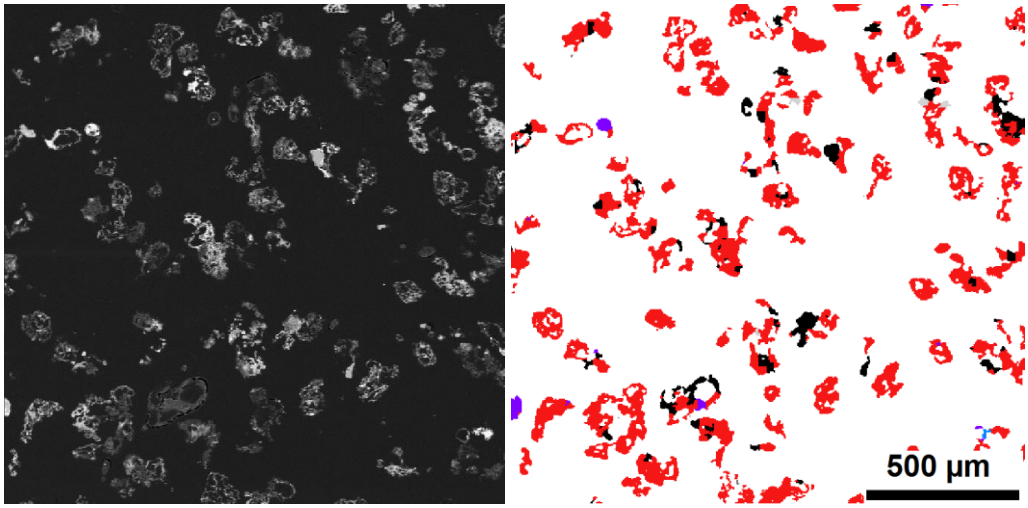

Figure 6.14. BSE image (left) and MLA image (right) of ash particles from the combustion of olive cake ash at 1300°C with no additive

Figures 6.15 & 6.16 show the grouped MLA images of the ashes produced at 1150°C with 40% and 50% kaolin respectively. As with the ungrouped images

of the same samples, the blue kaolinite is immediately identifiable. What is even more striking however is the clear presence of the potassium aluminium silicates. This visually demonstrates the effect of the kaolin additive. There is clear association between the fuel and additive, both in olive cake ash particles (Figure 6.15-A) and in the additive particles (Figure 6.15-B).

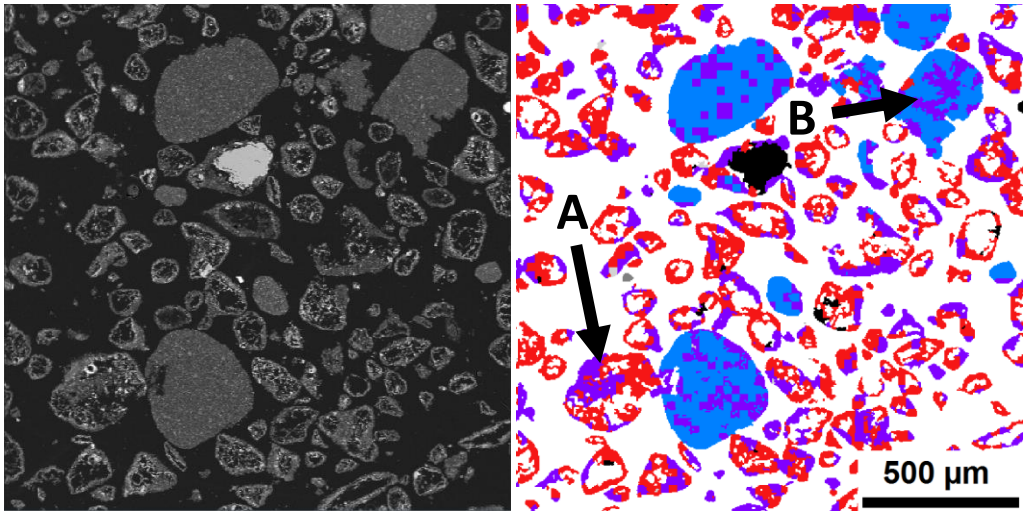

Figure 6.15. BSE image (left) and MLA image (right) of ash particles from the combustion of olive cake ash at 1150°C with 40% kaolin

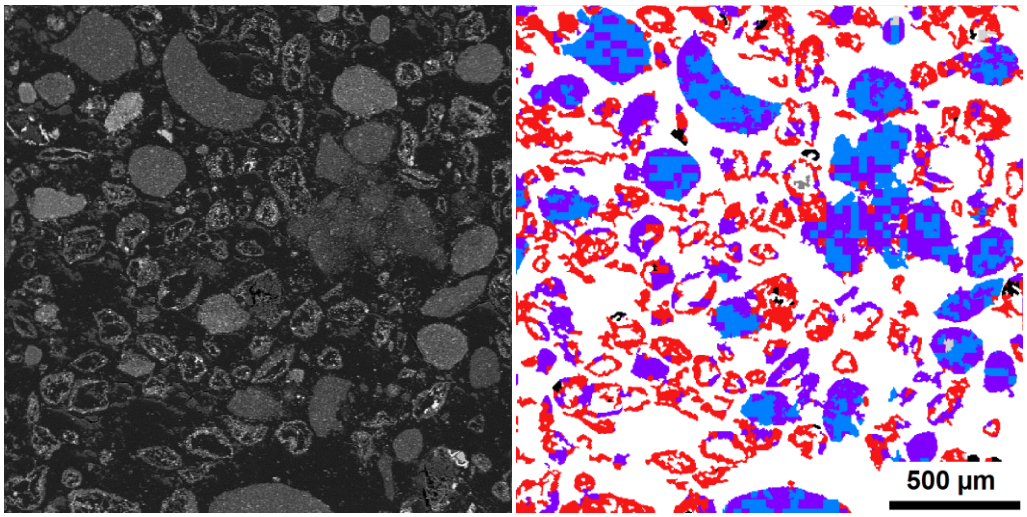

Figure 6.16. BSE image (left) and MLA image (right) of ash particles from the combustion of olive cake ash at 1150°C with 50% kaolin

The ashes from the experiments conducted at 1300°C with 40% and 50% kaolin are shown in Figures 6.17 & 6.18. Once again, the level of association is evidenced by the purple phases.

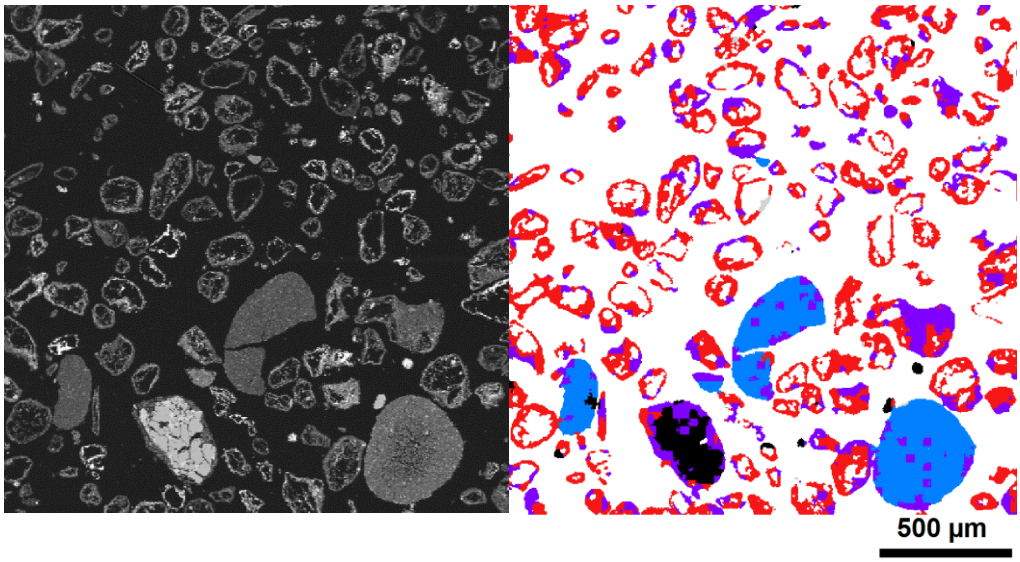

Figure 6.17. BSE image (left) and MLA image (right) of ash particles from the combustion of olive cake ash at 1300°C with 40% kaolin

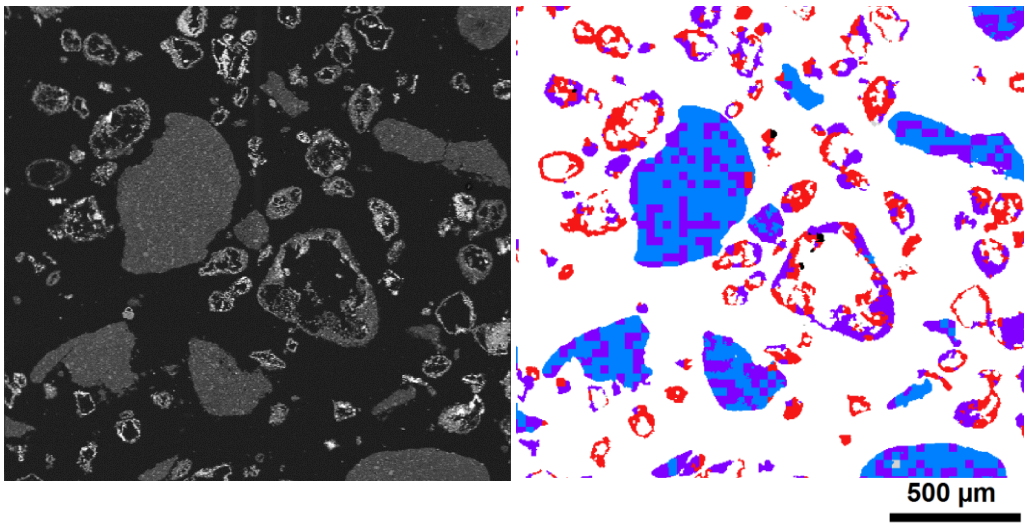

Figure 6.18. BSE image (left) and MLA image (right) of ash particles from the combustion of olive cake ash at 1300°C with 50% kaolin

6.8 Conclusions

The analysis conducted in this chapter provides information on the location of potassium within the ash samples. In the absence of kaolin, olive cake ash samples produced at 1150°C and 1300°C show conclusive evidence of potassium loss in the form of potassium oxide and chloride phases. Additionally, the migration of potassium to calcium containing silicates is clearly observed. In the presence of kaolin, preferential sorption of this migrating potassium into potassium aluminium silicate phases is clearly evidenced.

Furthermore, the majority of volatile potassium (up to 100%) is retained and fixed in these phases.

7 General Discussion and Relevance of Findings

7.1 Introduction

The use of kaolin as an aluminosilicate-based additive for the mitigation of potassium release during combustion of biomass has been investigated at length. Several different combustion conditions (fixed bed and PF) and biomass feedstocks (with different ash/alkali contents) were tested. A comparison between kaolin (as a perfect scenario, single mineral additive) with coal fly ash (as a real world, economically viable/practical additive) was conducted. XRF analysis was used to determine potassium balances. Finally, semi-quantitative mapping of $>10^4$ ash particles by MLA was conducted for a selection of samples to look for corroborating evidence of potassium retention.

7.2 The effect of kaolin on potassium retention in muffle furnace combustion

This was a convenient test that was run for simplicity and for later comparison with DTF experiments. It was found that in the absence of any additive, approximately 40% of K in olive cake was lost during combustion. This is in accordance with research previously reported (Clery et al., 2018). Where kaolin additive was used, moderate increases in ash yield were identified. This increase in mass was then determined to have occurred as a result of retention of potassium in the ash. This was evidenced by the use of alkali metal balances determined by XRF analysis. The highest level of volatile potassium retention measured was 40%. Poor retention was found for the kaolin layer experiment

relative to the quantity of kaolin used. This highlights the importance of mixing the biomass with the additive. In general, the levels of retention found in the muffle furnace at 815°C, were notably lower than those found in the drop tube furnace at higher temperatures. It is expected that the reason for this is that the reaction kinetics will be too slow at this temperature for total conversion to potassium aluminium silicates.

7.3 The effect of kaolin on potassium retention in drop tube furnace combustion of olive cake

These experiments were run as a means of testing the impact of kaolin under conditions representative of PF firing. In the first series of experiments conducted, a range of additive ratios were tested. It was found that as the ratio of additive increased, so did the level of K retention. It was clear that this increase in retention reduced as a threshold value was approached, indicating the kinetic limit for the reaction at that temperature. For the series conducted at 1300°C, this maximum level of retention was found to be of the order of 60-80% of volatile K while at 1150°C, 100% retention of volatile K is reached. These values for retention of K in olive cake are within the same range (70-100%) as previously reported by Clery et al. for the combustion of pellets suspended in air with an aluminosilicate additive (Clery et al., 2018). In Figure 7.1, the measured levels of K retention at 1150°C and 1300°C are shown with a logarithmic curve for each series.

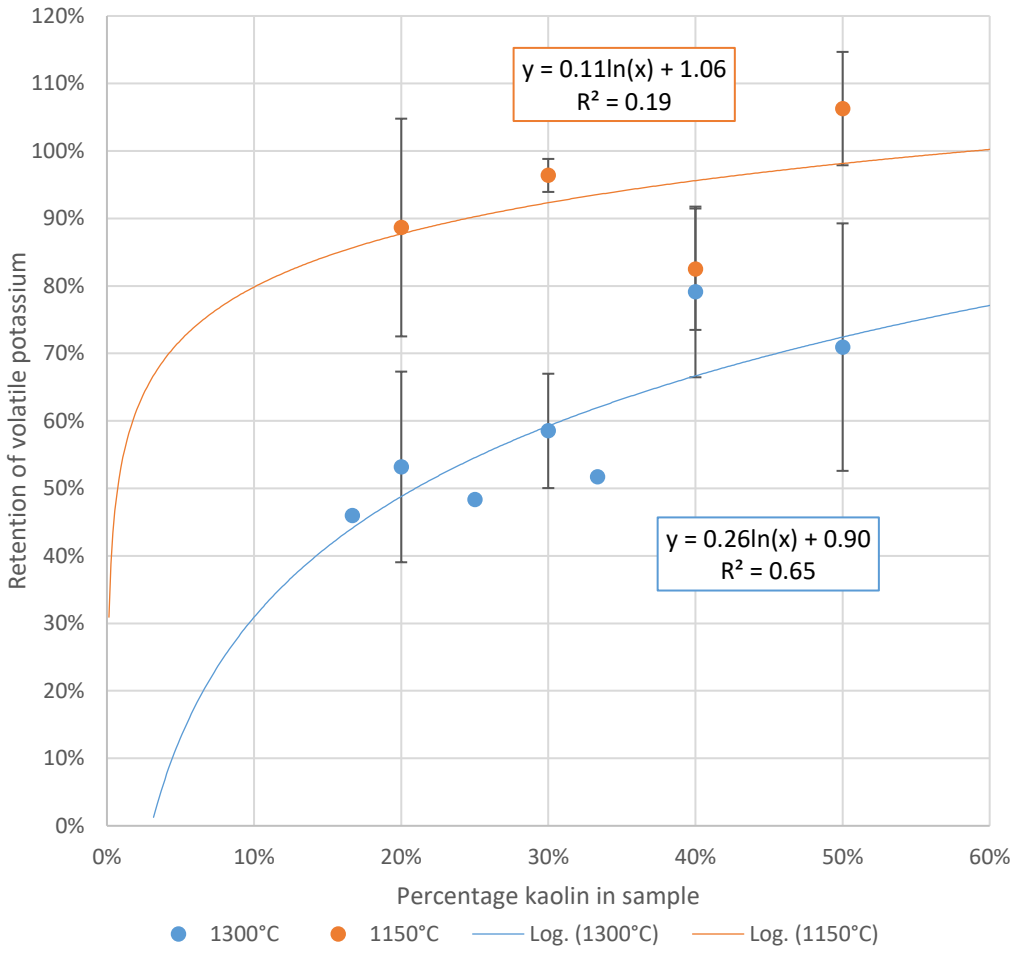

Figure 7.1. Retention of volatile potassium by kaolin addition at two temperatures in the drop tube furnace

It should be noted that these trendlines do not offer a perfect fit as they should both be expected to intercept at the origin. This is reflected in the low r^2 values for both trendlines and is due both to the variation caused by error, and also the lack of data points at very low additive ratios. However, they do offer some insight into the levels of K retention that might be achieved where lower additive ratios are used. They also visually demonstrate the effect of approaching the threshold value for additive ratio for each temperature. For industrial use of additives, it should be expected that the most attractive additive ratio would be the level at which the highest retention is achieved for

the smallest quantity of additive used. At 1300°C, this could be expected to be an additive ratio of 20% (equivalent to a raw fuel additive ratio of approx. 2%) where 50% K retention was measured. At 1150°C, the curve suggests that K retention of approximately 80% could be achieved with an additive ratio of just 10% (equivalent to a raw fuel additive ratio of approx. 1%).

7.4 The effect of temperature on potassium retention in drop tube furnace combustion of olive cake with kaolin

Experiments were conducted at four different temperatures in the DTF to determine the effect of combustion temperature on potassium retention. A curve of potassium retention against combustion temperature was found (Figure 7.2).

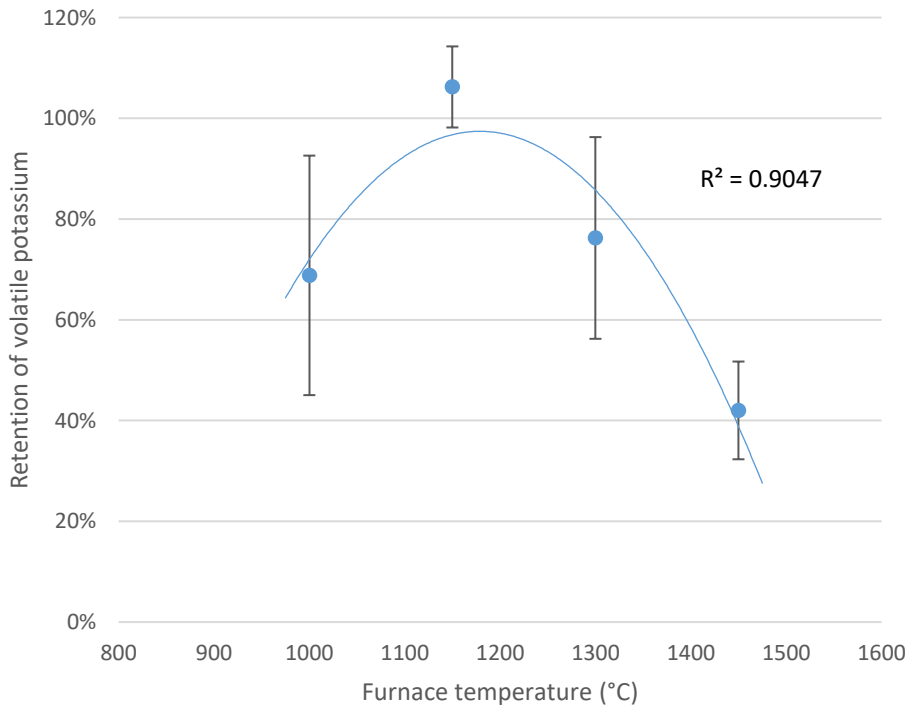

Figure 7.2. Effect of temperature on retention of volatile potassium in the drop tube furnace

At the lowest temperature tested, 1000°C, approximately 70% of volatile potassium was retained. The highest levels of retention were achieved at 1150°C where 100% of volatile potassium was recovered. As temperatures increase above 1150°C, the retention of K decreases. At such high temperatures it is clear that the addition reaction is under thermodynamic control. This was evidenced by the residence time experiment where it was shown that the retention of potassium does not change when shorter reaction times are used.

There are two potential explanations for this reduction in potassium retention at higher temperatures. The first is that the potassium aluminium silicate phases might not be stable or might volatilise at higher temperatures. However, it has been reported that the melting temperatures of the expected reaction products – kalsilite and leucite – are in excess of 1500°C (Yanqing; Niu et al., 2016). This is higher than the temperatures used in any experiments conducted in this research. The second is that the kaolinite might transform at high temperatures and become less susceptible to reaction with potassium. The deleterious effect of this additive degradation has been reported by Zheng et al. in their kinetic study of gaseous potassium capture (Zheng et al., 2008). In the study, the researchers found that kaolin was less effective at retaining gaseous KCl over a period of 1 hour between 1100°C and 1500°C Figure 7.3.

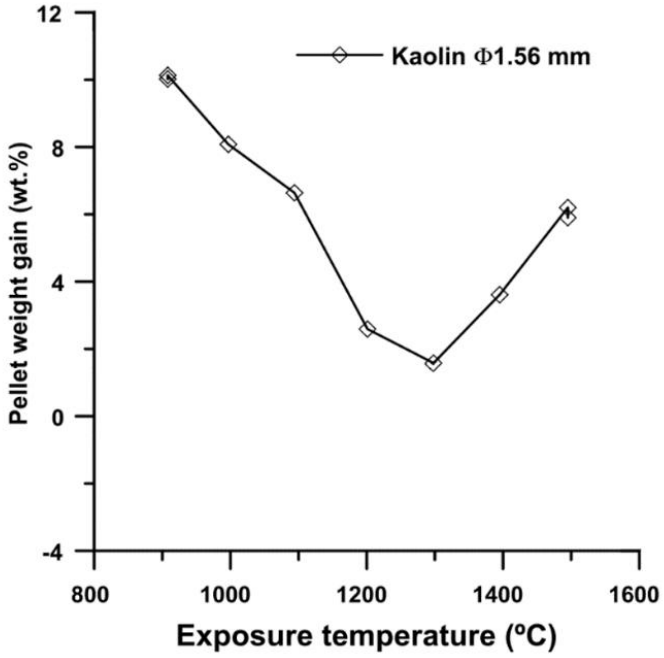

Figure 7.3. Effect of reaction temperature on kaolin pellet weight gain when exposed to 1000 ppmv KCl for 1 h (Zheng et al., 2008)

However, the results in this thesis indicate that retention is most effective at 1150°C. Furthermore, in an article from Paneru et al., it was reported that: "The present study shows that the interaction between potassium species and additive is possible in a short residence time and even at a high temperature (>1200°C) relevant for pulverized combustion conditions". The reason for this difference in results is clearly the duration of exposure to high temperature. With no apparent effect of additive degradation observed at 1150°C, it is likely that no such degradation occurs within the sub-one second timeframe of DTF combustion.

7.5 Mineral Liberation Analysis

Seven samples were analysed by mineral liberation analysis (MLA). These included the fuel source – olive cake ash prepared at 550°C – and the subsequent combustion ash fired with no additive, 40% kaolin and 50% kaolin,

at 1150°C and 1300°C. The objective of this analysis was to attempt to determine the form of the potassium (by association) in each sample and to identify any bulk transformations/migrations of potassium that may have occurred.

Figure 7.4 below shows the change in potassium content after combustion at 1150°C when compared with the starting 550°C ash. It can clearly be seen that potassium is lost in the form of “K Chlorine mix”, “K oxide”, “KSiP mix” and “P containing K oxide”. Where no additive is used, it can be seen that potassium migrates to form “CaMgK silicate mixture” and “carbon mixture”. Where aluminosilicate additive is used, none of this migration is observed. Instead, the formation of three potassium-containing aluminium silicate mixtures is observed.

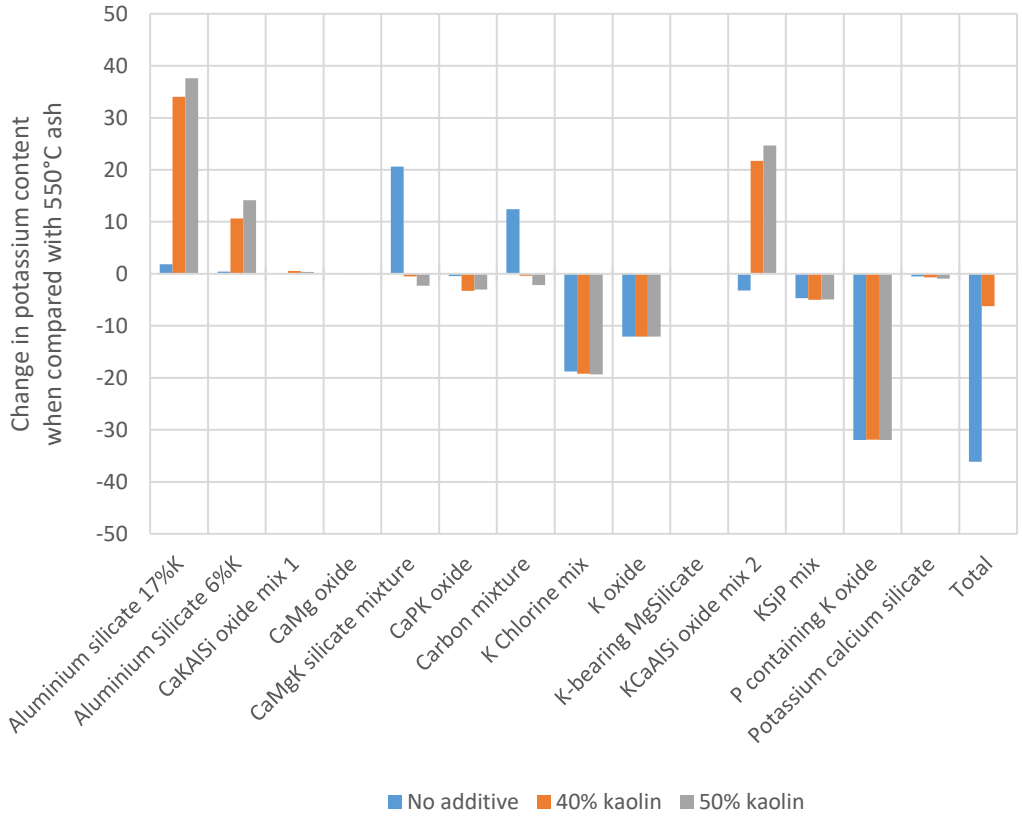

Figure 7.4. Change in potassium distribution from 550°C ash for experiments at 1150°C

To better understand the compositions of these mineral phases and to gain further insight into the reactions and transformations that are occurring, the molar ratios of elements within each of the main mineral phases has been determined. In Table 7.1, the molar ratios of elements of the four, volatile K-containing mineral phases are presented with respect to K.

Table 7.1. Molar ratios of elements in volatile, K-containing mineral phases with respect to K

	K	O	Cl	Na	P	Si
"K chlorine mix"	1.0	1.9	0.1			
"K oxide"	1.0	1.4				
"KSiP mix"	1.0	2.9		0.1	0.1	0.5
"P containing K oxide"	1.0	1.0			0.2	

The data in the table above shows that all four mineral phases comprise predominantly of potassium oxide. In Table 7.2 below, the molar ratios for the elements in the two potassium silicate phases are presented with respect to Si.

Table 7.2. Molar ratios of elements in potassium silicate mineral phases with respect to Si

	Si	Al	K	O	Ca	Mg	C	Fe	P
"CaMgK silicate mixture"	1.0	0.3	0.6	4.2	1.0	0.7		0.1	0.2
"Carbon mixture"	1.0	0.6	0.5	45.5	2.2	1.1	8.0	0.5	

Finally, the molar ratios for the potassium aluminium silicate phases which form in the presence of the additive, are shown in Table 7.3.

Table 7.3. Molar ratios of elements in potassium aluminium silicate phases with respect to Si

	Si	Al	K	O	Ca	Mg	P
"Aluminium Silicate 6%K"	1.0	0.8	0.2	2.3		0.1	
"Aluminium Silicate 17%K"	1.0	1.0	0.6	3.1			
"KCaAlSi oxide mix 2"	1.0	1.2	1.3	5.1	0.8		0.3

From the data in these tables it is possible to speculate on the presence of specific compounds by considering the ratios of elements. The two most commonly reported products from the reaction of K with kaolinite are kalsilite ($KAlSiO_4$) and leucite ($KAlSi_2O_6$). The presence of the elements K, Al and Si, in a ratio of 1:1:1 or 1:1:2 would give very strong evidence of the presence of these reaction products. For the two main aluminium silicate phases however ("Aluminium silicate 6%K" and "Aluminium silicate 17%K"), the level of K is low relative to Al and Si. It is likely that the reason for this is that the kaolin has not fully dispersed through the mixture and that these mineral phases contain unreacted kaolinite. Given that the K is expected to react to form either kalsilite or leucite, an indication about which product has been formed can be found by looking at the relative quantities of Al and Si. "Aluminium silicate 6%" has a reduced level of Al so it is possible that some leucite might be formed and present in this mineral phase. The final aluminium silicate mixture listed is

"KCaAlSi oxide mix 2". A ratio of K to Ca to Si to O of 2:1:1:4 would strongly indicate the presence of K_2CaSiO_4 – as previously reported in literature (Vassilev et al., 2014). The measured ratio for this mineral phase is 1.3:0.8:1.0:5.1, suggesting that the presence of some K_2CaSiO_4 is highly probable.

In research reported by Paneru et al. in 2016, the Gibbs free energy of formation of several potassium silicate and potassium aluminium silicate compounds from $KOH_{(g)}$, $KCl_{(g)}$ and $K_2SO_{4(g)}$ at 1200°C was presented (Paneru et al., 2016). This data is shown in Table 7.4.

Table 7.4. Gibbs free energy of formation of potassium silicates and potassium aluminium silicates at 1200°C (Paneru et al., 2016)

	From KOH(g)	From KCl (g)	From K_2SO_4 (g)
K_2SiO_3	-179 kJ	+	+
$K_2Si_2O_5$	-226 kJ	+	-8 kJ
$K_2Si_4O_9$	-255 kJ	+	-37 kJ
$KAlSiO_4$	-575 kJ	-318 kJ	-357 kJ
$KAlSi_2O_6$	-656 kJ	-399 kJ	-439 kJ

The data in the table above from Paneru et al. show that the formation of all potassium silicates from KCl have positive values for ΔG. This means that the reaction is not thermodynamically favourable. Likewise, with the potassium sulphates, the first potassium silicate has a positive ΔG of formation and the other silicates have small negative values for ΔG. There are significant negative ΔG values for the formation of potassium silicates from KOH which suggests that some migration of potassium to silicates can be expected from KOH. Where aluminosilicates are present, the potassium species have the opportunity to form potassium aluminium silicates. It can be seen in the table above that the formations of these products from KOH are much more preferable as both reactions have very negative ΔG energies. They are also

expected to be very stable with melting points of over 1500°C. Of further interest is that the formation of potassium aluminium silicates from potassium chlorides and sulphates have strongly negative ΔG energies. This means that it is thermodynamically favourable for the formation of these products and therefore, release of gaseous KCl and K_2SO_4 should be mitigated where aluminosilicates are present.

This reported thermodynamic data further evidences the conclusions drawn from the MLA data presented above. It was found that the predominant form of volatile potassium present in the olive cake was KOH. Migration of K to form potassium silicates was clearly identified and preferential migration to form potassium aluminium silicate phases where kaolinite was present was also observed.

7.6 Potassium retention in other feedstocks using kaolin

To investigate the effect of kaolin addition on the combustion of other biomasses, samples of miscanthus and wood were tested. Relative to other biomasses, miscanthus has a medium ash content (3.6%) and a medium K content (~11% K_2O in ash). Furthermore, at 815°C only around 25% of the K is lost. By comparison, olive cake has 33% K_2O in ash and 40% of this is volatile at 815°C. When fired with kaolin at 1150°C and 1300°C, significant increases in K_2O in the combustion ashes were measured. For both tests these increases were greater than 100% for volatile K_2O. With the small quantities of K_2O that were measured and when considering the relative errors found when analysing the olive cake samples, it is likely that this is a result of experimental error. It is

therefore difficult to draw substantive conclusions with specific values for K retention from the data from this experiment. However, despite the high relative error, it would appear that significant retention of volatile K did occur.

Wood has a very low ash content (<1%) and a medium K content (~17% K_2O in ash). However, 42% of the K in wood is volatile at 815°C. This higher absolute level of K and higher level of volatile K gives smaller relative errors. It was found that for the test with wood and kaolin at 1300°C, 75% of volatile K was retained in the combustion ash. This is very close to the level of retention found in olive cake at the same temperature.

The purpose of these experiments was to give a brief insight into how biomass fuels with different levels of K would respond to kaolin addition during combustion. The results suggest that as with olive cake, significant levels of K retention are possible by the use of kaolin addition. Further investigation with MLA should afford a much greater insight. Such information would include the form of K in both fuels and the migration behaviours during combustion – with and without additive.

7.7 The use of coal fly ash as additive

The use of coal fly ash as an alternative additive to kaolin was briefly investigated. The high availability and low cost of coal fly ash makes it an attractive option for industry as a source of aluminosilicates. Figure 7.5 is a ternary mineral diagram, previously reported by Wang et al. in 2012. The red circle encompasses mineral phases of a low melting point which are problematic in boilers. The use of aluminosilicate additives has the effect of

shifting the ratio of elements in the direction of the blue arrow by increasing the amount of Al_2O_3 present in the mixture. The minerals formed from these more alumina-rich mixtures have significantly higher melting temperatures.

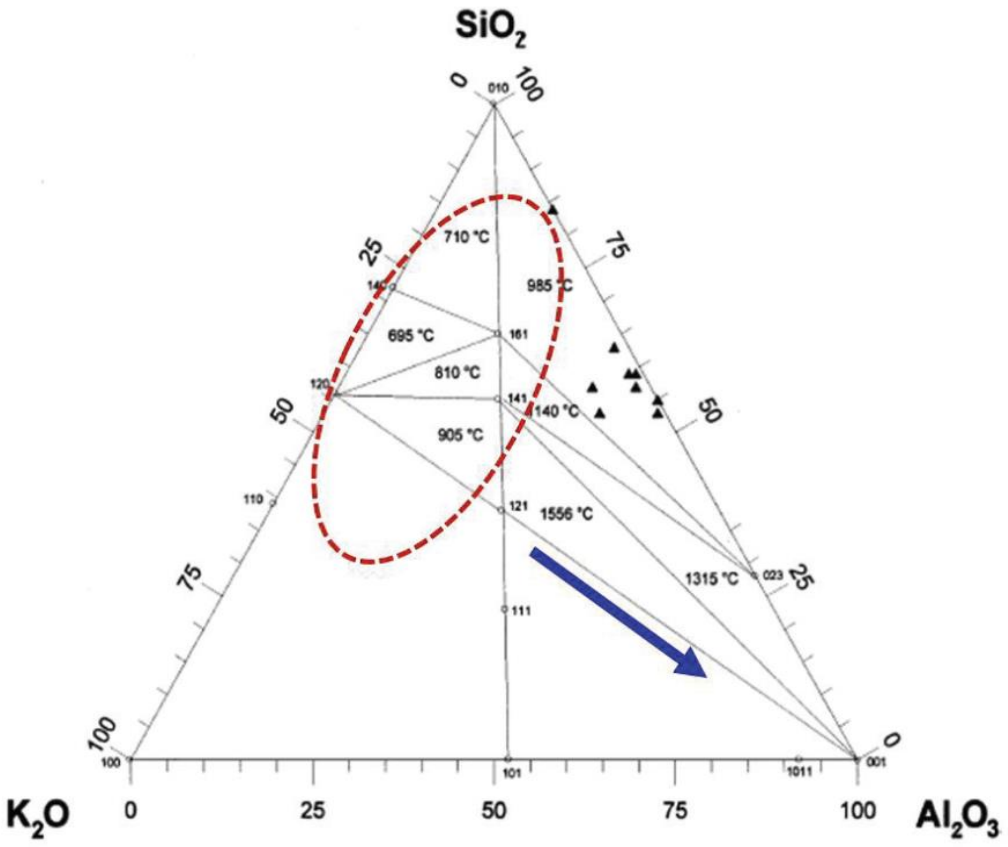

Figure 7.5. Formation of Potassium -Silicates and -Aluminium Silicates (Wang et al., 2012c)

It therefore seems clear that the ratio of alumina in any additive that is to be used is of critical significance. In Table 7.5, the relative quantities of silica and alumina are shown for kaolin and coal fly ash.

Table 7.5. Alumina and silica contents of kaolin and coal fly ash

	Al_2O_3	SiO_2
Kaolin	30.4	35.2
Coal fly ash	22.8	48.8

Units: wt%

In kaolin, it can be seen that the ratio of alumina to silica is almost 1:1. However, in the coal fly ash there is significantly more silica, with the ratio of alumina to

silica being less than 1:2. Tests with coal fly ash additive were conducted with olive cake at 1150°C and 1300°C and with wood at 1300°C. Under conditions which yielded 100% retention in olive cake with kaolin (1150°C, 50% additive), only 50% retention was found for coal fly ash. Furthermore, negligible retention was found with olive cake and coal fly ash at 1300°C – retention with kaolin was 76%. Negligible potassium retention was also found for wood with coal fly ash at 1300°C – retention with kaolin was 75%. These results further evidence that the ratio of alumina to silica is key in the level of formation of potassium aluminium silicates. Where it is preferable to use an additive with a lower ratio of alumina (such as coal fly ash), it might be possible to simply increase the level of additive in the mixture. Taking this approach will result in a higher level of silicates present in the mixture. It's possible that this would result in the formation of potassium silicate phases in addition to the formation of potassium aluminium silicates. This would be problematic as these phases are formed when no additive is used and could lead to silicate-melt induced slagging. However, as evidenced by the aforementioned MLA results, the formation of potassium aluminium silicates is more thermodynamically favourable than the migration of K species to potassium silicates. It should be possible to confirm if the favourable thermodynamics would overcome the effect of a higher relative silica content by undertaking further MLA research.

7.8 Relevance of research and areas for further work

The results of the research conducted in this study provide values for levels of K retention for three different fuels, in a range of combustion conditions where

aluminosilicate additives are used. Of particular relevance is the use of the drop tube furnace as a means of combustion which is representative of pulverised fuel firing. However, there are significant differences between drop tube furnace combustion and industrial scale PF combustion. These differences exist primarily due to the one-dimensional nature of the drop tube furnace. The clear next step to obtaining a thorough understanding of how aluminosilicate additives would behave in full scale power generation would be to conduct experiments on a pilot scale combustor such as the 1 MW_{th} combustion test facility at Uniper Technologies Ltd. In a pilot scale unit such as this, a burner more typical of those found on full scale boilers is used. These burners have significant differences to the combustion stream found in the DTF. Where the particles in the DTF are fed into the combustion chamber in a single stream within a laminar flow, solid fuel in the pilot rig is introduced to the furnace in large quantities within a highly turbulent air stream. Furthermore, due to the less uniform behaviour of incident particles, it can be expected that variations in heating rates and local gas compositions will arise.

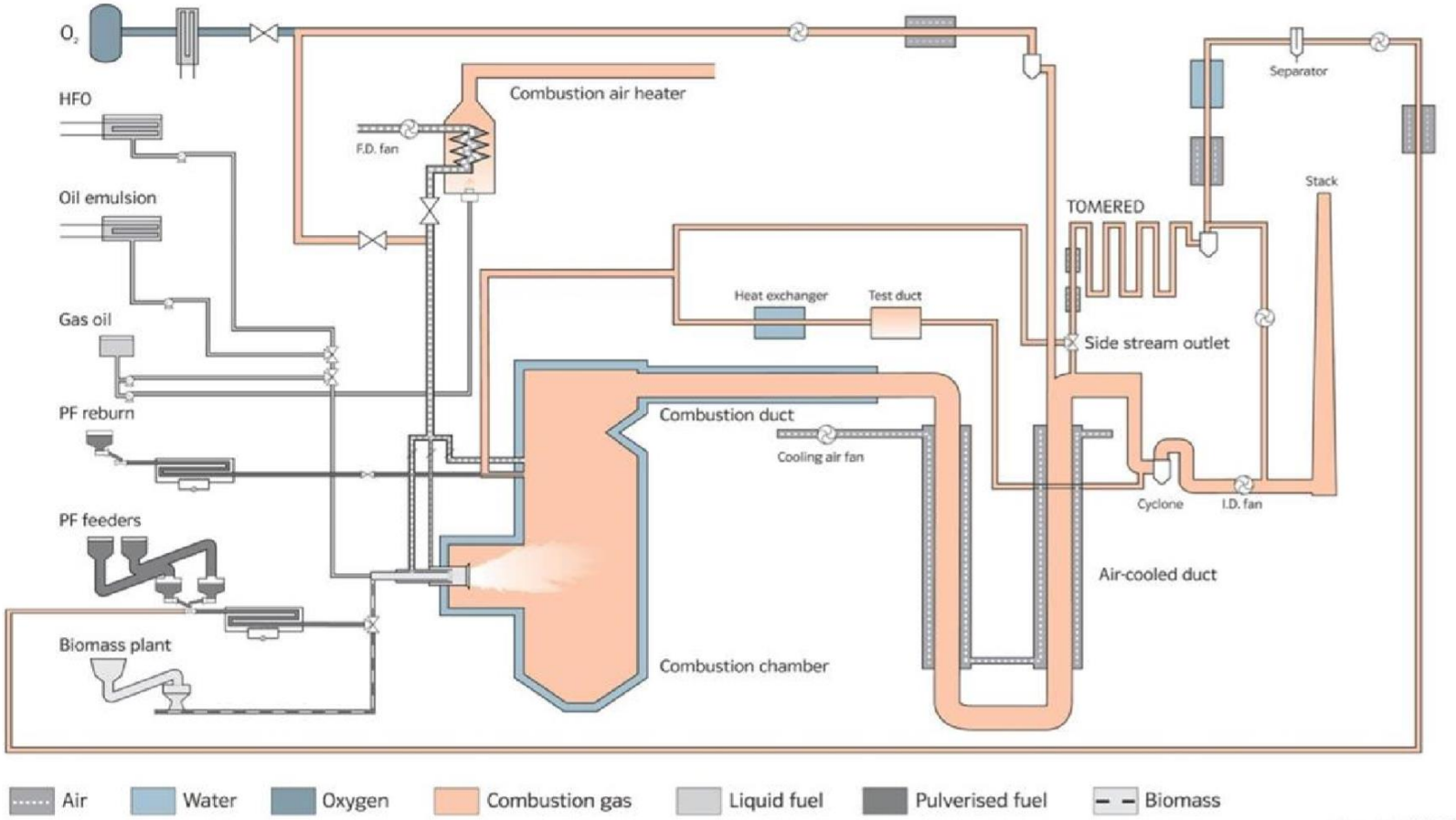

Figure 7.6. Process flow diagram of combustion test facilty at Uniper Technologies Ltd

Figure 7.6 depicts a process flow diagram of the combustion test facility at Uniper Technologies Ltd. A test rig such as this is fully fuel flexible and designed to be highly instrumental and controllable. It would therefore afford researchers the opportunity to conduct experiments on a great number of parameters which could inform industry on a wide range of operating procedures for the use of additives in biomass combustion. It could be expected that there may be a number of issues which manifest on the introduction of aluminosilicate additives. These could potentially vary a great deal depending on the method of introduction used. Such methods might include: the upstream production of pre-mixed fuel-additive pellets; the introduction of additive to the pulverised fuel stream immediately after milling; the introduction of additive to the combustion zone via a separate stream. The first method of producing pre-mixed pellets would have several advantages: it would mean that mixing could be carried out separate to the combustion process (even at a different facility if desired); no other streams would have to be run concurrently – reducing plant operating costs; and the fuel and additive would already be thoroughly integrated. However, the presence of the additive may be detrimental to the mills and therefore its mechanical properties should be taken into consideration. It would also result in a reduction in fuel throughput which would incur an energy cost. The adoption of the second method – introducing the additive to the fuel stream after milling – would mean that the additive bypassed the mills. It would also mean that different fuels could be used and fuel/additive ratios could be controlled. It's possible however that the presence of the non-volatile additive could negatively affect

fuel ignition and/or combustion. The third method of introducing the additive to the combustion zone via a separate stream might avoid this, but presents the risk of poorer alkali metal capture due to reduced integration of fuel and additive. This could be combatted by increasing the quantity of additive.

One key difference between the research conducted in this study and industrial scale biomass combustion is the use of ash prepared at 550°C instead of raw biomass. This allowed for the collection of significantly greater quantities of ash for analysis – essentially meaning that the experiments could be conducted on a larger scale than would be possible in the DTF with raw fuel. When raw olive cake is used, there is a tenfold increase in overall mass for the same amount of potassium. This means that only a tenth of the amount of additive could be used for the same effect. However, the extra mass could serve as a barrier between the problematic K and the additive – allowing volatile K to escape. When used in a highly turbulent flow such as that found in a conventional PF burner, this may be countered by greater mixing and therefore, high interaction of the biomass with the additive.

Finally, another area for further research is the investigation into different additives. A brief comparison between kaolin and coal fly ash was made in this research and showed that – with its higher ratio of alumina to silica – the kaolin performed better than the coal fly ash. However, given the obvious advantages of using coal fly ash as an additive, further investigation of this would be highly pertinent. MLA analysis in this area could offer great insight into the direct comparison between kaolin clay and coal fly ash. Not only is coal fly ash an

attractive proposition as an additive for its availability and low cost, but there are other, practical advantages with its use. Feeding kaolin clay can be problematic as it is hygroscopic and tends to clump. By comparison, coal fly ash might prove to be more agreeable in use, provided the appropriate quantity can be determined.

8 Conclusions

After combustion of olive cake in the muffle furnace, a small increase in the ash yield at 815°C was measured in the presence of the kaolin. In addition, XRF indicated that there was a greater amount of potassium in the ash when kaolin was used. This provides evidence of retention of volatile potassium in ash as a result of the use of the additive. The benefit of this test over the drop tube furnace tests is that all ash is retained in the crucibles so exact mass yields can be used for normalisation of results. 40% retention of volatile potassium was the highest recorded, with 5-15% for the lower additive ratios. At this temperature it is expected that the reaction will be under kinetic control and it was concluded that the reason for the relatively low retention rates at lower additive ratios was due to the kinetics being slower than at higher temperatures.

Very high levels of potassium retention were found for the DTF experiments with olive cake and kaolin. Across additive ratio ranges of 20-50% kaolin in olive cake ash at two temperatures (1150°C and 1300°C), the most effective additive ratio tested was found to be the highest ratio of 50% kaolin. At 1150°C a retention of 100% of volatile potassium was achieved. At 1300°C a maximum volatile potassium retention of 76% was found.

When the temperature range was extended to include 1000°C and 1450°C, it was found that as the temperature is increased from 1000°C to 1150°C the level of potassium retention increases from 70% to 100% and then as the temperature increases further to 1300°C and then 1450°C, the level of

retention reduces to 76% and then 42%. The reason for this was determined to be due to the slower kinetics at 1000°C while at temperatures above 1150°C, the reaction should be under thermodynamic control. To establish if this is indeed the case, an experiment was conducted under different residence times in the drop tube furnace.

Across residence times of 600, 200 and 100 ms, it was found that no decrease in retention was measured as the residence time decreased. This provides evidence for the reaction occurring instantaneously and therefore being under thermodynamic control.

Experiments with miscanthus suggested that very high levels of retention (up to 100%) were achieved at 1150°C and 1300°C when fired with 50% kaolin. However, miscanthus has significantly lower absolute levels of potassium in the ash and a lower proportion of the K in miscanthus is volatile. This means that the changes in K content for this experiment are much closer in value to those found for the experimental error – resulting in difficulty drawing solid conclusions here. Also investigated was the use of kaolin in the combustion of wood ash. This yielded volatile potassium retention of 75% at 1300°C.

Comparative experiments were conducted with coal fly ash as an alternative additive to kaolin. It was found that significantly lower retention of potassium was found when the same amount of additive was used on a mass basis. When fired at 1150°C in the drop tube furnace, 53% of potassium was retained in olive cake by the presence of coal fly ash, compared with 100% by the presence of kaolin. Less than 10% of the volatile potassium was retained by coal fly ash at

1300°C, compared with 76% when kaolin was used. In an experiment conducted with wood and coal fly ash at 1300°C, in the same additive ratio of 50% additive in biomass ash (by weight), negligible potassium retention was found. It is expected that the reason for this is the significantly lower alumina-silica ratio found in the sample of coal fly ash used when compared with kaolin. This is highly pertinent and a key point to take forward when considering fly ash sources for use as additives.

By the application of mineral liberation analysis, olive cake ash samples produced in the drop tube furnace with and without kaolin additive have been characterised. The distribution of potassium across individual mineral phases has been identified for all samples on a semi-quantitative basis. Further analysis of this data has provided a novel insight into the migration behaviour of potassium during combustion of olive cake both in the absence and presence of kaolin. For all high temperature ash samples, total loss of potassium oxide and chloride species was observed. Where no kaolin was used, migration of potassium to calcium-containing silicate phases was identified. In the presence of kaolin however, this migration was arrested in favour of the formation of the more thermodynamically favourable potassium aluminium silicates.

The establishment of this method for semi-quantitatively determining the migration of potassium during biomass combustion provides exciting scope for further research in this area. It is expected that the data obtained in this research could be fed into computational thermodynamic models.

Other areas of interest for future work would be to expand the MLA dataset to include the drop tube furnace ashes of other biomass feedstocks. The MLA has proved to be a powerful tool for the rapid discovery of potassium distribution within samples and its transformations. Broadening the biomasses analysed would greatly enhance the scope of the findings in terms of predicting the behaviour of potassium release.

Additionally, further coal fly ash experiments using samples with different alumina to silica ratios could offer substantial insight into how this key additive characteristic directly translates into its efficacy as an additive. This knowledge could be of great value such are the credentials of fly ash as a low cost, highly available waste product.

References

Aho, M., Ferrer, E., 2005. Importance of coal ash composition in protecting the boiler against chlorine deposition during combustion of chlorine-rich biomass. Fuel 84, 201–212. https://doi.org/10.1016/j.fuel.2004.08.022

Anderson, G.Q. a, Fergusson, M.J., 2006. Energy from biomass in the UK: Sources, processes and biodiversity implications. Ibis (Lond. 1859). 148, 180–183. https://doi.org/10.1111/j.1474-919X.2006.00535.x

Baxter, L., 2005. Biomass-coal co-combustion: Opportunity for affordable renewable energy. Fuel 84, 1295–1302. https://doi.org/10.1016/j.fuel.2004.09.023

Baxter, L., Nielsen, H., 1997. The effects of fuel-bound chlorine and alkali on corrosion initiation. Fuel Energy Abstr. 1091–1095.

Baxter, L.L., Miles, T.R., Jenkins, B.M., Milne, T., Dayton, D., Bryers, R.W., Oden, L.L., 1998. The behavior of inorganic material in biomass-fired power boilers: field and laboratory experiences. Fuel Process. Technol. 54, 47–78. https://doi.org/10.1016/S0378-3820(97)00060-X

Benson, S.A., McCollor, D.P., Eylands, K.E., Laumb, J.D., Jensen, R.R., 2012. Characterisation of particulate matter with computer-controlled scanning electron microscopy, in: Environmental Challenges and Greenhouse Gas Control for Fossil Fuel Utilization in the 21st Century. Springer Science & Business Media, pp. 29–30.

Biagini, E., Lippi, F., Petarca, L., Tognotti, L., 2002. Devolatilization rate of

biomasses and coal–biomass blends: an experimental investigation. Fuel 81, 1041–1050. https://doi.org/10.1016/S0016-2361(01)00204-6

Boerjan, W., Ralph, J., Baucher, M., 2003. Lignin biosynthesis. Annu. Rev. Plant Biol. 54, 519–46. https://doi.org/10.1146/annurev.arplant.54.031902.134938

Boström, D., Grimm, A., Boman, C., Björnbom, E., Öhman, M., 2009. Influence of kaolin and calcite additives on ash transformations in small-scale combustion of oat. Energy and Fuels 23, 5184–5190. https://doi.org/10.1021/ef900429f

BP, 2015. BP statistical review of world energy.

Broström, M., Kassman, H., Helgesson, A., Berg, M., Andersson, C., Backman, R., Nordin, A., 2007. Sulfation of corrosive alkali chlorides by ammonium sulfate in a biomass fired CFB boiler. Fuel Process. Technol. 88, 1171–1177. https://doi.org/10.1016/j.fuproc.2007.06.023

Cannell, M.G.R., 2003. Carbon sequestration and biomass energy offset: theoretical, potential and achievable capacities globally, in Europe and the UK. Biomass and Bioenergy 24, 97–116. https://doi.org/10.1016/S0961-9534(02)00103-4

Clayden, J., Greeves, N., Warren, S., Wothers, P., 2008. Organic Chemistry. Oxford University Press Inc.

Clery, D.S., Mason, P.E., Rayner, C.M., Jones, J.M., 2018. The effects of an additive on the release of potassium in biomass combustion. Fuel 214,

647–655. https://doi.org/10.1016/j.fuel.2017.11.040

Couch, G., 1994. Understanding slagging and fouling during pf combustion. IEA Coal Research, London.

Davidsson, K.O., Åmand, L.-E., Steenari, B.-M., Elled, a.-L., Eskilsson, D., Leckner, B., 2008. Countermeasures against alkali-related problems during combustion of biomass in a circulating fluidized bed boiler. Chem. Eng. Sci. 63, 5314–5329. https://doi.org/10.1016/j.ces.2008.07.012

Dayton, D., French, R., Milne, T., 1995. Direct observation of alkali vapor release during biomass combustion and gasification. 1. Application of molecular beam/mass spectrometry to switchgrass combustion. Energy & Fuels 855–865.

Dayton, D., Jenkins, B., Turn, S., 1999. Release of inorganic constituents from leached biomass during thermal conversion. Energy … 1977, 860–870.

DECC, 2018. UK Energy in Brief 29–30.

Fandrich, R., Gu, Y., Burrows, D., Moeller, K., 2007. Modern SEM-based mineral liberation analysis. Int. J. Miner. Process. 84, 310–320. https://doi.org/10.1016/j.minpro.2006.07.018

Farrow, T.S., 2013. A fundamental study of biomass oxy-fuel combustion and co-combustion. University of Nottingham.

Field, C.B., Campbell, J.E., Lobell, D.B., 2008. Biomass energy: the scale of the potential resource. Trends Ecol. Evol. 23, 65–72. https://doi.org/10.1016/j.tree.2007.12.001

Fu, Y., Li, Z., Zhou, A., Xiong, S., Yang, C., 2019. Evaluation of coal component liberation upon impact breakage by MLA. Fuel 258, 116136. https://doi.org/10.1016/j.fuel.2019.116136

Goodall, W.R., Scales, P.J., Butcher, A.R., 2005. The use of QEMSCAN and diagnostic leaching in the characterisation of visible gold in complex ores. Miner. Eng. 18, 877–886. https://doi.org/10.1016/j.mineng.2005.01.018

Gräbner, M., Lester, E., 2016. Proximate and ultimate analysis correction for kaolinite-rich Chinese coals using mineral liberation analysis. Fuel 186, 190–198. https://doi.org/10.1016/j.fuel.2016.08.074

Grimm, A., Skoglund, N., Bostr, D., Ohman, M., 2011. Bed Agglomeration Characteristics in Fluidized Quartz Bed Combustion of Phosphorus-Rich Biomass Fuels 937–947.

Gu, Y., 2003. Automated scanning electron microscope based mineral liberation analysis. J. Miner. Mater. Charact. Eng. 2, 33–41.

Gudka, B., Jones, J.M., Lea-Langton, A.R., Williams, A., Saddawi, A., 2016. A review of the mitigation of deposition and emission problems during biomass combustion through washing pre-treatment. J. Energy Inst. 89, 159–171. https://doi.org/10.1016/j.joei.2015.02.007

Gupta, R., Wall, T., Kajigaya, I., 1998. Computer-controlled scanning electron microscopy of minerals in coal—implications for ash deposition. Prog. Energy Combust. Sci. 24, 523–543.

Hupa, M., Karlström, O., Vainio, E., 2017. Biomass combustion technology

development - It is all about chemical details. Proc. Combust. Inst. 36, 113–134. https://doi.org/10.1016/j.proci.2016.06.152

Jones, J.M., Darvell, L.I., Bridgeman, T.G., Pourkashanian, M., Williams, a., 2007. An investigation of the thermal and catalytic behaviour of potassium in biomass combustion. Proc. Combust. Inst. 31, 1955–1963. https://doi.org/10.1016/j.proci.2006.07.093

Klass, D.L., 1998. Biomass for Renewable Energy, Fuels, and Chemicals. Elsevier.

Knudsen, J., Jensen, P., Dam-Johansen, K., 2004. Transformation and release to the gas phase of Cl, K, and S during combustion of annual biomass. Energy & Fuels 1385–1399.

Kutchko, B., Kim, a, 2006. Fly ash characterization by SEM–EDS. Fuel 85, 2537–2544. https://doi.org/10.1016/j.fuel.2006.05.016

Ladanai, S., Vinterbäck, J., 2009. Global Potential of Sustainable Biomass for Energy.

Le Manquais, K., 2011. Combustion Enhancing Additives for Coal Firing. University of Nottingham.

Levidow, L., Borda-Rodriguez, A., Papaioannou, T., 2014. UK bioenergy innovation priorities: Making expectations credible in state-industry arenas. Technol. Forecast. Soc. Change 87, 191–204. https://doi.org/10.1016/j.techfore.2013.12.011

Li, Z., Fu, Y., Yang, C., Yu, W., Liu, L., Qu, J., Zhao, W., 2018. Mineral liberation analysis on coal components separated using typical comminution

methods. Miner. Eng. 126, 74–81. https://doi.org/10.1016/j.mineng.2018.06.028

Liu, Y., Gupta, R., Sharma, A., Wall, T., Butcher, A., Miller, G., Gottlieb, P., French, D., 2005. Mineral matter–organic matter association characterisation by QEMSCAN and applications in coal utilisation. Fuel 84, 1259–1267. https://doi.org/10.1016/j.fuel.2004.07.015

Liu, Y., Gupta, R., Wall, T., 2007. Ash formation from excluded minerals including consideration of mineral-mineral associations. Energy & fuels 461–467.

Livingston, W.R., 2016. The status of large scale biomass firing: The milling and combustion of biomass materials in large pulverised coal boilers, IEA Bioenergy Task 32: Biomass Combustion and co-firing.

Livingston, W.R., 2014. The firing and co-firing of biomass in large pulverised fuel boilers.

Lu, G., Yan, Y., Cornwell, S., Whitehouse, M., Riley, G., 2008. Impact of co-firing coal and biomass on flame characteristics and stability. Fuel 87, 1133–1140. https://doi.org/10.1016/j.fuel.2007.07.005

Marsh, R., Steer, J.M., Fesenko, E., Cleary, V., Rahman, A., Griffiths, A.J., Williams, K.P., 2008. Biomass and waste co-firing in large-scale combustion systems, in: Proceedings of the ICE-Energy. pp. 115–126. https://doi.org/10.1680/ener.2008.161.3.115

Masiá, A.T., 2010. Characterisation and prediction of deposits in biomass co-

combustion.

Mason, P.E., Darvell, L.I., Jones, J.M., Pourkashanian, M., Williams, A., 2015. Single particle flame-combustion studies on solid biomass fuels. Fuel 151, 21–30. https://doi.org/10.1016/j.fuel.2014.11.088

Mason, P.E., Darvell, L.I., Jones, J.M., Williams, A., 2016. Observations on the release of gas-phase potassium during the combustion of single particles of biomass. Fuel 182, 110–117. https://doi.org/10.1016/j.fuel.2016.05.077

Miles, T., Miles Jr, T., Baxter, L., 1996. Boiler deposits from firing biomass fuels. Biomass and Bioenergy… 10, 125–138.

Moghtaderi, B., 2007. A study on the char burnout characteristics of coal and biomass blends. Fuel 86, 2431–2438. https://doi.org/10.1016/j.fuel.2007.01.004

Mohan, D., Pittman, C.U., Steele, P.H., 2006. Pyrolysis of Wood/Biomass for Bio-oil: A Critical Review. Energy & Fuels 20, 848–889. https://doi.org/10.1021/ef0502397

Munir, S., 2010. Potential Slagging and Fouling Problems associated with Biomass-Coal blends in Coal-fired Boilers. J. Pakistan Inst. Chem. Eng. 38, 1–11.

Neavel, R.C., 1979. Coal structure and coal science: overview and recommendations. ACS Div. Fuel Chem. Prepr. https://doi.org/doi:10.1021/ba-1981-0192.ch001 10.1021/ba-1981-

0192.ch001

Nielsen, H.P., Frandsen, F.J., Dam-Johansen, K., Baxter, L.L., 2000. Implications of chlorine-associated corrosion on the operation of biomass-fired boilers. Prog. Energy Combust. Sci. 26, 283–298. https://doi.org/10.1016/S0360-1285(00)00003-4

Niu, Yanqing;, Tan, H., Hui, S., 2016. Ash-related issues during biomass combustion: Alkali-induced slagging, silicate melt-induced slagging (ash fusion), agglomeration, corrosion, ash utilization, and related countermeasures. Prog. Energy Combust. Sci. 52, 1–61. https://doi.org/10.1016/j.pecs.2015.09.003

Niu, Yanqing, Wang, Z., Zhu, Y., Zhang, X., Tan, H., Hui, S., 2016. Experimental evaluation of additives and K2O-SiO2-Al2O3 diagrams on high-temperature silicate melt-induced slagging during biomass combustion. Fuel 179, 52–59. https://doi.org/10.1016/j.fuel.2016.03.077

Nutalapati, D., Gupta, R., Moghtaderi, B., Wall, T.F., 2007. Assessing slagging and fouling during biomass combustion: A thermodynamic approach allowing for alkali/ash reactions. Fuel Process. Technol. 88, 1044–1052. https://doi.org/10.1016/j.fuproc.2007.06.022

Öhman, M., Nordin, A., 2000. The role of kaolin in prevention of bed agglomeration during fluidized bed combustion of biomass fuels. Energy and Fuels 14, 618–624. https://doi.org/10.1021/ef990198c

Paneru, M., Babat, S., Maier, J., Scheffknecht, G., 2016. Role of potassium in

deposit formation during wood pellets combustion. Fuel Process. Technol. 141, 266–275. https://doi.org/10.1016/j.fuproc.2015.10.008

Pearson, P.J.G., Watson, J., 2012. UK Energy Policy 1980-2010, A history and lessons to be learnt, Energy Policy.

Pettersen, R.C., 1984. The Chemical Composition of Wood, in: Rowell, R. (Ed.), The Chemistry of Solid Wood, Advances in Chemistry. American Chemical Society, Washington, DC, pp. 57–126. https://doi.org/10.1021/ba-1984-0207

Pisupati, S.V.L.N., 1999. Coal Utilisation. Encycl. Br.

Ren, Q., Li, L., 2015. Co-combustion of Agricultural Straw with Municipal Sewage Sludge in a Fluidized Bed: Role of Phosphorus in Potassium Behavior. Energy & Fuels 29, 4321–4327. https://doi.org/10.1021/acs.energyfuels.5b00790

Saidur, R., Abdelaziz, E. a., Demirbas, A., Hossain, M.S., Mekhilef, S., 2011. A review on biomass as a fuel for boilers. Renew. Sustain. Energy Rev. 15, 2262–2289. https://doi.org/10.1016/j.rser.2011.02.015

Sami, M., Annamalai, K., Wooldridge, M., 2001. Co-firing of coal and biomass fuel blends. Prog. Energy Combust. Sci. 27, 171–214. https://doi.org/10.1016/S0360-1285(00)00020-4

Sánchez, O.J., Cardona, C. a, 2008. Trends in biotechnological production of fuel ethanol from different feedstocks. Bioresour. Technol. 99, 5270–95. https://doi.org/10.1016/j.biortech.2007.11.013

Schmitt, V.E.M., Kaltschmitt, M., 2013. Effect of straw proportion and Ca- and Al-containing additives on ash composition and sintering of wood–straw pellets. Fuel 109, 551–558. https://doi.org/10.1016/j.fuel.2013.02.064

Speight, J.G., 2015. Handbook of Coal Analysis, 2nd ed. John Wiley & Sons.

Steenari, B.-M., Lundberg, A., Pettersson, H., Wilewska-Bien, M., Andersson, D., 2009. Investigation of Ash Sintering during Combustion of Agricultural Residues and the Effect of Additives. Energy & Fuels 23, 5655–5662. https://doi.org/10.1021/ef900471u

Steenari, B.M., Lindqvist, O., 1998. High-temperature reactions of straw ash and the anti-sintering additives kaolin and dolomite. Biomass and Bioenergy 14, 67–76. https://doi.org/10.1016/S0961-9534(97)00035-4

Straker, P., Shipstone, J., Nicholson, A., 2016. Biomass Combustion. US 2016/0040873 A1.

Thornley, P., 2006. Increasing biomass based power generation in the UK. Energy Policy 34, 2087–2099. https://doi.org/10.1016/j.enpol.2005.02.006

Tobiasen, L., Skytte, R., Pedersen, L.S., Pedersen, S.T., Lindberg, M.A., 2007. Deposit characteristic after injection of additives to a Danish straw-fired suspension boiler. Fuel Process. Technol. 88, 1108–1117. https://doi.org/10.1016/j.fuproc.2007.06.017

Tortosa Masiá, a. a., Buhre, B.J.P., Gupta, R.P., Wall, T.F., 2007. Characterising ash of biomass and waste. Fuel Process. Technol. 88, 1071–1081.

https://doi.org/10.1016/j.fuproc.2007.06.011

Tran, K.Q., Iisa, K., Steenari, B.M., Lindqvist, O., 2005. A kinetic study of gaseous alkali capture by kaolin in the fixed bed reactor equipped with an alkali detector. Fuel 84, 169–175. https://doi.org/10.1016/j.fuel.2004.08.019

UK Government, 2013. Biomass Energy Centre [WWW Document]. URL http://www.biomassenergycentre.org.uk/

UK Government, 2011. Planning our electric future: a White Paper for secure, affordable and low-carbon electricity.

Vamvuka, D., Zografos, D., Alevizos, G., 2008. Control methods for mitigating biomass ash-related problems in fluidized beds. Bioresour. Technol. 99, 3534–44. https://doi.org/10.1016/j.biortech.2007.07.049

Van Krevelen, D.W., 1993. Coal: Typology - Physics - Chemistry - Constitution, Third Edit. ed. Elsevier.

van Lith, S., Alonso-Ramírez, V., Jensen, P. a., Frandsen, F.J., Glarborg, P., 2006. Release to the gas phase of inorganic elements during wood combustion. Part 1: development and evaluation of quantification methods. Energy & Fuels 20, 964–978.

van Lith, S.C., Jensen, P. a., Frandsen, F.J., Glarborg, P., 2008. Release to the Gas Phase of Inorganic Elements during Wood Combustion. Part 2: Influence of Fuel Composition. Energy & Fuels 22, 1598–1609. https://doi.org/10.1021/ef060613i

Vassilev, S. V., Baxter, D., Andersen, L.K., Vassileva, C.G., 2010. An overview of

the chemical composition of biomass. Fuel 89, 913–933. https://doi.org/10.1016/j.fuel.2009.10.022

Vassilev, S. V., Baxter, D., Vassileva, C.G., 2014. An overview of the behaviour of biomass during combustion: Part II. Ash fusion and ash formation mechanisms of biomass types. Fuel 117, 152–183. https://doi.org/10.1016/j.fuel.2013.09.024

Vassilev, S. V., Tascón, J.M.D., 2003. Methods for characterization of inorganic and mineral matter in coal: A critical overview. Energy and Fuels 17, 271–281. https://doi.org/10.1021/ef020113z

Vassilev, S. V., Vassileva, C.G., 2005. Methods for Characterization of Composition of Fly Ashes from Coal-Fired Power Stations: A Critical Overview. Energy & Fuels 19, 1084–1098. https://doi.org/10.1021/ef049694d

Vassilev, S. V., Vassileva, C.G., Vassilev, V.S., 2015. Advantages and disadvantages of composition and properties of biomass in comparison with coal: An overview. Fuel 158, 330–350. https://doi.org/10.1016/j.fuel.2015.05.050

Vassilev, S. V, Kitanob, K., Takedab, S., Tsurueb, T., 1995. Influence of mineral and chemical composition of coal ashes on their fusibility 3820.

Wang, L., Becidan, M., Skreiberg, O., 2012a. Sintering behavior of agricultural residues ashes and effects of additives. Energy and Fuels 26, 5917–5929. https://doi.org/10.1021/ef3004366

Wang, L., Hustad, J.E., Skreiberg, Ø., Skjevrak, G., Grønli, M., 2012b. A critical review on additives to reduce ash related operation problems in biomass combustion applications. Energy Procedia 20, 20–29. https://doi.org/10.1016/j.egypro.2012.03.004

Wang, L., Skjevrak, G., Hustad, J., Skreiberg, Ø., 2013. Investigation of biomass ash sintering characteristics and the effect of additives. Energy & Fuels.

Wang, L., Skjevrak, G., Hustad, J.E., Grønli, M., Skreiberg, Ø., 2012c. Effects of additives on barley straw and husk ashes sintering characteristics. Energy Procedia 20, 30–39. https://doi.org/10.1016/j.egypro.2012.03.005

Wigmans, T., Haringa, H., Moulijn, J.A., 1983. Nature, activity and stability of active sites during alkali metal carbonate-catalysed gasification reactions of coal char. Fuel 62, 185–189. https://doi.org/10.1016/0016-2361(83)90195-3

Wornat, M.J., Hurt, R.H., Yang, N.Y.C., Headley, T.J., 1995. Structural and compositional transformations of biomass chars during combustion. Combust. Flame 100, 131–143. https://doi.org/10.1016/0010-2180(94)00055-W

Wu, H., Bashir, M.S., Jensen, P.A., Sander, B., Glarborg, P., 2013. Impact of coal fly ash addition on ash transformation and deposition in a full-scale wood suspension-firing boiler. Fuel 113, 632–643. https://doi.org/10.1016/j.fuel.2013.06.018

Wu, H., Glarborg, P., Frandsen, F.J., Dam-Johansen, K., Jensen, P.A., 2011. Dust-

firing of straw and additives: Ash chemistry and deposition behavior. Energy and Fuels 25, 2862–2873. https://doi.org/10.1021/ef200452d

Yongtie, C., Wenming, Y., Zhimin, Z., Mingchen, X., Boon, S.K., Subbaiah, P., 2017. Modelling of ash deposition in biomass boilers: A review. Energy Procedia 143, 623–628. https://doi.org/10.1016/j.egypro.2017.12.737

Zbogar, A., Frandsen, F., Jensen, P.A., Glarborg, P., 2009. Shedding of ash deposits. Prog. Energy Combust. Sci. 35, 31–56. https://doi.org/10.1016/j.pecs.2008.07.001

Zheng, Y., Jensen, P.A., Jensen, A.D., 2008. A kinetic study of gaseous potassium capture by coal minerals in a high temperature fixed-bed reactor. Fuel 87, 3304–3312. https://doi.org/10.1016/j.fuel.2008.05.003

Appendices

Chapter 4 Appendices

XRF Results – Values for potassium oxide

Additive Ratio	**Kaolin Layer**				**1:1 Ratio (50% kaolin)**			
Sample number	30	31	32	Mean	33	34	35	Mean
Uncorrected (UoB)	8.4%	11.2%	11.2%	10.2%	17.9%	17.6%	17.1%	17.5%
Corrected	7.5%	9.9%	9.9%	9.1%	15.9%	15.6%	15.2%	15.6%
Normalised to mass yield	5.6%	7.5%	7.4%	6.8%	12.9%	13.0%	12.1%	12.7%
Normalised to 0% kaolin	18.7%	19.9%	23.0%	20.5%	25.7%	26.0%	24.2%	25.3%

Additive Ratio	**2:1 Ratio (33.3% kaolin)**				**3:1 Ratio (25% kaolin)**			
Sample number	36	37	38	Mean	40	41	42	Mean
Uncorrected (UoB)	20.5%	19.7%	19.7%	19.9%	22.7%	22.7%	22.6%	22.7%
Corrected	18.2%	17.5%	17.5%	17.7%	20.2%	20.2%	20.1%	20.1%
Normalised to mass yield	15.1%	14.4%	14.2%	14.6%	15.5%	15.9%	15.6%	15.6%
Normalised to 0% kaolin	22.8%	21.7%	21.4%	21.9%	20.7%	21.1%	20.8%	20.9%

Additive Ratio	**4:1 Ratio (20% kaolin)**				**5:1 Ratio (16.7% kaolin)**			
Sample number	43	44	45	Mean	46	47	48	Mean
Uncorrected (UoB)	22.6%	22.6%	24.7%	23.3%	24.7%	25.0%	26.0%	25.2%
Corrected	20.1%	20.1%	21.9%	20.7%	21.9%	22.2%	23.1%	22.4%
Normalised to mass yield	16.5%	16.9%	18.7%	17.4%	18.0%	18.0%	19.1%	18.4%
Normalised to 0% kaolin	20.6%	21.2%	23.4%	21.8%	21.8%	21.7%	23.0%	22.1%

	Fuel and additive mixed					Kaolin Layer
% kaolin	**16.67%**	**20%**	**25%**	**33%**	**50%**	**66.8%**
stdev	0.6%	1.2%	0.2%	0.6%	0.8%	1.8%
2* stdev	1.2%	2.4%	0.4%	1.2%	1.6%	3.6%
% K2O	22.1%	21.8%	20.9%	22.0%	25.3%	20.5%
% Vol. K	15.0%	11.9%	5.0%	13.5%	39.8%	2.3%
stdev	4.5%	9.4%	1.5%	4.6%	6.1%	14.1%
2* stdev	9.0%	18.9%	3.0%	9.3%	12.3%	28.1%

Chapter 5 Appendices

XRF Results – Values for potassium oxide

1300°C Additive ratio experiment - phase 1					
% kaolin	**17%**	**20%**	**25%**	**33%**	**50%**
uncorrected value (UoB)	26.6%	25.5%	24.4%	22.1%	16.8%
corrected value	23.7%	22.7%	21.7%	19.6%	14.9%
normalised to mass yields	21.8%	20.9%	19.8%	17.9%	13.7%
normalised to 0% additive	26.1%	26.1%	26.4%	26.9%	27.4%
% volatile K2O	46.0%	45.6%	48.3%	51.7%	55.7%

1300°C Additive ratio experiment - phase 2				
% kaolin	**20%**	**30%**	**40%**	**50%**
uncorrected mean value (UoB)	26.8%	23.9%	22.2%	18.4 %
corrected mean value	23.8%	21.3%	19.7%	16.3%
normalised to mass yields	21.9%	19.4%	18.2%	15.0%
normalised to 0% additive	27.4%	27.7%	30.4%	30.0%
stdev *2	1.9%	1.1%	1.6%	2.4%
% volatile K2O	55.7%	58.5%	79.1%	76.0%

1300°C Additive ratio experiment - combined results							
% kaolin	**17%**	**20%**	**25%**	**30%**	**33%**	**40%**	**50%**
Absolute K2O content	26.1%	27.0%	26.4%	27.7%	26.9%	30.4%	29.3%
stdev *2		1.8%		1.1%		1.6%	2.4%
% volatile K2O	46.0%	53.2%	48.3%	58.5%	51.7%	79.1%	70.9%

Temperature experiment - 50% kaolin				
Temperature (°C)	**1000**	**1150**	**1300**	**1450**
uncorrected mean value (UoB)	18.1%	**16.8%	18.4%	16.3%
corrected mean value	16.1%	18.1%	16.3%	14.5%
normalised to mass yields	14.6%	16.9%	15.0%	12.6%
normalised to 0% additive	29.2%	33.8%	30.0%	25.2%
stdev *2	3.1%	1.0%	2.6%	1.2%
% vol. K	68.8%	106.2%	76.3%	42.0%
stdev *2	23.8%	8.0%	20.0%	9.7%

**value measured at UoN

Residence time experiment - 50% kaolin			
Residence time (ms)	**600**	**200**	**100**
uncorrected mean value (UoB)	18.4%	19.6%	19.5%
corrected mean value	16.3%	17.4%	17.3%
normalised to mass yields	15.0%	16.1%	15.9%
normalised to 0% additive	30.0%	32.2%	31.7%
stdev *2	2.6%	1.1%	2.7%
% vol. K	76.3%	93.1%	87.4%
stdev *2	20.0%	8.0%	20.0%

Miscanthus experiment - 50% kaolin		
Temperature (°C)	**1150**	**1300**
uncorrected mean value (UoN)	7.4%	6.9%
corrected mean value	7.9%	7.4%
normalised to mass yields	6.7%	6.3%
normalised to 0% additive	13.4%	12.6%
stdev*2	0.1%	1.9%
% vol. K	190.3%	148.3%

Wood additive experiments - 1300°C		
additive	50% kaolin	50% Coal Fly Ash
uncorrected mean value (UoN)	8.6%	5.5%
corrected mean value	9.2%	5.9%
normalised to mass yields	7.6%	5.0%
normalised to 0% additive	15.2%	10.0%
% vol. K	75.2%	3.5%

olive cake and coal fly ash experiments		
Temperature (°C)	**1150**	**1300**
uncorrected mean value (UoN)	14.0%	10.8%
corrected mean value	15.0%	11.6%
normalised to mass yields	13.7%	10.6%
normalised to 0% additive	27.4%	21.2%
stdev *2	0.0%	0.0%
% vol. K	52.8%	8.7%
stdev *2	1.1%	1.3%